Doctoral theses at NTNU, 2019:251

Di Wan

Hydrogen-Assisted Fatigue Crack Growth in Ferritic Steels

ISBN 978-82-326-4098-0 (printed ver.)
ISBN 978-82-326-4099-7 (electronic ver.)
ISSN 1503-8181

NTNU
Norwegian University of Science and Technology

NTNU
Norwegian University of Science and Technology

Doctoral theses at NTNU, 2019:251

NTNU
Norwegian University of Science and Technology
Thesis for the Degree of
Philosophiae Doctor
Faculty of Engineering
Department of Mechanical and Industrial Engineering

Di Wan

Hydrogen-Assisted Fatigue Crack Growth in Ferritic Steels

Thesis for the Degree of Philosophiae Doctor

Trondheim, September 2019

Norwegian University of Science and Technology
Faculty of Engineering
Department of Mechanical and Industrial Engineering

NTNU
Norwegian University of
Science and Technology

NTNU
Norwegian University of Science and Technology

Thesis for the Degree of Philosophiae Doctor

Faculty of Engineering
Department of Mechanical and Industrial Engineering

ISBN 978-82-326-4098-0 (printed ver.)
ISBN 978-82-326-4099-7 (electronic ver.)
ISSN 1503-8181

Doctoral theses at NTNU, 2019:251

Printed by NTNU Grafisk senter

"Scio me nihil scire."

"I know that I know nothing."

--- Socrates (ca. 470 BC – 399 BC, classical Greek philosopher)

Preface

This dissertation is submitted to the Norwegian University of Science and Technology (NTNU), in fulfillment of requirements for the Doctor of Philosophy degree. The work has been conducted in the period from September 2015 to September 2018 under the supervision of Prof. Afrooz Barnoush. The main experimental work was carried out in the NTNU Nanomechanical lab and Metallography lab at the Department of Mechanical and Industrial Engineering.

The thesis was financially supported through the HyF-Lex project (Petromaks 2 Programm, Project No. 244068/E30) by the Research Council of Norway (RCN).

The thesis comprises a summary of the PhD work and five articles published in scientific journals or conferences.

Di Wan

August, 2019

Acknowledgements

First and foremost, I would like to thank my supervisor Prof. Afrooz Barnoush, without whom this PhD project could not be established. You are a great professor and always inspire me in thinking deeper and deeper. Most of the great ideas came up in my PhD study were given by your creative thinking and innovative brainstorming. Your attitude towards science also encouraged me a lot in doing rigorous work and being responsible for the work. You are not only a professor, but also a close friend whenever I have problem with my life here in Trondheim. Thank you very much for giving me the great opportunity working in your group!

I would also like to thank my co-supervisor Dr. Nousha Kheradmand. You helped me a lot in the lab work. You showed me lots of practical tips in doing tests and trusted me a lot and allowed me work independently in the labs. This gave me a great freedom in practicing my skills and developing my new experimental setups. Thanks a lot for your help, Nousha!

Then I would like to thank my closest working partner Dr. Antonio Alvaro at SINTEF Industry. You are the correct one who delivered the necessary materials, specimens and testing details. Your deep knowledge in fatigue testing helped me a lot in writing the papers as well as doing the investigations. Wish you all the best with your new position as a leader in the lab!

My sincere gratitude goes also to those who supported me in my PhD study, including but not limiting to: Prof. Yanjun Li, Dr. Dongdong Zhao, Dr. Hailong Jia, Dr. Feng Qian, Dr. Jisheng Qin, Dr. Yijiang Xu and Dr. Yun Deng, Mr. Jan Inge Meling, Mr. Dong Wang and Mrs. Xu Lu, Mr. Feng Lu, Dr. Lu Wang and Mrs. Xiaoxue Zhang, Dr. Bo Jiang and Dr. Yan Ma, Ms. Lu Xia, Mr. Shaoquan Wang and many others.

A special hug should be given to my beloved parents who encouraged me all the time. Thank you for your patience and support during my study abroad, and thanks for understanding and respecting my decision in my life.

Finally, it has been a great pleasure to work in the Department of Mechanical and Industrial Engineering (MTP) at NTNU. I would like to express my grateful gratitude to all the friends, colleagues and collaborators. Thank you all!

Di Wan, Trondheim

Table of Contents

List of Papers

1. **D. Wan**, Y. Deng, A. Barnoush, Hydrogen embrittlement effect observed by in-situ hydrogen plasma charging on a ferritic alloy, *Scripta Mater.* 151 (2018) 24-27.
2. **D. Wan**, A. Alvaro, V. Olden, A. Barnoush, Hydrogen-enhanced fatigue crack growth behaviors in a ferritic Fe-3wt%Si steel studied by fractography and dislocation structure analysis, *Int. J. Hydrog. Energy* 44 (2019) 5030-42.
3. **D. Wan**, Y. Deng, J. I. Meling, A. Alvaro, A. Barnoush, Hydrogen-enhanced fatigue crack growth in a pre-cracked single-edge notched tensile specimen under in-situ hydrogen-plasma charging inside an environmental scanning electron microscope, *Acta Mater.* 170 (2019) 87-99.
4. **D. Wan,** A. Barnoush, Plasticity in cryogenic brittle fracture of ferritic steels: dislocation versus twinning, *Mater. Sci. Eng., A* 744 (2019) 335-339.
5. **D. Wan**, A. Alvaro, V. Olden, A. Barnoush, Hydrogen-assisted fatigue crack growth in ferritic steels – a fractographic study, *MATEC Web of Conferences*, 2018, p. 03004. (conference paper)

Contributions to Conferences

1. **D. Wan**, A. Barnoush, (2016) Observation of Dislocations in Scanning Electron Microscope. Nano@NTNU Symposium. NTNU; Trondheim, Norway. 2016-11-18 - 2016-11-19. (poster)
2. **D. Wan**, A. Alvaro, V. Olden, A. Barnoush, (2018) A fractographic study of hydrogen-enhanced fatigue crack propagation in a Fe-3wt.%Si ferritic alloy. The 12th International Fatigue Congress. SF2M Fatigue technical committee; Futuroscope, Poitiers. 2018-05-27 - 2018-06-01. (oral presentation)
3. **D. Wan**, A. Alvaro, A. Barnoush, Hydrogen-assisted fatigue crack propagation in a ferritic steel. Materials Science and Engineering 2018 (MSE); Darmstadt, Germany. 2018-09-26 - 2018-09-28. (poster)
4. **D. Wan**, A. Barnoush, In-situ crack growth observation and advanced characterization of the fracture process zone in an ESEM. Materials Science and Engineering 2018 (MSE); Darmstadt, Germany. 2018-09-26 - 2018-09-28. (oral presentation)
5. Y. Deng, T. Hajilou, **D. Wan**, N. Kheradmand, A. Barnoush, (2016) Hydrogen embrittlement investigated by novel critical experiments. HEmS Workshop; 2016-09-23 - 2016-09-23. (oral presentation)
6. A. Barnoush, Y. Deng, T. Hajilou, **D. Wan**, X. Lu, D. Wang, N. Kheradmand, (2017) Understanding the hydrogen embrittlement by novel critical experiments. Invited lecture at University of Science and Technology Beijing. University of Science and Technology Beijing; Beijing. 2017-08-28 - 2017-08-28. (oral presentation)
7. A. Barnoush, T. Hajilou, Y. Deng, B.R.S. Rogne, **D. Wan**, X. Lu, D. Wang, (2017) Critical experiments for understanding the hydrogen embrittlement. The 2017 world conference on advances in structural engineering and mechanics. Int'l Association of Structural Engineering & Mechanics; Ilsan. 2017-08-28 - 2017-09-01. (oral presentation)

Contributions to Other Works

1. Y. Deng, T. Hajilou, **D. Wan**, N. Kheradmand, A. Barnoush, In-situ micro-cantilever bending test in environmental scanning electron microscope: Real time observation of hydrogen enhanced cracking, Scripta Mater. 127 (2017) 19-23.
2. A. Alvaro, **D. Wan**, V. Olden, A. Barnoush, Hydrogen Enhanced Fatigue Crack Growth Rates in a Ferritic Fe-3wt%Si Alloy, Procedia Structural Integrity 13 (2018) 1514-1520.
3. A. Alvaro, **D. Wan**, V. Olden, A. Barnoush, Hydrogen Enhanced Fatigue Crack Growth Rates in a Ferritic Fe-3wt%Si Alloy and a X70 pipeline steel, Eng. Fract. Mech. (*in press*) (2019).
4. T. Depover, T. Hajilou, **D. Wan**, D. Wang, A. Barnoush, Assessment of the potential of hydrogen plasma charging as compared to conventional electrochemical hydrogen charging on dual phase steel, Mater. Sci. Eng., A 754 (2019) 613-621.
5. T. Depover, **D. Wan**, D. Wang, A. Barnoush, K. Verbeken, Hydrogen embrittlement evaluation by hydrogen plasma charging of TRIP-assisted steel, Int. J. Alloy Compd, (*submitted*) (2019).
6. F. Qian, S. Jin, **D. Wan**, G. Sha, Y. Li, Synergistic effects of Cd and Cr on engineering dispersoid-strengthened aluminium alloy for high-temperature applications, (*to be submitted*) (2019).
7. S. Guan, K. Solberg, **D. Wan**, F. Berto, T. Welo, T.M. Yue, K.C. Chan, Formation of fully equiaxed grain microstructure in additively manufactured AlCoCrFeNiTi0.5 high entropy alloy, Mater. Design (*under review*) (2019).
8. S. Guan, **D. Wan**, K. Solberg, F. Berto, T. Welo, T.M. Yue, K.C. Chan, Additive manufacturing of fine-grained and dislocation-populated CrMnFeCoNi high entropy alloy by laser engineered net shaping, Mater. Sci. Eng., A 761 (2019).
9. S.Q. Zhang, S.H. Jiao, J.H. Ding, **D. Wan**, Z.Y. Liu, G.D. Wang, Super long-range diffusion of carbon during proeutectoid ferrite transformation, Journal of Central South University 26(3) (2019) 560-566.
10. D. Wang, X. Lu, Y. Deng, **D. Wan**, Z. Li, A. Barnoush, Effect of hydrogen-induced surface steps on the nanomechanical behavior of a CoCrFeMnNi high-entropy alloy revealed by in-situ electrochemical nanoindentation, Intermetallics (*under review*) (2019).

11. D. Wang, X. Lu, **D. Wan**, Z. Li, A. Barnoush, In-situ observation of martensitic transformation in an interstitial metastable high-entropy alloy during cathodic hydrogen charging, Scripta Mater. 173 (2019) 56-60.
12. X. Lu, D. Wang, **D. Wan**, Z.B. Zhang, N. Kheradmand, A. Barnoush, Effect of electrochemical charging on the hydrogen embrittlement susceptibility of alloy 718, Acta Mater. 179 (2019) 36-48.

List of Abbreviations

AIDE	adsorption-induced decohesion
ASTM	American standard for testing and materials
CT	compact tension
DC	dislocation cell
EBSD	electron backscattered diffraction
ECCI	electron channeling contrast imaging
ESEM	environmental scanning electron microscope
EU	European Union
FCG	fatigue crack growth
FCGR	fatigue crack growth rate
FIB	focused ion beam
GND	geometrically necessary dislocation
H	hydrogen
HDDW	highly densed dislocation wall
HE	hydrogen embrittlement
HEDE	hydrogen-enhanced decohesion
HELP	hydrogen-enhanced localized plasticity
HER	hydrogen evolution reaction
HESIV	hydrogen-enhanced strain-induced vacancy formation
ID	individual dislocation
NTNU	Norwegian University of Science and Technology
RCN	Research Council of Norway
SEM	scanning electron microscopy
SENT	single-edge notched tension
SPM	scanning probe microscopy
SSD	statistically stored dislocation
TEM	transmission electron microscopy
WP	work package

List of Figures

List of Tables

Part I

1. Introduction

1.1 Background

This PhD project is a part of the project "field life extension through controlling the combined material degradation of fatigue and hydrogen (HyF-Lex)". The HyF-Lex project seeks to increase the fundamental understanding of the mechanisms inherent to hydrogen assisted fatigue crack growth in steels, as well as contributing to a model framework for assessment of hydrogen-assisted fatigue.

One of the primary targets of the PETROMAKS 2 program[1] is higher recovery rates in new and existing fields. As described in thematic priority area 4, the aging of infrastructure is a main challenge to achieving this objective. Increasing the lifetime requires the management of material degradation. This is clearly pointed out in the technology target area TTA4 in the OG21[2] strategy document. The understanding and assessment of degradation mechanisms, including the combined degradation effects is an important knowledge gap. Therefore, the HyF-Lex project will investigate the synergistic degradation from combined fatigue and hydrogen embrittlement effect. This would improve the basis for lifetime assessment. It will also provide information valuable for defining guidelines for design and use under hydrogen-assisted fatigue, which is currently lacking. Degradation from combined fatigue and hydrogen embrittlement is also a challenge for drilling components such as, for instance, drill heads and tubing hangers. Extended reach drilling for the development of smaller fields from existing ones is targeted in the thematic priority area 3 and TTA3 of the OG21 strategy document. HyF-Lex also shares an interface with the ENERGIX program[3]. The insight obtained in the project is also relevant for the hydrogen society emerging in the European Union (EU), Japan and USA.

The structure of the HyF-Lex project is schematically shown in Figure 1-1.

[1] PETROMAKS 2 program: A large-scale program of the Research Council of Norway for the optimal management of petroleum resources – 2013-2022.
[2] OG21: Oil and gas in the 21st century, Norway's technology strategy for the 21st century.
[3] ENERGIX program: A large-scale program of the Research Council of Norway for energy research – 2013-2022.

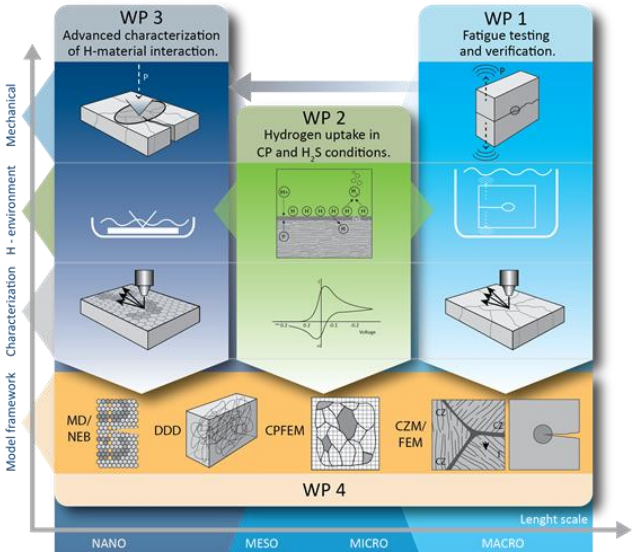

Figure 1-1 Structrue of the HyF-Lex project. The present PhD thesis focuses on the WP3.

1.2 Objectives and scope

The PhD study holds the responsibility of the WP3 of the HyF-Lex project, which focuses on the in-situ crack growth tests and advanced materials characterization work. The materials were provided by SINTEF Industry through WP1 (fatigue testing and verification). The samples include compact tension (CT) specimens tested by fatigue crack growth rate testing in lab air and cathodic charging conditions and small-scale tensile specimens with fatigue pre-cracking. The failed CT specimens were further prepared by metallographic methods and investigated by scanning electron microscopy (SEM). The pre-cracked tensile specimens were further tested by in-situ small-scale tensile testing inside the environmental scanning electron microscope (ESEM) with different environmental conditions.

The scope of the work is defined as follows:

- Understanding the state-of-the-art fundamentals of hydrogen embrittlement in structural materials.
- Understanding the fundamentals of fatigue and cyclic loading behaviors of steels.
- Understanding and mastering different advanced characterization methods suitable for the project.

- Performing advanced characterization work (mainly SEM-based techniques) on different samples received from WP partners and other testing manners.
- Analyzing testing data from different methods and evaluate the applicability of the present mechanism models.
- Providing necessary results and contributions to other WP partners (mainly the modelling partners) of the HyF-Lex project.

1.3 Thesis overview

To meet the goals of the PhD project, we first did the macroscopic FCGR tests with in-situ electrochemical hydrogen charging and the corresponding characterizations, and the results showed inspiring aspects on the study of hydrogen-assisted fatigue crack growth in ferritic steels. However, some problems still exist in the macro-scale studies such as the ambiguity from the local stress state and the neighboring crystal orientation influences. Following the problems, we designed the well-defined crack in an oligocrystalline tensile specimen that can constrain as many parameters as possible. To assure that the hydrogen could be properly charged into the chamber of an environmental scanning electron microscope, we developed the novel approach of using hydrogen plasma instead of conventional hydrogen gas and checked the effect of hydrogen plasma on the tensile properties of the ferritic specimens by in-situ tensile testing. When the hydrogen effect was confirmed, we performed the critical tests on the pre-cracked oligocrystalline tensile specimens by cyclic loading and observed the fatigue crack growth behaviors via both in-situ and ex-situ approaches. The results from these tests are consistent with each other and agree with that from other approaches in the candidate's research group.

This thesis was written based on a collection of research papers that resulted from the PhD study. Part I is the introduction part to the PhD work containing background and a literature review followed by the main results from the study. Part II comprises the research papers that have been published in scientific journals or conferences. The papers are listed below, and a summary of the papers is presented in Chapter 6.

Journal papers:

D. Wan, Y. Deng, A. Barnoush, Hydrogen embrittlement effect observed by in-situ hydrogen plasma charging on a ferritic alloy, Scripta Mater. 151 (2018) 24-27.

D. Wan, A. Alvaro, V. Olden, A. Barnoush, Hydrogen-enhanced fatigue crack growth behaviors in a ferritic Fe-3wt%Si steel studied by fractography and dislocation structure analysis, Int. J. Hydrog. Energy 44(10) (2019) 5030-5042.

D. Wan, Y. Deng, J.I. Meling, A. Alvaro, A. Barnoush, Hydrogen-enhanced fatigue crack growth in a single-edge notched tensile specimen under in-situ hydrogen charging inside an environmental scanning electron microscope, Acta Mater. 170 (2019) 87-99.

D. Wan, A. Barnoush, Plasticity in cryogenic brittle fracture of ferritic steels: Dislocation versus twinning, Mater. Sci. Eng., A 744 (2019) 335-339.

Conference papers:

D. Wan, A. Alvaro, V. Olden, A. Barnoush, Hydrogen-assisted fatigue crack growth in ferritic steels – a fractographic study, MATEC Web of Conferences, 2018, p. 03004.

Statement of Author Contributions:

DW & AB designed the experiments. DW conducted the tests and analyzed the data. AA delivered the raw materials and specimens. VO was the manager of related work packages. YD joined the discussions. JIM helped in the numerical method analysis. AB was the manager of the whole project. All authors joined the manuscript writing and revising.

2. State of the Art

2.1 Hydrogen embrittlement

Johnson [1] is generally acknowledged as the first one who launched the study field of the hydrogen embrittlement phenomenon in 1874. The practical outcome of this phenomenon is denoted as unwanted earlier failure of the material, namely a decreased ductility, or increased brittleness, in the presence of hydrogen. To cause this phenomenon, three main factors should be accounted, i.e.: the material itself, mechanical loading condition and the environment. These factors have been schematically summarized by Barnoush [2] in Figure 2-1.

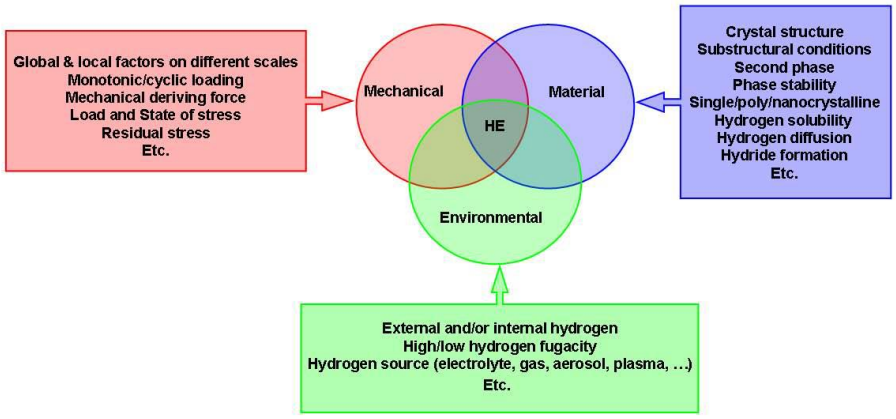

Figure 2-1 Global description of hydrogen embrittlement interaction aspects. Adopted from Ref. [2].

2.1.1 Phenomenology

A significant effect from the hydrogen is the mechanical behavior change. Many researchers have found softening or hardening effects in different materials after different hydrogen charging procedures. In 1987, Kimura and Matsui [3] reported a summary on the occurrence of hydrogen-induced softening and hardening in iron. The hardening effect could be simply explained by solid solution hardening mechanism, while the softening effect was explained by a hydrogen-enhanced dislocation mobility, both for edge and screw dislocations [3].

In 1983, Kimura et al. [4] reported the three-stage work hardening behavior of an Fe single crystal oriented for single slip during hydrogen charging between 296 and 200 K.

Conventionally, when hydrogen is not presented, the tensile behavior of single crystals can be divided into three stages, i.e. stage I as easy glide regime, stage II as a large linear increase of strength and stage III as a decrease of the hardening rate (dynamic recovery) [5]. When hydrogen is presented, however, the three stages can change depending on the crystal orientation and temperature. The stage I' (prime means hydrogen is presented) is associated with single slip by the motion of primary screw dislocations. The stage II' associates with the long-range motion of secondary screw dislocations and the stage III' also shows a softening behavior of the single crystal. The main difference between the hydrogen-free and the hydrogen-charged cases falls in the first two stages when hydrogen is presented, the material shows more significant softening behavior, which is due to the increased mobility of screw dislocations by hydrogen [4]. This has been supported by the slip line observation and dislocation structure observation in Ref. [4]. Interestingly, the hydrogen-charged specimens show a longer uniform elongation compared to the hydrogen-free cases, but the fractographs show a semi-brittle manner in the case with hydrogen as compared to a 100% ductile case without hydrogen.

When it comes to commercial materials such as high strength steels, the vital degradation is a ductility loss in terms of the tensile elongation when comparing testing cases in hydrogenated specimens with the cases in air. Depover and his coworkers did intensive work on different high strength steels with different microstructures by tensile tests on hydrogen-charged specimens [6-19]. Most of the results show a slight increase in the strength with a significant reduction in the elongation to fracture. The fractography shows a brittle-like surface in hydrogen cases versus a ductile surface in the hydrogen-free cases. By thermal desorption analysis (TDS), the mechanical degradation was concluded as being caused by trapped hydrogen, and the configuration of different type of carbides can influence the hydrogen trapping situation in materials.

2.1.2 Hydrogen entry into materials

A first step to initiate the embrittlement effect is the entry of hydrogen into the materials. In literature, different charging methods have been used to let hydrogen enter metals and alloys. This section shortly summarizes some commonly used methods and their theoretical backgrounds.

Gaseous phase hydrogen

From gaseous phase, the hydrogen can enter the material via three different stages, i.e. physisorption, chemisorption, and absorption [2]. This can be seen in the schematic in Figure 2-2.

- Physisorption is a result from the van der Waals forces between the surface (Fe for example) and the adsorbent (H_2 molecules), and a multi-layer fluid will be formed, as described in Figure 2-2b. This is a reversible procedure that normally happens instantaneously with an enthalpy change corresponding to the heat of condensation of the gaseous adsorbent (20 kJ/mol or less) [2]. This is a long-range reaction.
- Chemisorption is the process described in Figure 2-2c. This procedure is a result from short-range chemical reactions between the surface atom (e.g. Fe) and the adsorbent (H_2). An energy barrier for the dissociation of H_2 molecule and the formation of hydrogen - metal bond has to be overcome, which is typically in the range of 20~150 kJ/mol and thus significantly higher than the energy for physisorption. Since this is a short-range interaction, typically only monolayers are involved, and is either a slowly reversible or irreversible procedure [2, 20].
- The last stage is the absorption that involves the introduction of the products from chemisorption into the bulk lattice of the metal, as described in Figure 2-2d. The capacity of hydrogen absorption, however, depends on the metal type and microstructures.

The hydrogen in the physisorption or chemisorption stages can be referred to as "adsorbed hydrogen", in contrast to the "absorbed hydrogen" in the final stage.

In the present PhD work, the gaseous hydrogen charging was not conducted, but instead, the results from literature by this method was compared and discussed.

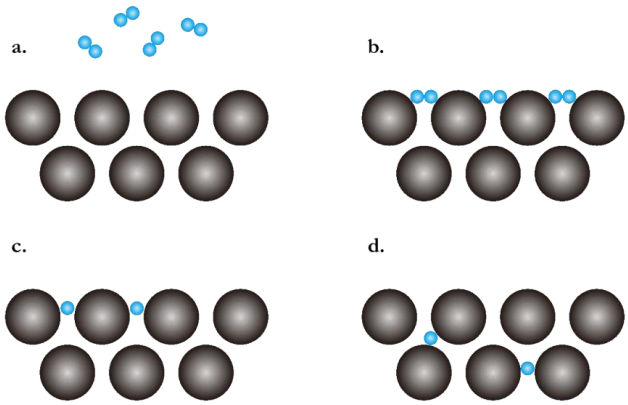

Figure 2-2 Schematic of hydrogen entry from gaseous phase: a. H_2 molecules approaching the material surface, b. physisorption, c. chemisorption, and d. absorption. (Small blue balls indicate hydrogen atoms or molecules and big gray balls indicate metal atoms.)

Cathodic charging

Electrochemical hydrogen charging by means of cathodic polarization is commonly used in the hydrogen embrittlement study. Depending on the condition of the electrolyte, the overall hydrogen evolution reaction (HER) can be identified as two cases:

$$2H_3O^+ + 2e^- \rightarrow H_2 + 2H_2O \text{ (in acid solutions)} \quad \textbf{Eq. 1}$$

$$2H_2O + 2e^- \rightarrow H_2 + 2OH^- \text{ (in alkaline solutions)} \quad \textbf{Eq. 2}$$

It is generally accepted that two successive processes contribute to the overall HERs in both cases. The first step is either the discharge of hydrated protons in acid solutions or the electrolysis of water in alkaline solutions:

$$H_3O^+ + M + e^- \rightarrow MH_{ads} + H_2O \text{ (in acid solutions)} \quad \textbf{Eq. 3}$$

$$H_2O + M + e^- \rightarrow MH_{ads} + OH^- \text{ (in alkaline solutions)} \quad \textbf{Eq. 4}$$

Here the MH_{ads} means the hydrogen atoms adsorbed on the metal surface. The second step following the first is associated with the detachment of the hydrogen atoms from the metal surface. The chemical desorption (also called catalytic recombination) occurs in both acid and alkaline solutions as:

$$MH_{ads} + MH_{ads} \rightarrow H_2 + 2M \quad \textbf{Eq. 5}$$

And the electrochemical desorption occurs as:

$$MH_{ads} + H_3O^+ + e^- \rightarrow H_2 + H_2O + M \quad \text{(in acid solutions)} \qquad \textbf{Eq. 6}$$

$$MH_{ads} + H_2O + e^- \rightarrow H_2 + OH^- + M \quad \text{(in alkaline solutions)} \qquad \textbf{Eq. 7}$$

The entry of hydrogen into metals has been summarized as two alternative models [2]. The fist model was developed by Bockris and others [21-24] and the reaction sequence at the cathode surface is as follows (in acid):

$$H_3O^+ + M + e^- \xrightarrow[k_1]{\text{slow}} MH_{ads} + H_2O \qquad \textbf{Eq. 8}$$

$$MH_{ads} \underset{k_{-2}}{\overset{k_2}{\longleftrightarrow}} MH_{abs} \qquad \textbf{Eq. 9}$$

$$MH_{ads} + MH_{ads} \xrightarrow{k_3} H_2 + 2M \qquad \textbf{Eq. 10}$$

Where the MH_{ads} and the MH_{abs} refer to that the hydrogen adsorbed on the metal surface and absorbed directly beneath the metal surface, respectively. k_1, k_2, k_{-2}, and k_3 are the rate constants.

The second model was proposed by Bagotskaya and Frumkin [25] and the reaction sequence at the cathode surface is as follows:

$$H_3O^+ + M + e^- \underset{k_{-4}}{\overset{k_4}{\longleftrightarrow}} MH_{abs} + H_2O \qquad \textbf{Eq. 11}$$

$$H_3O^+ + M + e^- \xrightarrow{k_1} MH_{ads} + H_2O \qquad \textbf{Eq. 12}$$

$$MH_{ads} + MH_{ads} \xrightarrow{k_3} H_2 + 2M \qquad \textbf{Eq. 13}$$

Where k_3 and k_{-4} are the rate constants.

Both models consider an intermediate stage through which the electrolytic hydrogen enters the metal surface. The first model claims the intermediate stage is the adsorbed state and is identical to the reaction leads to hydrogen evolution. In this model the hydrogen entry rate is proportional to the coverage of the metal surface by the adsorbed hydrogen. The second model claims that the intermediate stage is not identical to the HER but to the reaction of hydrogen discharge. Thus, the rate constants in the two models are not the same.

In the present PhD study, cathodic charging was used in the macro-scaled tests to evaluate the hydrogen-assisted fatigue behaviors. More details follow in the experimental chapter.

Water vapor and intermetallics

Recently, an innovative methodology to study the hydrogen embrittlement effect of some special materials has been develop, which is based on the chemical reaction between water vapor molecules and some metallic constituents (e.g. Al). The fact is that water vapor can react with the metal producing hydrogen and oxides. The reaction can be written as (Al as an example):

$$2Al+3H_2O \rightarrow Al_2O_3+6H^+ +6e^- \qquad \text{Eq. 14}$$

Consequently, the produced atomic hydrogen can segregate at the stressed areas including micro-cracks, second phase boundaries, and other kinds of crystal defects and promote brittle fracture. This methodology has been successfully applied to evaluate the environmental embrittlement behaviors of Fe-Al and Ni-Al intermetallics [26-32].

This method has not been directly conducted in the present PhD project. The candidate joined the discussion with Dr. Yun Deng and the analysis of the results of the embrittlement behaviors in FeAl (50 at%) [30].

Plasma

As is stated before, the hydrogen needs to be dissociated into atomic form to initiate the embrittlement effect. To make this procedure more active, a novel approach can be introduced prior to the conventional tests, which becomes the idea of using plasma phase instead of molecular form of hydrogen. According to the report by Narita [33], the concentration of hydrogen can reach a value that is four orders of magnitude higher than that calculated from the gaseous hydrogen for the pressure used. In 1987, Kimura et al. [34] used this method to charge pure iron and got a significant softening effect on the mechanical performance of the charged specimen compared with the same material charged by helium plasma. However, some difficulties can arise from this approach, such as the temperature change and the surface damage. As is also stated by Kimura et al. [3], the heating from the plasma phase on the specimen can make the thermal procedure different. Furthermore, direct exposure of the specimen in plasma phase can modify the surface such as removing oxides or causing blisters [34-40]. As the techniques have been developing during the last decades, a new approach called "remote plasma" is now available in some commercial setups. By this approach, the plasma phase is mostly activated and stored near the afterglow of the plasma source, and only the active part of

this phase can take part in the reactions in the chamber. This setup can effectively charge the material with least heating and surface damage [35]. The effectiveness of this method has been proven by the candidate on an Fe-3wt%Si steel [41].

This charging method is the major novelty of the present PhD study, and has been applied to different materials under various loading conditions to study the hydrogen embrittlement effect.

2.1.3 Mechanisms

Since begin of the hydrogen embrittlement studies, a number of mechanisms have been proposed to explain this unfavorable behavior. They are summarized intensively in some review articles or book chapters, e.g. [42-45]. The proposed mechanisms include:

- High hydrogen pressure bubble or void; [46, 47]
- Hydrogen-enhanced localized plasticity (HELP); [48-53]
- Hydrogen-enhanced decohesion (HEDE); [44, 54-57]
- Adsorption-induced dislocation emission (AIDE); [42, 58-60]
- Hydrogen-enhanced strain-induced vacancy formation (HESIV); [61, 62]
- And so on.

Among these mechanisms, the HELP, HEDE and AIDE are the most popular ones and have successfully explained many experimental discoveries. Unfortunately, however, there is still no concrete conclusion on the accurate mechanism that could clarify all details.

HELP

The HELP mechanism postulates an enhanced dislocation activity by hydrogen in comparison with the hydrogen-free case. Consequently, the dislocation slipping will be "localized" by the introduction of hydrogen [49]. The enhanced dislocation mobility has been proven by in-situ TEM observations with environmental cell on Ni [50]. The localized slipping can also be seen in the confined plastic zone near the fracture surface of a hydrogenated specimen. This mechanism can easily explain the softening effect of hydrogen on materials, and the hardening phenomenon could be explained by atmospheric dragging, strain rate effect or high hydrogen concentration gradient near the sample surface, despite an enhanced dislocation mobility [49]. This mechanism can be schematically

described by Figure 2-3. The schematic shows that when dislocations approach obstacles, the total elastic energy is minimized due to hydrogen, and the resistance to dislocation motion due to obstacles is therefore decreased and consequently, the dislocation velocities are increased [63].

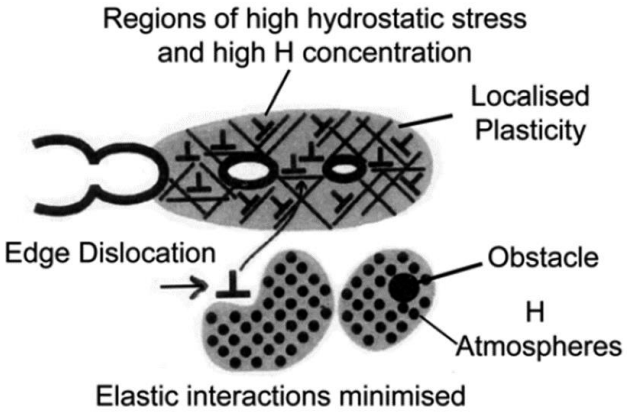

Figure 2-3 Schematic illustration of the HELP mechanism with regions of high hydrogen concentration giving increased localized plasticity. Adopted from Ref. [63].

However, as far as the candidate knows, some uncertainties can arise from the in-situ TEM observations. Due to the sample geometry in TEM (as thin foils), the two surfaces of the specimen can have strong influences on the results of the observations. The influence from the so-called "image force" could not be easily ignored. When pressurized gaseous hydrogen was charged into the small TEM chamber, this effect should be carefully treated in order to avoid the uncertainties. Instead, another technique that is suitable for the observation of plasticity in bulk materials was used by the candidate, which is called electron channeling contrast imaging (ECCI, details see section 2.3.2). This method can give some statistically more reliable results on bulk specimens that experience less influence from the surfaces.

HEDE

The HEDE mechanism was first proposed by Troiano [64] and further developed by Oriani et al. [56, 57, 65, 66] and Gerberich et al. [44, 67]. The basic suggestion in this mechanism is that the presence of H decreases the binding energy of interfaces. Consequently, upon mechanical loading, the boundaries in the materials become the weak points and can lead to a straight separation there. This can explain some intergranular

fracture type. However, direct evidence of the HEDE mechanism is difficult to be obtained by experimental approach due to technical limitations. But this mechanism can be supported by some numerical methods, particularly ab-initio calculations [68, 69]. When hydrogen concentration is increased, a decreased fracture energy can be observed. This relation can be efficiently shown in Figure 2-4. A higher hydrogen concentration yields a lower cohesive energy for surface decohesion.

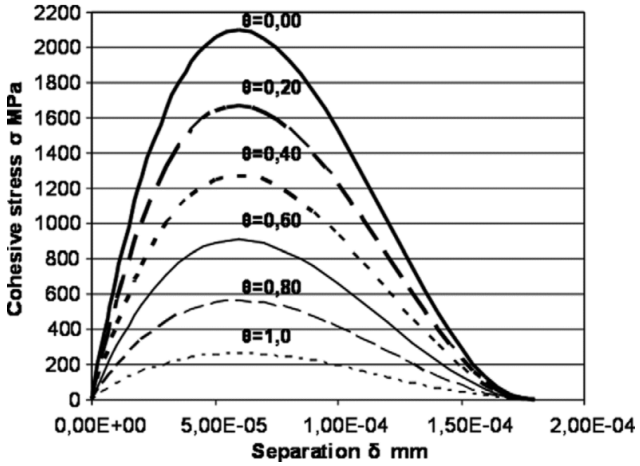

Figure 2-4 The cohesive energy for surface decohesion with different hydrogen coverage (θ). A larger θ value means a higher hydrogen concentration. [70]

This mechanism, on the one hand, can successfully explain some brittle fractographic morphology, on the other hand, however, is weak in explaining the fracture in relation to plastic (dislocation) activities.

AIDE

The AIDE mechanism explains the HE phenomenon from the aspects of both HELP and HEDE mechanisms. It is based on the weakening of interatomic bonding energy by hydrogen (HEDE) with the crack growth occurring by localized slip (HELP), and it is first proposed by Lynch [42, 58-60, 63]. The embrittling factor associates with the adsorbed hydrogen on the surface that weakens the substrate interatomic bonds and facilitates the emission of dislocations from the crack tip. This mechanism can be schematically described by Figure 2-5. The adsorbed hydrogen at the crack tip facilitates dislocation emission and help in crack opening. The void formation ahead of the crack tip helps in

maintaining small crack tip opening angles. Furthermore, the microvoid coalescence helps in crack growth and leave dimple structure on the fracture surface. [63]

The AIDE mechanism is successful in explaining the dimple structure on the fracture surface and ductile crack growth in the presence of hydrogen.

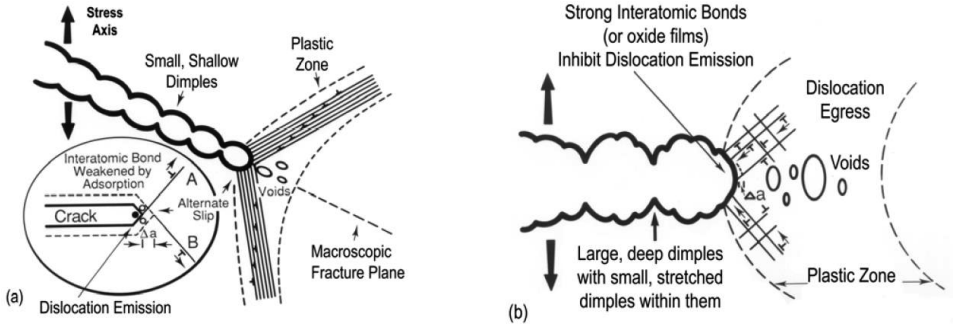

Figure 2-5 (a) the AIDE mechanism for transgranular crack growth involving alternate-slip from crack tips with voids formation ahead of the crack tip and (b) ductile crack growth involving coalescence of cracks with voids by egress of dislocations nucleated from near-crack-tip sources. Adopted from Refs.[59, 63].

Defactant concept

In the recent years, a relatively new concept called "defactant" model has been proposed by Kirchheim [71-73] and draws researchers' attention in the field of hydrogen embrittlement. "Defactant" is short for "**def**ect **act**ing **a**g**ent**", in analogy to a surfactant (**surf**ace **act**ing **a**g**ent**). This is a term denoting solute atoms that segregates to defects in a material. Within this framework, surfactants are also one sub-group of defactants [74].

When it comes to the interaction between metal and hydrogen, the solute hydrogen atom can be seen as a defactant that lowers the dislocation formation energy. This can be used as a proof for the enhanced dislocation activities and localized plasticity by the defactant, when hydrogen segregates to defects, as proposed by the HELP mechanism. It has been directly proven by both numerical methods yielding a lowered defect formation energy [71-73] and nanoindentation experiments showing an enhanced homogeneous dislocation nucleation in different materials [75-79].

Nevertheless, there is hardly a single mechanism that could explain all the phenomena and researchers are more and more favoring the combination and interaction between multiple mechanisms to explain the HE problem more reasonably, such as the HELP-mediated-HEDE mechanism. This could be a new direction in the future study on HE.

2.2 Fatigue crack growth (FCG)

Fatigue is one failure mechanism of structures that originates from cyclic loading. This damage has been discussed in scientific society for over 100 years. It was assessed that fatigue damage could cost $119 billion per year, according to the economic analyses by Battelle Laboratory under contract to US government in 1983 [80]. This economic loss is nevertheless growing since the largest fraction of fractures in metallic structures is associated with cyclic loads.

The fatigue procedure can be roughly divided into three stages, i.e. stage I as crack initiation, stage II as stable fatigue crack growth (FCG) and stage III as final rupture. The first two stages are deeply studied and carefully considered in many engineering aspects. The present PhD thesis has a focus on the stable FCG stage during cyclic loading. This stage is classically described by the Paris' law (or Paris-Erdogan law) [81], in which the straightforward mathematical relation can be described by Eq. 15:

$$\frac{da}{dN} = C \cdot \Delta K \qquad \textbf{Eq. 15}$$

where a is the crack length, N is the number of cycles and da/dN is the crack growth rate, which denotes the crack growth per loading cycle. On the right-hand side, C and m are constants that depend on the material, environment, stress ratio, etc, and ΔK is the range of the stress intensity factor during the cyclic loading, which is defined by Eq. 16:

$$\Delta K = K_{\max} - K_{\min} \qquad \textbf{Eq. 16}$$

where K_{max} and K_{min} are the maximum and minimum stress intensity factor during one loading cycle, respectively.

This relation can satisfactorily describe the stable FCG procedure (the stage II) for a wide range of materials. Engineers rely on this relation a lot since it can give a rough estimation on the FCGR and tell how long the structure can still be in service without repairing the existing cracks.

It is interesting to note that most continuum models for FCG are based on a mechanism that involves ductile striation formation, which is based on the alternative slipping behaviors of the dislocations ahead of the crack tip [82]. For example, Forsyth [83] summarized the damage and crack growth mechanisms in aluminum alloys when subjected to fatigue loading, and a two-stage fracture mechanism has been shown based on some microscopic evidence. In the first stage, the crack growth has been associated with the slip behaviors according to the geometrical constraints of the crystallography (slip plane crack), and the crack will mainly grow along the active slip bands. When the main crack has reached a critical length, it will eventually progress along the direction that is determined by the maximum tensile stress components. This stage involves the cross-slipping process that is associated with many more slip planes than the easy glide phase and therefore can be identified with the blunting of the crack tip and the growth during the cycle. A curved ductile striation appearance of the fractography is one of the evidences of this mechanism. Note that the types of dislocations as well as their sensitivity to strain rate, temperature or environmental conditions can be decisive in the deformation as well as the crack growth procedure. And on the other hand, these conditions can be a control parameter to validate the dislocation-based mechanisms. Some materials, nevertheless, behave differently during this stage, and the final fractography can show different features. This can make the evaluation much more complicated.

2.3 Materials characterization

2.3.1 Small scale mechanical testing

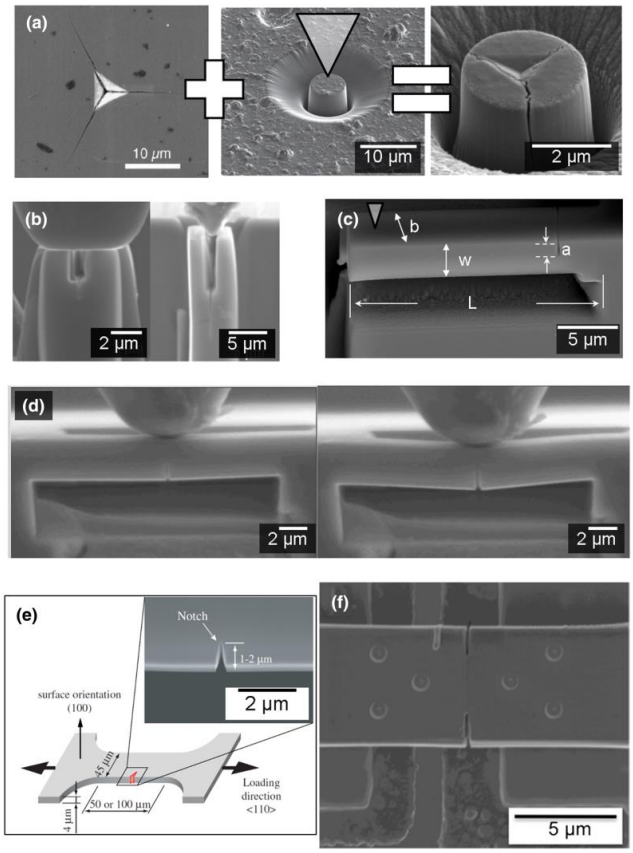

Figure 2-6 A summary of micro-scale fracture testing geometries: (a) indentation-based methods; (b) double cantilever bending using flat punch compression or wedge splitting; (c) single cantilever bending; (d) clamped beam bending; (e) single edge notch tension; and (f) double edge notch tension. Adopted from Ref. [84].

The conventional mechanical tests such as tensile tests, cyclic loading tests, fracture toughness tests, dynamic loading tests and so on, are normally conducted at a continuum-level according to the American Standard for Testing and Materials (ASTM) or other relevant standards, which describe the exact sample geometries. However, the need for testing materials at small scales such as micro- to nano-scales is gradually increasing nowadays. One reason is that the small scale devices in application need testing and evaluation. Another reason is that the evaluation at continuum level is a general average of the properties from the contributions of each small units at finer scales. In large applications, the microstructure of the materials is normally varying, and the large scale tests are difficult to predict the behaviors at such locations. Figure 2-6 shows a summary

of the sample geometries for micro-scale fracture testing with corresponding scale bars. Detailed description of this summary can be found if Ref. [84].

However, the realization of the miniature testing is challenging due to several reason: 1) the sample fabrication needs high precision at very fine scale and the sample can be easily contaminated during the fabrication process; 2) the testing device needs to acquire accurate data with high precision and high sensitivity, and thus the testing environment should be kept as stable as possible; 3) the size effect of materials should be carefully treated during data analysis, and the evaluation criteria should be re-validated at such scales.

The miniature mechanical testing approaches to evaluate the micro- and nano-mechanical properties, especially with environmental influences, such as electrochemical nanoindentation (ECNI) [2, 75-77, 85-94], electrochemical cantilever bending (ECCB) [6, 94-96] and micro-cantilever bending in ESEM [28-31, 97] have been developed by the research group of the candidate. Detailed description can be found in the above-mentioned references. To avoid the disadvantages of the miniature testing approach, a compromise has been considered by the candidate such that a material with coarse microstructure (grain size at mm level) and specially designed sample geometry at mm level to reveal the behavior at a specific microstructural feature. By advanced characterizations, the meso-scale testing result [98] is in good agreement with the macro-scale testing [99-101] and micro- to nano-scale testing [29, 31, 96].

2.3.2 Scanning electron microscopy

Electron channeling contrast imaging (ECCI)

The ECCI technique has been proven to be an excellent SEM technique that can reveal fine-scaled structure up to individual dislocation level in bulk specimens [102]. This technique is using the signal from backscattered electrons (BSEs) and was developed based on the fact that the defects in the crystal have a different diffraction condition in comparison with the matrix due to a shift in orientation, crystallography or chemical composition. When the matrix is exactly in the so-called channeling condition, the intensity of the BSE signal is the lowest, which corresponds to the electron channeling contrast (ECC), and in contrast, the defects will be in the backscattering condition and give rise to a high BSE intensity. As a result, the defects can be revealed on the BSE image. The theory of this imaging technique is now well developed such that several advantages can be

obtained: 1) the penetration depth and diffraction vector can be easily estimated according to the theory (e.g. Ref. [102]); 2) the field of view is relatively large such that good statistics can be obtained; 3) the investigation can be done on bulk specimens, and influence from sample surfaces is strictly limited, as different from the thin film specimens; 4) the sample preparation is rather simple within metallography lab, and expensive instruments such as ion-beam-based fabrication can be skipped. This technique has been widely used to investigate deformation structures resulted from dislocations, stacking faults, and/or twins in a variety of materials, e.g. austenitic steels [103-111], ferritic steels [112-116], aluminum and its alloys [117, 118], titanium alloys [119], and nickel alloys [120-122]. Figure 3-1 shows some examples of different crystal defects such as highly-densed dislocation walls (HDDWs), dislocation cells (DCs), individual dislocations (IDs), stacking faults (SFs) and twins in various materials. It is worth noting that the dislocations observed by ECCI are mostly statistically stored dislocations (SSDs). As another important type of dislocations, the geometrically necessary dislocations (GNDs) are difficult to be fully observed due to the varying contrast, although they are sometimes visible. Other accompanying techniques such as electron backscatter diffraction (EBSD) will be helpful in further determining GNDs. The ECCI technique has been intensively used in the present PhD project regarding investigation on the deformation of the materials.

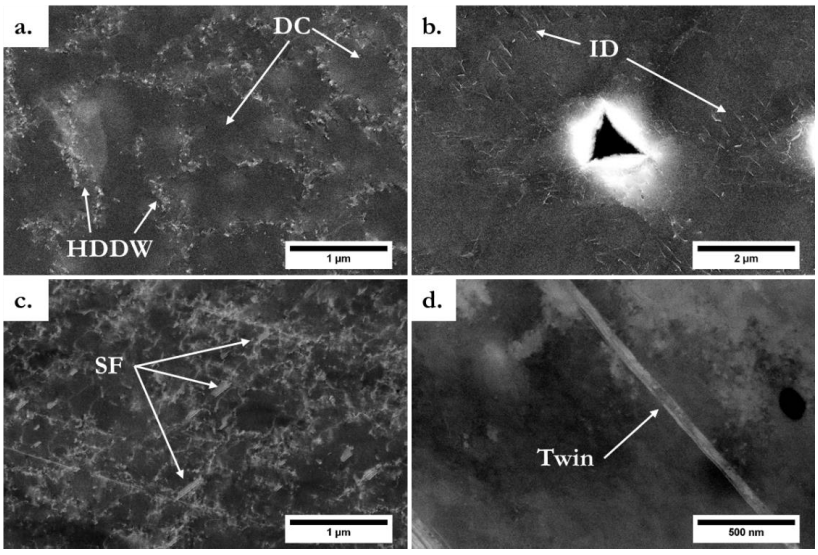

Figure 2-7 Examples of ECC images: a. highly-densed dislocation walls and dislocation cells in a cyclically deformed nickel single crystal (material curtesy of Guillaume Hachet), b. individual dislocations near a nanoindent in Fe-3wt%Si steel, c. stacking faults (SFs) accompanying dislocations in a deformed 304 stainless

steel (material curtesy of Yuhei Ogawa), and d. a nano-scaled twin in a deformed CrCoNiFeMn high-entropy alloy (material curtesy of Shuai Guan).

2.3.3 Transmission electron microscopy

Thanks to the modern development of techniques, the TEM has equipped various additional devices to fulfil different objectives of materials characterization. The TEM loading cell allows external mechanical loading to the TEM specimen, and the environmental chamber allows the tests to be done in different environmental conditions. This combination has promoted the field of environment-assisted cracking of materials a lot because of the high-resolution characterization proofs at small-scale levels. The most famous proof of the HELP mechanism came from an observation via in-situ TEM with an environmental chamber. Figure 2-8 shows the reduction of the separation distance between dislocations in a pileup of a deformed 310s stainless steel [50]. It can be seen that when the hydrogen gas pressure was increased, the distance between dislocations in the pileup was reduced. The overall shift in position of the dislocations is more evident in the overlapped subfigure f). This is a strongly supportive proof to the HELP mechanism that claims an enhanced dislocation mobility by hydrogen.

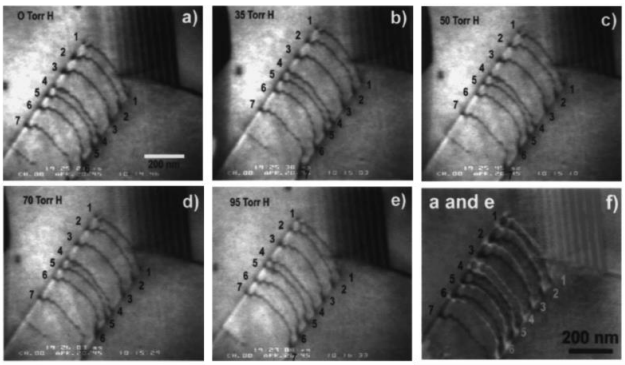

Figure 2-8 Reduction of the separation distance between dislocations in a pileup in 310s stainless steel due to solute hydrogen [123]. The hydrogen gas pressures are indicated. Image f is a composite image made from a positive of image a (black dislocations) and a negative of image e (white dislocations). Adopted from Ref. [50].

However, some opposite results could also be found in a recent publication by Xie et al. [124]. It can be seen from Figure 2-9 that after hydrogenation, some tiny changes in the configuration of dislocations are found (see caption for more details). Furthermore, tiny blisters (as indicated by the black arrows) can also be found on the surface of the tested aluminum micro-pillar. After careful analysis, the observed absence of dislocation motion

is concluded as the effect of hydrogen, which is referred to as "hydrogen locking of dislocations".

As a summary, TEM is an excellent technique that helps in the observation of very fine-scaled microstructural changes due to a different environment when equipped with auxiliary devices. High-resolution images could be captured at a "sub-dislocation" level to reveal the key changes in the materials. Unfortunately, due to time limitation, this technique was not fully conducted in the present PhD study. Preliminary samples have been prepared from the study in Ref. [98] and could be further studied in the future.

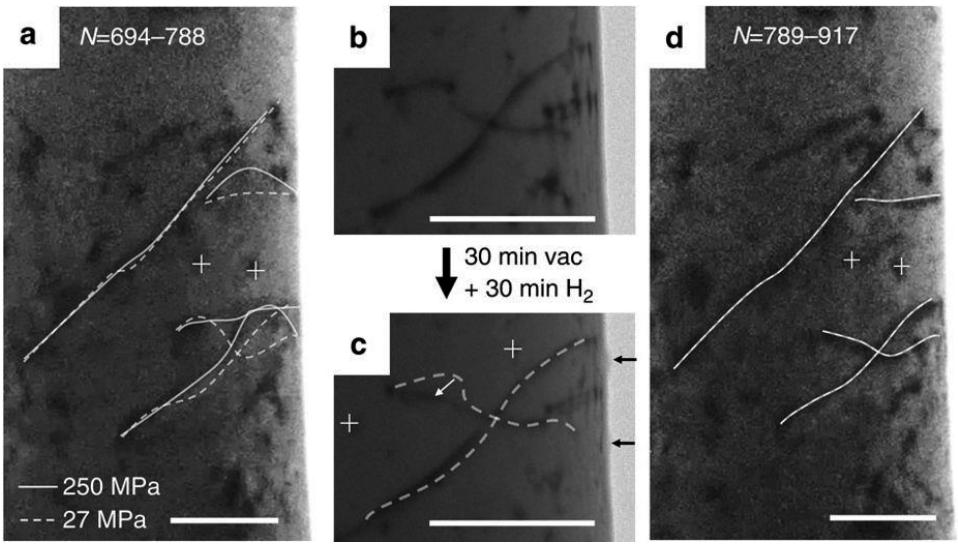

Figure 2-9 Effect of hydrogenation on dislocation movements. (a) Dislocation response to cyclic loads before hydrogenation. All the four observed dislocations ceased their motion immediately after hydrogenation under the same loading stress. (b) and (c) Respective positions of the four mobile dislocations before and after the hydrogenation, during which a curved segment of dislocation was relaxed due to the loss of pinning point. Besides, tiny blisters appeared on the surface (marked with black arrows). Dislocation positions in (b) is superimposed onto (c) with white dashed line for reference. (d) Dislocation response to the same cyclic load after hydrogenation. All dislocations ceased their motion. All scale bars are 200 nm. Adopted from Ref. [124].

3. Materials and Methods

3.1 Materials

The main model material used in the PhD study is one type of Fe-3wt%Si alloy. The chemical composition of this material is shown in Table 3-1. This material has a simple ferritic structure with the grain size of about 300 μm. The initial microstructure of the as-received material was investigated by optical microscope and shown in Figure 3-1.

Table 3-1 Chemical composition of the model Fe-3wt%Si alloy.

Elem.	C	Si	Mn	P	S	Cr	Ni	Mo
wt%	0.018	3.000	0.055	0.008	0.003	0.010	0.006	0.003
Elem.	Cu	Al	Ti	Nb	V	B	Zr	Fe
wt%	0.013	0.015	0.001	0.002	0.001	0.0002	0.0010	Bal.

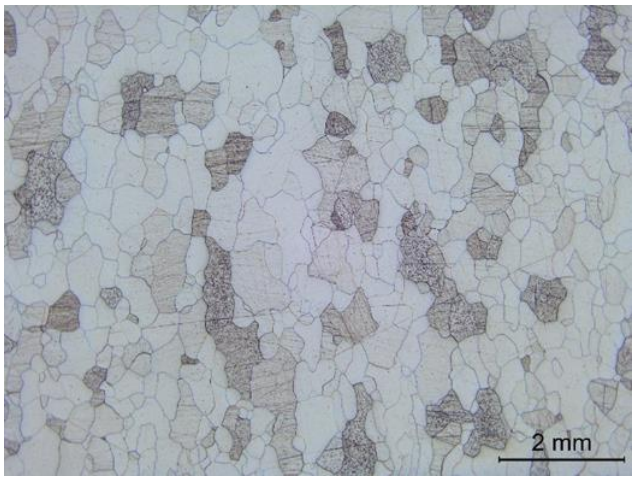

Figure 3-1 Microstructure of the model Fe-3wt%Si steel: pure ferrite with average grain size of about 300 μm.

For macro-scaled testing, a type of X70 pipeline steel was tested as a case study. The material has the chemical composition as shown in Table 3-2 and the as-received microstructure is a ferritic-pearlitic structure as shown in Figure 3-2.

Table 3-2 Chemical composition of the tested X70 pipeline steel.

Elem.	C	Si	Mn	P	S	Cu	Ni	Fe
wt%	0.090	0.3	0.710	0.010	0.001	0.300	0.250	Bal.

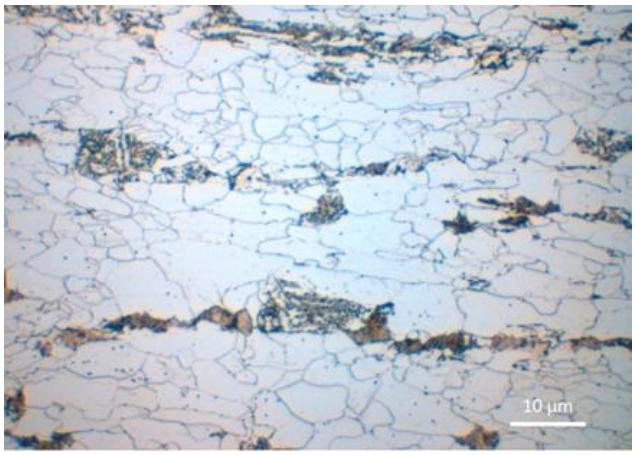

Figure 3-2 Microstructure of the tested X70 pipeline steel: ferritic-pearlitic structure.

3.2 Hydrogen charging methods

The hydrogen charging methods concerned in the PhD study are in-situ cathodic charging and H-plasma charging. As is stated in the literature review part, the diffusion rate of hydrogen in FCC and BCC materials is significantly different. FCC structure has a higher solubility of hydrogen, but hydrogen diffuses slowly in the lattice. While BCC structure has a much lower solubility of hydrogen, but vice versa hydrogen has a much higher diffusivity [125]. Therefore, it is critical to use ex-situ hydrogen charging in the study of BCC materials since most hydrogen atoms can escape out of the specimen.

3.2.1 Cathodic hydrogen charging

Cathodic hydrogen charging was used for the fatigue crack growth rate testing on CT specimens. Neutral 0.1 M Na_2SO_4 solution was adopted as the electrolyte in order to avoid corrosion effects. A constant potential of -1400 mV_{SCE} was used during the tests. Multimeters were used during the whole test in order to check the values and keep the circuit run as designed.

3.2.2 H-plasma charging

The innovative H-plasma charging method was adopted for the in-situ tests in the ESEM. A commercial Evactron® Zephyr (XEI Scientific Inc., USA) plasma source was used to excite plasma from H_2 as working gas. The gaseous H_2 was produced by a hydrogen generator using electrolysis principle from distilled water. A hydrogen sensor was used to

detect and confirm the production of H_2 gas as well as give warning when it is above the safe level.

The plasma source in the PhD study is producing remote plasma, which means the excitation and storage of plasma is mainly in the vicinity of the plasma generator. In this case, only active plasma could take part in the reaction with the testing material and there is no direct exposure of the specimen surface to the plasma phase, which could reduce the direct damage of the plasma-material reaction. The effect of H-plasma in the hydrogen embrittlement study is validated by using the ferritic Fe-3wt%Si model alloy [41].

3.3 Mechanical testing

3.3.1 FCGR testing

The FCGR tests were carried out both in air and in-situ electrochemical charging conditions at room temperature. CT specimens were cut from the as-received Fe-3wt%Si steel according to the ASTM E647-13 standard. The geometry of the tested specimens have been described and schematically presented in the corresponding publications [99-101, 126]. The test frequencies were chosen to be 0.1 Hz, 1 Hz and 10 Hz at the load ratio of R=0.5, in order to eliminate the influence of crack closure. The crack length a is measured from the center of the holes (where the load was applied) to the crack tip by optical microscopy. Before tests, a pre-crack was produced by fatigue according to the procedure described in Ref.[127]. First, a lower bound threshold stress intensity factor, i.e. ΔK_{th}, ranging from 10-12 MPa√m was used to initiate the crack from the notch. Then a reduction in the ΔK value of 5% was adopted stepwise until the target K-value was reached, and the crack growth stabilized. Typically, these pre-cracks were in the range of 2~4 mm after approximately 500 000 cycles for this material. It should be noted that when the pre-crack procedure stopped, the crack front was not necessarily a straight line over the thickness, since the middle part sensed the highest level of hydrostatic stress while the edge parts were less stressed. To get the crack further growing, a 5% increase in the ΔK from the last step of pre-cracking procedure was used in order to minimize the effect of the plastic zone from the pre-cracking procedure present ahead of the crack. An alternate current-potential drop (AC-PD) crack growth rate measure box was used during the test to record the FCGR behavior. At the end of the test the specimens were cracked in liquid nitrogen and the the da/dN vs ΔK curves were obtained from start/stop surface measurements. The testing setup is shown in Figure 3-3.

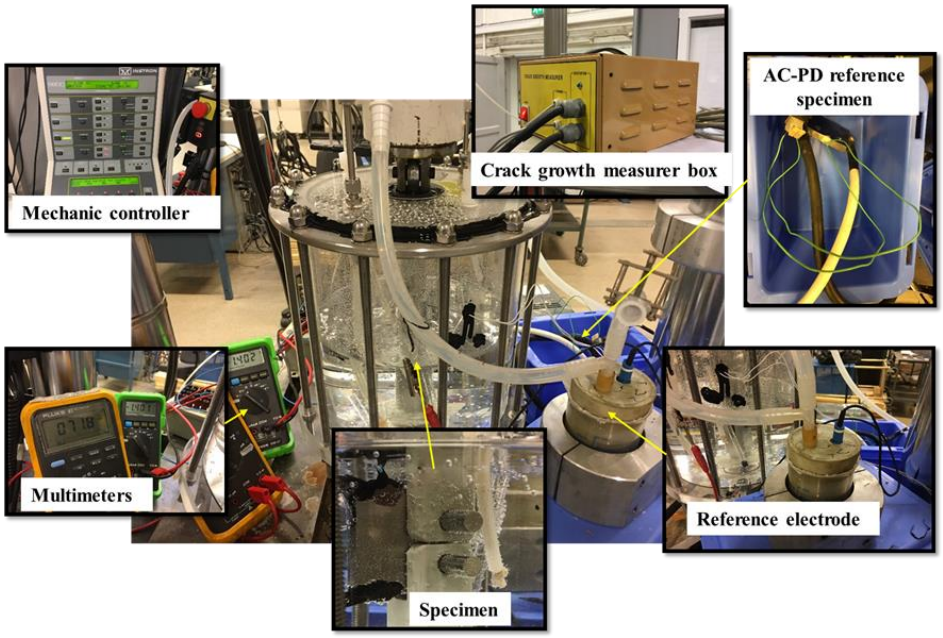

Figure 3-3 Experimental setup for FCGR testing. The major parts are highlighted and indicated. The mechanic controller and crack growth measurer box were connected outside of the main picture frame.

3.3.2 Tensile testing

Small-scale tensile testing was used in the PhD project to reveal the mechanical behavior in different environmental conditions. The specimens are dog-bone shaped with the dimension of the gauge area approx. 20 mm x 6 mm x 1.5 mm. The load was exerted by the tensile/ compression module from Kammrath & Weiss GmbH (Germany) with a maximum loading capacity of 5000 N. In the present PhD project, two different loading paths were applied, i.e. monotonic slow strain rate testing and cyclic loading testing. The monotonic loading was used for proving the embrittlement effect of the H-plasma phase and the cyclic loading was used for the small-scale FCG tests on SENT specimens.

3.4 Electron backscatter diffraction (EBSD)

The EBSD technique was used in microstructure analysis, texture analysis, orientation analysis as well as deformation analysis of the PhD project. The Nordif camera was used to acquire the diffraction patterns, and the OIM software was used for indexing and data analysis. The investigated surface of the specimen was place with a 70° tilting angle at a

working distance of about 10~15 mm. The SEM (Quanta 650 FEG, ThermoFisher Scientific Inc, USA) was operated at 20 kV accelerating voltage and with an aperture of 100 μm. The spot size was adjusted to an optimum value for different specimens (normally in the range 3.5~5.5).

3.5 Electron channeling contrast imaging (ECCI)

The ECCI technique was used for deformation structure analysis at the level of grain to dislocation. The SEM (Quanta 650 FEG, Thermo Fisher Inc., USA) was equipped with a four-quadrant solid state backscatter electron (BSE) detector, which collects the BSE signals from the specimen surface. The diffraction condition was carefully controlled by tilting and rotating the sample stage until the optimum channeling contrast was obtained. The accelerating voltage was normally set as 20 ~ 30 kV and the working distance was normally in the range of 6 ~ 10 mm, depending on the materials' conditions.

3.6 Focused ion beam (FIB) and transmission electron microscopy (TEM)

To achieve higher resolution characterization in specific regions, the FIB lift-out technique combined with TEM has been developed in the recent years. It has the advantage of combining accurate selecting of the investigation area by FIB and high resolution investigation by TEM. This could benefit the investigation on some localized features. In the present PhD project, the TEM foils were cut by FIB (NTNU Nanolab) from the fracture surface with specialized features (H-induced "quasi-cleavage" features) and the investigation was scheduled to be done by TEM. However, due to time limitations, this has not been completely finished by the date of thesis submission. This could be a potential outlook of this PhD project and those who are interested in this field can continue this topic in the future.

4. Main Results

4.1 Fatigue crack growth rate behavior with hydrogen influence

In this section, only the macro-scaled FCGR testing results are shown. This part of tests were done in collaboration with the partner in WP1 (SINTEF Industry). The major results are in the form of FCGR vs. stress intensity factor range (da/dN – ΔK) curves and the corresponding characterizations.

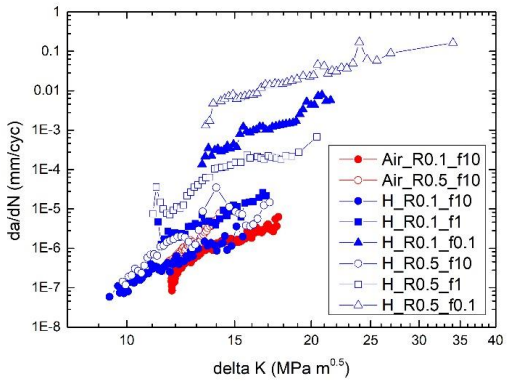

Figure 4-1 da/dN vs. ΔK of the model Fe-3wt%Si steel.

Figure 4-1 shows the FCGR behavior of the model Fe-3wt%Si steel under different conditions. It is clearly shown that when H was in-situ cathodically charged, the FCGR could increase up to 1000 times in comparison with the reference test in air. In the tested frequency range (0.1 Hz, 1 Hz and 10 Hz), a higher frequency made the FCGR became slower. This was explained by the H diffusion process. When higher frequencies were adopted, the H had less time to diffuse into the material and thus a less pronounced hydrogen embrittlement effect should be expected. The R=0.1 and R=0.5 cases show the same trend and similar accelerating factors.

Similarly, a type of X70 pipeline steel with ferritic-pearlitic structure was tested by the same setup and the FCGR data is shown in Figure 4-2. The main difference is a clear change in the acceleration of FCGR. When f=10 Hz, only a small increase in the FCGR can be seen throughout the whole tested ΔK range, while when f=0.1 Hz, a strongly accelerated FCGR of about 1000x can be seen throughout the whole range. However, a clear transformation in the f=1 Hz data can be seen that happens at a ΔK value of about 15 MPa$\sqrt{m}$. The

acceleration in FCGR becomes more and more significant as the ΔK value is getting higher, up to the acceleration level in the f=0.1 Hz case.

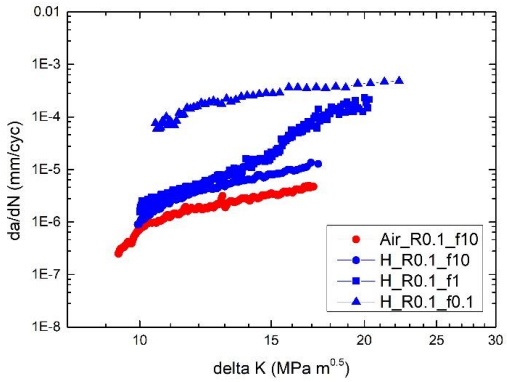

Figure 4-2 da/dN vs. ΔK of a type of X70 pipeline steel.

By fractographic analysis, the difference in the FCGR can be quantitatively correlated with a change in the fracture morphology. Figure 4-3 shows the case of the tested X70 pipeline steel. When tested in air and in hydrogen at f=10 Hz (less significant acceleration), only transgranular (TG) ductile striations can be seen on the fracture surface (Figure 4-3a and b). In the f=0.1 Hz case, a "saturated" acceleration in FCGR can be assumed, and the fractographic morphology shows complete "quasi-cleavage (QC)" feature (Figure 4-3d). In the transition case of f=1 Hz, a mixed feature of both TG and QC can be seen (Figure 4-3c). In the tested X70 pipeline steel specimens, no intergranular (IG) fracture feature can be seen. While in the model Fe-3wt%Si steel, a small fraction of IG feature can be detected. This part of result was published in [99-101].

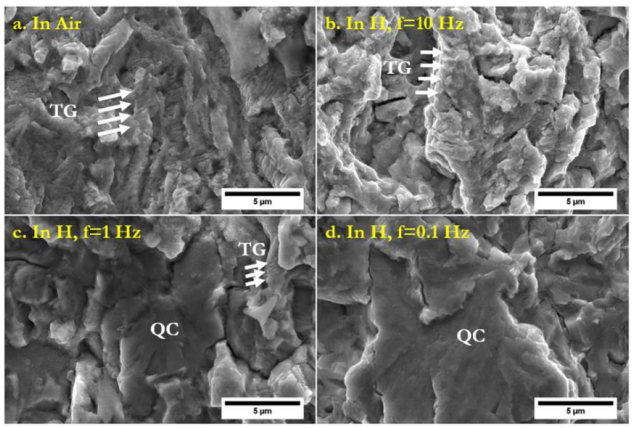

Figure 4-3 Representative images of the different fractographic morphologies of the tested X70 pipeline steel at ΔK=15 MPa $\sqrt{m}$, global crack growth direction is from top to bottom: a) in air; b) In hydrogen, 10 Hz; b) In hydrogen, 1 Hz; b) In hydrogen, 0.1 Hz.

4.2 In-situ tensile and fatigue crack growth testing

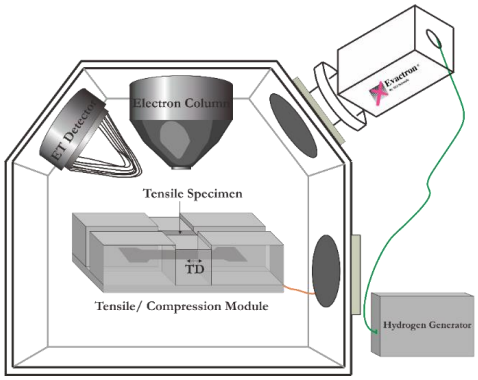

Figure 4-4 Schematic of the designed setup for in-situ mechanical testing with hydrogen plasma. (TD: tensile direction)

To achieve in-situ H-charging in the ESEM, we developed the innovative hydrogen plasma charging method on the ferritic specimens. Under this charging condition, monotonic tensile testing and fatigue crack growth testing with cyclic loading were realized. The setup is schematically shown in Figure 4-4. A commercial plasma source was attached to the flange of the ESEM, and a hydrogen generator (electrolysis of pure water) was used as the gas source (gaseous hydrogen with 99.99% purity level) for plasma excitation. The tensile/ compression module was installed directly to the stage of the ESEM and the communication cables were connected via another flange of the ESEM.

By this setup, in-situ loading combining in-situ hydrogen charging is possible and semi-in-situ imaging can be done by interrupting the test and changing the environment back to vacuum condition. Figure 4-5 shows a brief view on the crack tip resulting from different loading conditions. At the two tested frequencies (ultra-low frequency, ULF, 0.015 Hz; low frequency, LF, 0.15 Hz), the hydrogen-charged cases show a significant acceleration in the FCGR by 100 cycles at a similar ΔK level (9.8 µm vs 3.3 µm and 9.7 µm vs 4.9 µm, respectively). The semi-in-situ BSE imaging shows a clearly reduced plastic zone in the hydrogen cases compared to the vacuum cases. Details in Ref. [98].

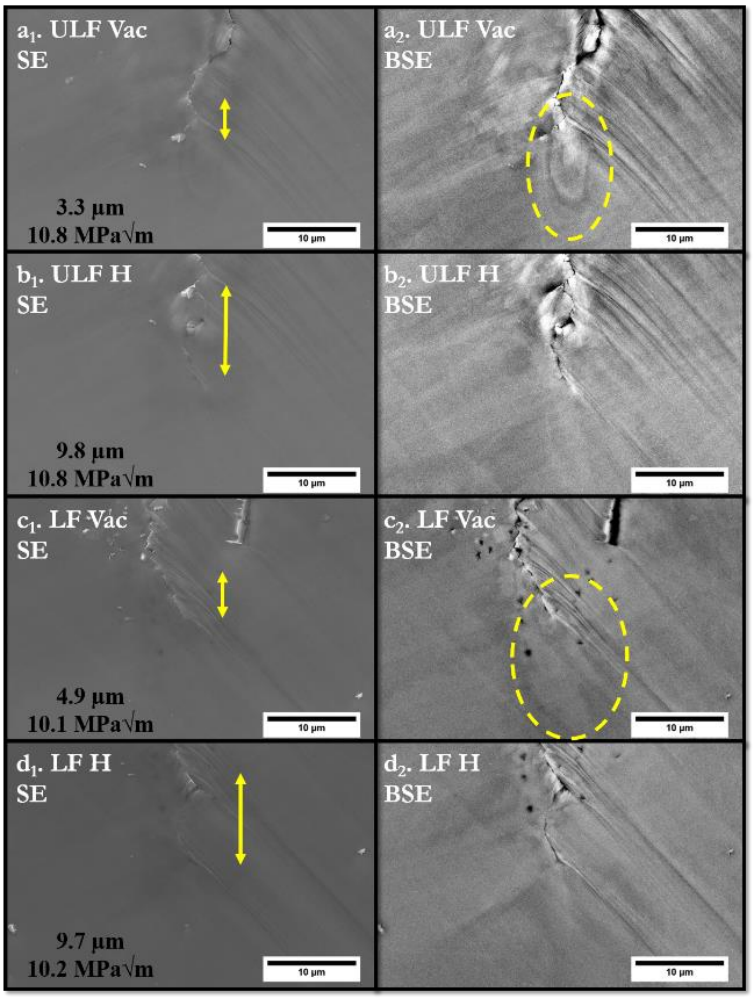

Figure 4-5 Crack-tip characterization in different conditions as marked in each subfigure. The double-arrow lines indicate the crack advance during the loading segment of 100 cycles. The corresponding crack growth and ΔK level are marked in each subfigure. The left column (a_1 to d_1) shows the SE images and the right

column (a_2 to d_2) shows the BSE images. The global FCG direction is from top to bottom for all subfigures. (ULF: ultra-low frequency at 0.015 Hz; LF: low frequency at 0.15 Hz)

4.3 Other results

During the PhD study, some results from collaboration with other affiliations and "side results" that were out of the task plan of the PhD project were also studied and published or in preparation for publication by the candidate. This part of results is summarized in the chapter "Contributions to Other Works".

5. Conclusions and Suggestions for Future Work

To sum up, the present PhD project realized the characterization work on the fracture behaviors of various materials regarding both monotonic loading and cyclic loading, especially with focus on the environmental effect. Some major conclusions can be drawn as follows:

- Hydrogen significantly reduced the ductility of steels both under monotonic loading and cyclic loading, and the major change in the fracture surface is the fraction of "quasi-cleavage" features: a higher amount of hydrogen will lead to a larger fraction of the "quasi-cleavage" features.
- The plastic deformation zone associated with the hydrogen-assisted fracture was characterized by advanced scanning electron microscopy, and it showed that when hydrogen was present, the plasticity accompanied by the fracture was strongly restricted.
- The embrittlement effect of the hydrogen-plasma was revealed by in-situ tensile and cyclic loading tests. The characterizations confirmed the effect was in the similar manner as other hydrogen-charging methods such as electrochemical charging or gaseous H_2 charging.
- The cryogenic fracture procedure of the Fe-3wt%Si steel was accompanied by plastic deformation in the form of dislocation emission and twinning. The EBSD characterizations confirmed the {111}-60° twinning relation and the ECCI characterizations showed the microstructure.

However, due to time and technical limitations, some work could not be realized in the presented PhD study. Some of the outlooks and suggestions are listed by the candidate as follows:

- It is necessary to know the exact hydrogen concentration in the system for hydrogen embrittlement studies. However, due to technical limitations, this could not be measured in the case of plasma charging for the time being. The candidate suggests researchers working in the field of plasma physics could give some contribution to this issue either by experimental or numerical methods.
- The in-situ imaging procedure is not possible in the plasma environment since this phase causes charging and arcing problems with the electron signal detectors and may damage the electron microscope. People working in the field of producing

electron microscopy devices are encouraged to produce "plasma-resistant" detectors for this field of study.

- Although the ECCI technique is able to capture some fine structures with a relatively high resolution, it is not enough to resolve very fine deformation structure (single dislocation lines, for instance) with the present setup, especially under in-situ conditions. The following researchers are suggested to improve the experimental setup to fit more requirements of the study.
- The combination of EBSD and ECCI in studying the low-temperature fracture behaviors of Fe-3wt%Si steel seems to be promising. More quantitative works could be done to shed some light on the study of the low-temperature effects on diverse materials, and this could be useful in understanding the materials behaviors as well as guiding the engineering work in the arctic regions.

6. Summary of Papers

This chapter is a short summary of the papers that have been published by the candidate within the PhD period. Full-texts of these papers are attached as the second part of the PhD thesis.

Paper 1: Hydrogen embrittlement effect observed by in-situ hydrogen plasma charging on a ferritic alloy

D. Wan, Y. Deng, A. Barnoush, Scripta Mater. 151 (2018) 24-27.

Abstract: To study the hydrogen embrittlement (HE) effect, a novel in-situ slow strain rate tensile test together with in-situ hydrogen (H) charging by H-plasma was conducted in an environmental scanning electron microscope (ESEM). The introduction of H-plasma gave a reduction in tensile elongation by about 5% in comparison with a reference test in vacuum. Fractographic observation clearly showed the difference in the resulted features on the fracture surfaces. Electron backscatter diffraction (EBSD) was conducted to elucidate the characteristics of the cracks. Such investigations can help to refresh the existing knowledge in HE study.

Keywords: hydrogen embrittlement; in-situ test; Fe-3wt.%Si; plasma; crack.

Graphical Abstract:

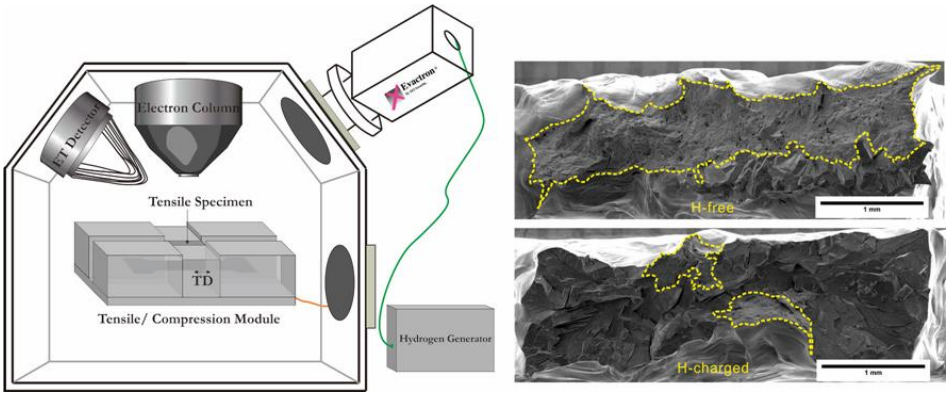

Paper 2: Hydrogen-enhanced fatigue crack growth behaviors in a ferritic Fe-3wt%Si steel studied by fractography and dislocation structure analysis

D. Wan, A. Alvaro, V. Olden, A. Barnoush, Int. J. Hydrog. Energy 44 (2019) 5030-42.

Abstract: The effect of hydrogen (H) on the fatigue behavior is of significant importance for metallic structures. In this study, the hydrogen-enhanced fatigue crack growth rate (FCGR) tests on in-situ electrochemically H-charged ferritic Fe-3wt%Si steel with coarse grain size were conducted. Results showed strong difference between the H-charged and the non-charged conditions (reference test in laboratory air) and were in good agreement with the results from literature. With H-charging, the fracture morphology changed from transgranular (TG) type to "quasi-cleavage" ("QC"), with a different fraction depending on the loading frequency. With the help of electron channeling contrast imaging (ECCI) inside a scanning electron microscope (SEM), a relatively large area in the failed bulk specimen could be easily observed with high-resolution down to dislocation level. In this work, the dislocation sub-structure immediately under the fracture surfaces were investigated by ECCI to depict the difference in the plasticity evolution during fatigue crack growth (FCG). Based on the analysis, the H-enhanced FCG mechanisms were discussed.

Keywords: hydrogen embrittlement; fractography; Fe-3wt%Si; fatigue crack growth (FCG); SEM; ECCI.

Highlights:

- In-situ electrochemical hydrogen charging enhances the FCGR by up to 1000x
- Transgranular, intergranular and "quasi-cleavage" features are identified
- The enhanced FCGR is related to the area fraction of "quasi-cleavage" features
- The dislocation cell formation is restricted in the hydrogen-charged cases

Paper 3: Hydrogen-enhanced fatigue crack growth in a pre-cracked single-edge notched tensile specimen under in-situ hydrogen-plasma charging inside an environmental scanning electron microscope

D. Wan, Y. Deng, J. I. Meling, A. Alvaro, A. Barnoush, Acta Mater. 170 (2019) 87-99.

Abstract: Fatigue crack growth (FCG) test was done on a pre-cracked single-edge notched tensile (SENT) specimen with oligocrystalline ferritic structure. Innovative in-situ hydrogen (H)- charging by plasma inside an environmental scanning electron microscope (ESEM) was adopted to directly observe the H influence on the FCG behavior of this material. Diverse in-situ and post-mortem characterization methods including secondary electron imaging, backscatter electron imaging, electron backscatter diffraction (EBSD) and scanning probe microscopy (SPM) were used to investigate the material's behavior. It was observed that the crack growth rate was enhanced by about one magnitude when H was charged, in comparison with the reference test in vacuum (Vac). The FCG procedure was concluded as strongly associated with the plasticity evolution in the vicinity of the crack-tip. A simple model based on the restricted plasticity was proposed for the H-enhanced FCG behavior. A peculiar frequency dependency of the H-enhanced FCG behavior was observed at low loading frequencies (0.015 Hz ~ 0.15 Hz): under the same in-situ H-charging condition, a lower frequency gave a slower crack growth rate and vice versa. This behavior was explained by the thermally activated dislocation motion correlated with the plasticity shielding effect during crack growth.

Keywords: fatigue crack growth (FCG); hydrogen embrittlement; SENT specimen; EBSD; SEM.

Graphical Abstract:

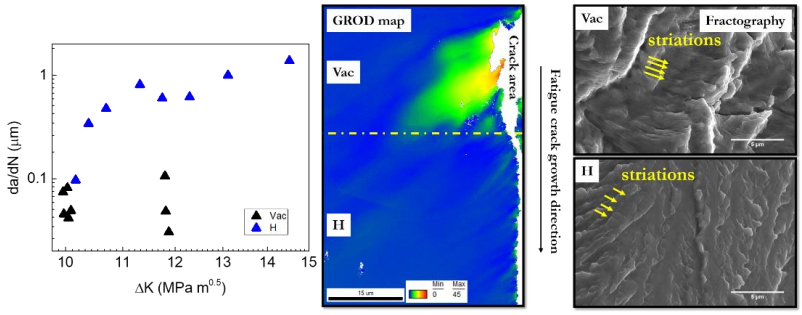

Paper 4: Plasticity in cryogenic brittle fracture of ferritic steels: dislocation versus twinning

D. Wan, A. Barnoush, Mater. Sci. Eng., A 744 (2019) 335-339.

Abstract: The sub-surface deformation structure after cryogenic (77 K) brittle fracture in a ferritic steel was characterized by scanning electron microscopy (SEM). Twin-like structures were found in many grains below the fracture surface. Electron backscatter diffraction (EBSD) was used to identify the crystallography of the structures, and the twin relation in body-centered cubic (BCC) systems was indexed. The twins in the sub-surface area were characterized further by electron channeling contrast imaging (ECCI). This study clarifies the low temperature brittle fracture behavior in the ferritic Fe-3wt%Si steel consists of both cleavage and plastic deformation in the form of dislocation activities and twinning.

Keywords: cleavage fracture, twinning, scanning electron microscopy, EBSD, ECCI, BCC.

Graphical Abstract:

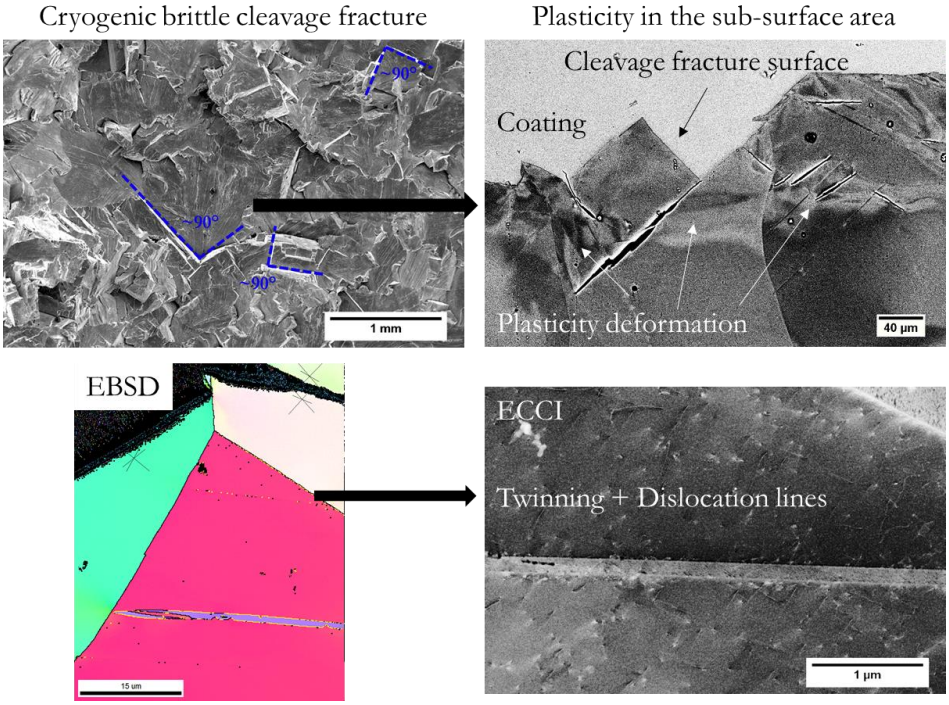

Paper 5: Hydrogen-assisted fatigue crack growth in ferritic steels – a fractographic study

D. Wan, A. Alvaro, V. Olden, A. Barnoush, MATEC Web of Conferences, 2018, p. 03004. (conference paper)

Abstract: Fatigue crack growth (FCG) behavior of a Fe-3wt.%Si ferritic alloy under different environmental conditions using in-situ electrochemical (cathodic) hydrogen (H) charging has been investigated. Three frequencies have been applied. Results clearly show that the FCG rate increased by a factor spanning from 20 to 1000 times, depending on the loading frequencies, when compared to the reference test in air. Lower frequency leads to higher FCG rate. A comprehensive fractographic analysis was carried out: the area fraction of different fracture surface features was measured and taken into statistical analysis. Based on these investigations, the possible mechanisms of H-enhanced FCG are discussed. Similar tests in high-pressure H gas from other studies were also compared and discussed. These results give a preliminary understanding of H effect in fatigue crack propagation procedure in ferritic alloys.

Reference

[1] W.H. Johnson, On Some Remarkable Changes Produced in Iron and Steel by the Action of Hydrogen and Acids, Proc. R. Soc. London 23(156-163) (1875) 168-179, DOI: 10.1098/rspl.1874.0024.

[2] A. Barnoush, Hydrogen embrittlement, revisited by in situ electrochemical nanoindentation, Materialwiss. Werkstofftech., Universität des Saarlandes, Aachen, 2009, p. 256.

[3] H. Kimura, H. Matsui, Mechanism of hydrogen-induced softening and hardening in iron, Scripta Metall. 21(3) (1987) 319-324, DOI: 10.1016/0036-9748(87)90221-3.

[4] A. Kimura, H. Matsui, H. Kimura, The work-hardening behaviour of hydrogen-charged high purity iron single crystals at temperatures between 296 and 200 K, Mater. Sci. Eng. 58(2) (1983) 211-222, DOI: 10.1016/0025-5416(83)90047-2.

[5] G. Gottstein, Physical Foundations of Materials Science, Springer-Verlag Berlin Heidelberg, New York, 2004.

[6] T. Depover, T. Hajilou, D. Wan, D. Wang, A. Barnoush, K. Verbeken, Assessment of the potential of hydrogen plasma charging as compared to conventional electrochemical hydrogen charging on dual phase steel, Mater. Sci. Eng., A 754 (2019) 613-621, DOI: 10.1016/j.msea.2019.03.097.

[7] T. Depover, A. Laureys, D. Perez Escobar, E. Van den Eeckhout, E. Wallaert, K. Verbeken, Understanding the Interaction between a Steel Microstructure and Hydrogen, Materials (Basel) 11(5) (2018), DOI: 10.3390/ma11050698.

[8] T. Depover, O. Monbaliu, E. Wallaert, K. Verbeken, Effect of Ti, Mo and Cr based precipitates on the hydrogen trapping and embrittlement of Fe–C–X Q&T alloys, Int. J. Hydrog. Energy 40(47) (2015) 16977-16984, DOI: 10.1016/j.ijhydene.2015.06.157.

[9] T. Depover, D. Pérez Escobar, E. Wallaert, Z. Zermout, K. Verbeken, Effect of hydrogen charging on the mechanical properties of advanced high strength steels, Int. J. Hydrog. Energy 39(9) (2014) 4647-4656, DOI: 10.1016/j.ijhydene.2013.12.190.

[10] T. Depover, E. Van den Eeckhout, K. Verbeken, Hydrogen induced mechanical degradation in tungsten alloyed steels, Mater. Charact. 136 (2018) 84-93, DOI: 10.1016/j.matchar.2017.12.017.

[11] T. Depover, K. Verbeken, Evaluation of the role of Mo2C in hydrogen induced ductility loss in Q&T FeCMo alloys, Int. J. Hydrog. Energy 41(32) (2016) 14310-14329, DOI: 10.1016/j.ijhydene.2016.05.176.

[12] T. Depover, K. Verbeken, Hydrogen trapping and hydrogen induced mechanical degradation in lab cast Fe-C-Cr alloys, Mater. Sci. Eng., A 669 (2016) 134-149, DOI: 10.1016/j.msea.2016.05.018.

[13] T. Depover, K. Verbeken, Evaluation of the effect of V 4 C 3 precipitates on the hydrogen induced mechanical degradation in Fe-C-V alloys, Mater. Sci. Eng., A 675 (2016) 299-313, DOI: 10.1016/j.msea.2016.08.053.

[14] T. Depover, K. Verbeken, The effect of TiC on the hydrogen induced ductility loss and trapping behavior of Fe-C-Ti alloys, Corros. Sci. 112 (2016) 308-326, DOI: 10.1016/j.corsci.2016.07.013.

[15] T. Depover, K. Verbeken, The detrimental effect of hydrogen at dislocations on the hydrogen embrittlement susceptibility of Fe-C-X alloys: An experimental proof of the HELP mechanism, Int. J. Hydrog. Energy 43(5) (2018) 3050-3061, DOI: 10.1016/j.ijhydene.2017.12.109.

[16] T. Depover, K. Verbeken, Thermal desorption spectroscopy study of the hydrogen trapping ability of W based precipitates in a Q&T matrix, Int. J. Hydrog. Energy 43(11) (2018) 5760-5769, DOI: 10.1016/j.ijhydene.2018.01.184.

[17] T. Depover, E. Wallaert, K. Verbeken, Fractographic analysis of the role of hydrogen diffusion on the hydrogen embrittlement susceptibility of DP steel, Mater. Sci. Eng., A 649 (2016) 201-208, DOI: 10.1016/j.msea.2015.09.124.

[18] T. Depover, E. Wallaert, K. Verbeken, On the synergy of diffusible hydrogen content and hydrogen diffusivity in the mechanical degradation of laboratory cast Fe-C alloys, Mater. Sci. Eng., A 664 (2016) 195-205, DOI: 10.1016/j.msea.2016.03.107.

[19] T. Depover, D. Wan, D. Wang, A. Barnoush, K. Verbeken, Hydrogen embrittlement evaluation by hydrogen plasma charging of TRIP-assisted steel, Acta Mater. (2019).

[20] Hydrogen Fuel: Production, Transport, and Storage, CRC Press, Boca Raton, 2008.

[21] J.M. Bockris, Modern Aspects of Electrode Kinetics, Annu. Rev. Phys. Chem. 5(1) (1954) 477-500, DOI: 10.1146/annurev.pc.05.100154.002401.

[22] J.O.M. Bockris, Recent Developments in the Study of Hydrogen Overpotential, Chem. Rev. 43(3) (1948) 525-577, DOI: 10.1021/cr60136a005.

[23] J.O.M. Bockris, E.C. Potter, The Mechanism of Hydrogen Evolution at Nickel Cathodes in Aqueous Solutions, The Journal of Chemical Physics 20(4) (1952) 614-628, DOI: 10.1063/1.1700503.

[24] H. Flitt, J. Bockris, Hydrogen/metal interactions with special reference to electrochemical approaches, Int. J. Hydrog. Energy 6(2) (1981) 119-138, DOI: 10.1016/0360-3199(81)90001-x.

[25] J. Bockris, A. Reddy, Modern Electrochemistry: An Introduction to an Interdisciplinary Area, Springer US1970.

[26] C.T. Liu, E.H. Lee, C.G. Mckamey, An environmental effect as the major cause for room-temperature embrittlement in FeAl, Scripta Metall. 23(6) (1989) 875-880, DOI: Doi 10.1016/0036-9748(89)90263-9.

[27] C.T. Liu, C.L. Fu, E.P. George, G.S. Painter, Environmental Embrittlement in FeAl Aluminides, ISIJ Int. 31(10) (1991) 1192-1200, DOI: 10.2355/isijinternational.31.1192.

[28] Y. Deng, Environmentally assisted cracking revisited via novel miniature fracture mechanics approach in environmental scanning electron microscope, Department of

Mechanical and Industrial Engineering, Norwegian University of Science and Technology, Trondheim, 2019.

[29] Y. Deng, A. Barnoush, Hydrogen embrittlement revealed via novel in situ fracture experiments using notched micro-cantilever specimens, Acta Mater. 142 (2018) 236-247, DOI: 10.1016/j.actamat.2017.09.057.

[30] Y. Deng, T. Hajilou, D. Wan, N. Kheradmand, A. Barnoush, In-situ micro-cantilever bending test in environmental scanning electron microscope: Real time observation of hydrogen enhanced cracking, Scripta Mater. 127 (2017) 19-23, DOI: 10.1016/j.scriptamat.2016.08.026.

[31] B.R.S. Rogne, N. Kheradmand, Y. Deng, A. Barnoush, In situ micromechanical testing in environmental scanning electron microscope: A new insight into hydrogen-assisted cracking, Acta Mater. 144 (2018) 257-268, DOI: 10.1016/j.actamat.2017.10.037.

[32] L.M. Pike, C.T. Liu, Environmental and Strain Rate Effects on the Ductility and Yield Strength of Fe-40Al, Scripta Mater. 38(10) (1998) 1475-1480, DOI: 10.1016/s1359-6462(98)00087-6.

[33] N. Narita, Embrittlement of Fe-Si alloy crystals by hydrogen glow discharge, Scripta Metall. 18(9) (1984) 985-988, DOI: 10.1016/0036-9748(84)90274-6.

[34] A. Kimura, H.K. Birnbaum, Plastic softening by hydrogen plasma charging in pure iron, Scripta Metall. 21(1) (1987) 53-57, DOI: 10.1016/0036-9748(87)90406-6.

[35] C.G. Morgan, R. Vane, Removal of Carbon Contamination using Hydrogen with Low-Power Downstream Plasma Cleaning. https://evactron.com/wp-content/uploads/2016/10/cleaningwithh2advlith2011.pdf, 2011).

[36] A. Vesel, A. Drenik, R. Zaplotnik, M. Mozetic, M. Balat-Pichelin, Reduction of thin oxide films on tungsten substrate with highly reactive cold hydrogen plasma, Surf. Interface Anal. 42(6-7) (2010) 1168-1171, DOI: 10.1002/sia.3185.

[37] M. Ishii, K. Nakashima, I. Tajima, M. Yamamoto, Properties of silicon surface cleaned by hydrogen plasma, Appl. Phys. Lett. 58(13) (1991) 1378-1380, DOI: 10.1063/1.105211.

[38] B. Anthony, In situ cleaning of silicon substrate surfaces by remote plasma-excited hydrogen, Journal of Vacuum Science & Technology B: Microelectronics and Nanometer Structures 7(4) (1989) 621, DOI: 10.1116/1.584805.

[39] S.J. Jeng, G.S. Oehrlein, G.J. Scilla, Hydrogen plasma induced defects in silicon, Appl. Phys. Lett. 53(18) (1988) 1735-1737, DOI: 10.1063/1.99810.

[40] R.P.H. Chang, C.C. Chang, S. Darack, Hydrogen plasma etching of semiconductors and their oxides, Journal of Vacuum Science and Technology 20(1) (1982) 45-50, DOI: 10.1116/1.571307.

[41] D. Wan, Y. Deng, A. Barnoush, Hydrogen embrittlement effect observed by in-situ hydrogen plasma charging on a ferritic alloy, Scripta Mater. 151 (2018) 24-27, DOI: 10.1016/j.scriptamat.2018.03.038.

[42] S. Lynch, Hydrogen embrittlement phenomena and mechanisms, Corros. Rev. 30(3-4) (2012) 105-123, DOI: 10.1515/corrrev-2012-0502.

[43] I.M. Robertson, P. Sofronis, A. Nagao, M.L. Martin, S. Wang, D.W. Gross, K.E. Nygren, Hydrogen Embrittlement Understood, Metall. Mater. Trans. B 46(3) (2015) 1085-1103, DOI: 10.1007/s11663-015-0325-y.

[44] W.W. Gerberich, P.G. Marsh, J.W. Hoehn, Hydrogen Induced Cracking Mechanisms - Are There Critical Experiments?, in: A.W. Thompson, N.R. Moody (Eds.), Hydrogen Effects in Materials, Minerals, Metals & Materials Society (TMS), Warrendale, Pennsylvania, USA, 1996, pp. 539-554.

[45] A. Nagao, M. Dadfarnia, B.P. Somerday, P. Sofronis, R.O. Ritchie, Hydrogen-enhanced-plasticity mediated decohesion for hydrogen-induced intergranular and "quasi-cleavage" fracture of lath martensitic steels, J. Mech. Phys. Solids 112 (2018) 403-430, DOI: 10.1016/j.jmps.2017.12.016.

[46] C.A. Zapffe, C.E. Sims, Hydrogen Embrittlement, Internal Stress and Defects in Steel, Am. Instit. Min. Metall. Eng. 145 (1941) 225-261.

[47] A.S. Tetelman, W.D. Robertson, Direct observation and analysis of crack propagation in iron-3% silicon single crystals, Acta Metall. 11(5) (1963) 415-426, DOI: 10.1016/0001-6160(63)90166-4.

[48] C.D. Beachem, A new model for hydrogen-assisted cracking (hydrogen "embrittlement"), Metall. Mater. Trans. B 3(2) (1972) 441-455, DOI: 10.1007/bf02642048.

[49] H.K. Birnbaum, P. Sofronis, Hydrogen-enhanced localized plasticity—a mechanism for hydrogen-related fracture, Mater. Sci. Eng., A 176(1-2) (1994) 191-202, DOI: 10.1016/0921-5093(94)90975-x.

[50] I.M. Robertson, The effect of hydrogen on dislocation dynamics, Eng. Fract. Mech. 64(5) (1999) 649-673, DOI: 10.1016/S0013-7944(99)00094-6.

[51] I.M. Robertson, H.K. Birnbaum, An Hvem Study of Hydrogen Effects on the Deformation and Fracture of Nickel, Acta Metall. 34(3) (1986) 353-366, DOI: 10.1016/0001-6160(86)90071-4.

[52] I.M. Robertson, H.K. Birnbaum, P. Sofronis, Hydrogen Effects on Plasticity, in: J.P. Hirth, L. Kubin (Eds.), Dislocations in Solids, Elsevier, Amsterdam, 2010, pp. 249-293.

[53] S. Wang, A. Nagao, P. Sofronis, I.M. Robertson, Hydrogen-modified dislocation structures in a cyclically deformed ferritic-pearlitic low carbon steel, Acta Mater. 144 (2018) 164-176, DOI: 10.1016/j.actamat.2017.10.034.

[54] R.P. Gangloff, Critical issues in hydrogen assisted cracking of structural alloys, in: S.A. Shipilov, R.H. Jones, J.-M. Olive, R.B. Rebak (Eds.), Environment-Induced Cracking of Materials, Elsevier, Amsterdam, 2008, pp. 141-165.

[55] I.H. Katzarov, A.T. Paxton, Hydrogen embrittlement II. Analysis of hydrogen-enhanced decohesion across (111) planes in α-Fe, Phys. Rev. Mater. 1(3) (2017), DOI: 10.1103/PhysRevMaterials.1.033603.

[56] R.A. Oriani, Whitney Award Lecture—1987:Hydrogen—The Versatile Embrittler, Corrosion 43(7) (1987) 390-397, DOI: 10.5006/1.3583875.

[57] R.A. Oriani, P.H. Josephic, Equilibrium and kinetic studies of the hydrogen-assisted cracking of steel, Acta Metall. 25(9) (1977) 979-988, DOI: 10.1016/0001-6160(77)90126-2.

[58] S.P. Lynch, Environmentally Assisted Cracking - Overview of Evidence for an Adsorption-Induced Localized-Slip Process, Acta Metall. 36(10) (1988) 2639-2661, DOI: 10.1016/0001-6160(88)90113-7.

[59] S.P. Lynch, Metallographic contributions to understanding mechanisms of environmentally assisted cracking, Metallography 23(2) (1989) 147-171, DOI: 10.1016/0026-0800(89)90016-5.

[60] S.P. Lynch, Comments on "A unified model of environment-assisted cracking", Scripta Mater. 61(3) (2009) 331-334, DOI: 10.1016/j.scriptamat.2009.02.031.

[61] O. Barrera, D. Bombac, Y. Chen, T.D. Daff, E. Galindo-Nava, P. Gong, D. Haley, R. Horton, I. Katzarov, J.R. Kermode, C. Liverani, M. Stopher, F. Sweeney, Understanding and mitigating hydrogen embrittlement of steels: a review of experimental, modelling and design progress from atomistic to continuum, J. Mater. Sci. 53(9) (2018) 6251-6290, DOI: 10.1007/s10853-017-1978-5.

[62] M. Nagumo, Hydrogen related failure of steels – a new aspect, Mater. Sci. Technol. 20(8) (2004) 940-950, DOI: 10.1179/026708304225019687.

[63] S.P. Lynch, Progress Towards Understanding Mechanisms Of Hydrogen Embrittlement And Stress Corrosion Cracking, CORROSION 2007, NACE International, Nashville, Tennessee, 2007.

[64] A.R. Troiano, The Role of Hydrogen and Other Interstitials in the Mechanical Behavior of Metals (1959 Edward De Mille Campbell Memorial Lecture), Metallography Microstructure and Analysis 5(6) (2016) 557-569, DOI: 10.1007/s13632-016-0319-4.

[65] R.A. Oriani, The diffusion and trapping of hydrogen in steel, Acta Metall. 18(1) (1970) 147-157, DOI: 10.1016/0001-6160(70)90078-7.

[66] R.A. Oriani, A mechanistic theory of hydrogen embrittlement of steels, Berichte der Bunsengesellschaft für physikalische Chemie 76(8) (1972) 848-857, DOI: 10.1002/bbpc.19720760864.

[67] W.W. Gerberich, R.A. Oriani, M.J. Lji, X. Chen, T. Foecke, The necessity of both plasticity and brittleness in the fracture thresholds of iron, Philos. Mag. A 63(2) (1991) 363-376, DOI: 10.1080/01418619108204854.

[68] D.E. Jiang, E.A. Carter, First principles assessment of ideal fracture energies of materials with mobile impurities: implications for hydrogen embrittlement of metals, Acta Mater. 52(16) (2004) 4801-4807, DOI: 10.1016/j.actamat.2004.06.037.

[69] M. Yamaguchi, M. Shiga, H. Kaburaki, Grain Boundary Decohesion by Sulfur Segregation in Ferromagnetic Iron and Nickel - A First-Principles Study-, Mater. Trans. 47(11) (2006) 2682-2689, DOI: 10.2320/matertrans.47.2682.

[70] V. Olden, C. Thaulow, R. Johnsen, E. Østby, T. Berstad, Application of hydrogen influenced cohesive laws in the prediction of hydrogen induced stress cracking in 25%Cr duplex stainless steel, Eng. Fract. Mech. 75(8) (2008) 2333-2351, DOI: 10.1016/j.engfracmech.2007.09.003.

[71] R. Kirchheim, Reducing grain boundary, dislocation line and vacancy formation energies by solute segregation. I. Theoretical background, Acta Mater. 55(15) (2007) 5129-5138, DOI: 10.1016/j.actamat.2007.05.047.

[72] R. Kirchheim, Reducing grain boundary, dislocation line and vacancy formation energies by solute segregationII. Experimental evidence and consequences, Acta Mater. 55(15) (2007) 5139-5148, DOI: 10.1016/j.actamat.2007.05.033.

[73] R. Kirchheim, On the solute-defect interaction in the framework of a defactant concept, Int. J. Mater. Res. 100(4) (2009) 483-487, DOI: 10.3139/146.110065.

[74] R. Kirchheim, Solid solution softening and hardening by mobile solute atoms with special focus on hydrogen, Scripta Mater. 67(9) (2012) 767-770, DOI: 10.1016/j.scriptamat.2012.07.022.

[75] A. Barnoush, N. Kheradmand, T. Hajilou, Correlation between the hydrogen chemical potential and pop-in load during in situ electrochemical nanoindentation, Scripta Mater. 108 (2015) 76-79, DOI: 10.1016/j.scriptamat.2015.06.021.

[76] A. Barnoush, H. Vehoff, In situ electrochemical nanoindentation: A technique for local examination of hydrogen embrittlement, Corros. Sci. 50(1) (2008) 259-267, DOI: 10.1016/j.corsci.2007.05.026.

[77] A. Barnoush, H. Vehoff, Recent developments in the study of hydrogen embrittlement: Hydrogen effect on dislocation nucleation, Acta Mater. 58(16) (2010) 5274-5285, DOI: 10.1016/j.actamat.2010.05.057.

[78] A. Barnoush, M. Zamanzade, H. Vehoff, Direct observation of hydrogen-enhanced plasticity in super duplex stainless steel by means of in situ electrochemical methods, Scripta Mater. 62(5) (2010) 242-245, DOI: 10.1016/j.scriptamat.2009.11.007.

[79] D. Wang, X. Lu, Y. Deng, X. Guo, A. Barnoush, Effect of hydrogen on nanomechanical properties in Fe-22Mn-0.6C TWIP steel revealed by in-situ electrochemical nanoindentation, Acta Mater. 166 (2019) 618-629, DOI: 10.1016/j.actamat.2018.12.055.

[80] P. Peralta, C. Laird, Fatigue of Metals, in: D.E. Laughlin, K. Hono (Eds.), Physical Metallurgy (Fifth Edition), Elsevier, Amsterdam, 2014, pp. 1765-1880.

[81] P. Paris, F. Erdogan, A critical analysis of crack propagation laws, Journal of Basic Engineering 85(4) (1963) 528-533, DOI: 10.1115/1.3656900.

[82] R.O. Ritchie, J.F. Knott, Mechanisms of fatigue crack growth in low alloy steel, Acta Metall. 21(5) (1973) 639-648, DOI: 10.1016/0001-6160(73)90073-4.

[83] P.J.E. Forsyth, Fatigue damage and crack growth in aluminium alloys, Acta Metall. 11(7) (1963) 703-715, DOI: 10.1016/0001-6160(63)90008-7.

[84] B.N. Jaya, V. Jayaram, Fracture Testing at Small-Length Scales: From Plasticity in Si to Brittleness in Pt, JOM 68(1) (2015) 94-108, DOI: 10.1007/s11837-015-1489-2.

[85] A. Barnoush, Correlation between dislocation density and nanomechanical response during nanoindentation, Acta Mater. 60(3) (2012) 1268-1277, DOI: 10.1016/j.actamat.2011.11.034.

[86] A. Barnoush, M. Asgari, R. Johnsen, Resolving the hydrogen effect on dislocation nucleation and mobility by electrochemical nanoindentation, Scripta Mater. 66(6) (2012) 414-417, DOI: 10.1016/j.scriptamat.2011.12.004.

[87] A. Barnoush, M. Asgari, R. Johnsen, R. Hoel, Hydrogen effect on nanomechanical properties of the nitrided steel, Metall. Mater. Trans. A 44(2) (2013) 766-775, DOI: 10.1007/s11661-012-1462-4.

[88] A. Barnoush, C. Bies, H. Vehoff, In situ electrochemical nanoindentation of FeAl (100) single crystal: Hydrogen effect on dislocation nucleation, J. Mater. Res. 24(3) (2009) 1105-1113, DOI: 10.1557/jmr.2009.0084.

[89] A. Barnoush, J. Dake, N. Kheradmand, H. Vehoff, Examination of hydrogen embrittlement in FeAl by means of in situ electrochemical micropillar compression and nanoindentation techniques, Intermetallics 18(7) (2010) 1385-1389, DOI: 10.1016/j.intermet.2010.01.001.

[90] A. Barnoush, H. Vehoff, In situ electrochemical nanoindentation of a nickel (111) single crystal: hydrogen effect on pop-in behaviour, Zeitschrift fuer Metallkunde/Materials Research and Advanced Techniques 97(9) (2006) 1224-1229.

[91] A. Barnoush, H. Vehoff, Electrochemical nanoindentation: A new approach to probe hydrogen/deformation interaction, Scripta Mater. 55(2) (2006) 195-198, DOI: 10.1016/j.scriptamat.2006.03.041.

[92] A. Barnoush, H. Vehoff, Hydrogen embrittlement of aluminum in aqueous environments examined by in situ electrochemical nanoindentation, Scripta Mater. 58(9) (2008) 747-750, DOI: 10.1016/j.scriptamat.2007.12.019.

[93] A. Barnoush, H. Vehoff, In situ electrochemical nanoindentation: A nanomechanical approach to rank hydrogen embrittlement in extremely small volumes, Proceedings of the 2008 International Hydrogen Conference - Effects of Hydrogen on Materials, 2009, pp. 187-194.

[94] T. Hajilou, M.S.B. Hope, A.H. Zavieh, N. Kheradmand, R. Johnsen, A. Barnoush, In situ small-scale hydrogen embrittlement testing made easy: An electrolyte for preserving surface integrity at nano-scale during hydrogen charging, Int. J. Hydrog. Energy 43(27) (2018) 12516-12529, DOI: 10.1016/j.ijhydene.2018.04.168.

[95] T. Hajilou, Y. Deng, N. Kheradmand, A. Barnoush, Hydrogen enhanced cracking studies on Fe-3wt%Si single and bi-crystal microcantilevers, Philos Trans A Math Phys Eng Sci 375(2098) (2017), DOI: 10.1098/rsta.2016.0410.

[96] T. Hajilou, Y. Deng, B.R. Rogne, N. Kheradmand, A. Barnoush, In situ electrochemical microcantilever bending test: A new insight into hydrogen enhanced cracking, Scripta Mater. 132 (2017) 17-21, DOI: 10.1016/j.scriptamat.2017.01.019.

[97] Y. Deng, T. Hajilou, A. Barnoush, Hydrogen-enhanced cracking revealed by in situ micro-cantilever bending test inside environmental scanning electron microscope, Philosophical Transactions of the Royal Society A: Mathematical, Physical and Engineering Sciences 375(2098) (2017), DOI: 10.1098/rsta.2017.0106.

[98] D. Wan, Y. Deng, J.I.H. Meling, A. Alvaro, A. Barnoush, Hydrogen-enhanced fatigue crack growth in a single-edge notched tensile specimen under in-situ hydrogen charging inside an environmental scanning electron microscope, Acta Mater. 170 (2019) 87-99, DOI: 10.1016/j.actamat.2019.03.032.

[99] A. Alvaro, D. Wan, V. Olden, A. Barnoush, Hydrogen Enhanced Fatigue Crack Growth Rates in a Ferritic Fe-3wt%Si Alloy, Procedia Structural Integrity 13 (2018) 1514-1520, DOI: 10.1016/j.prostr.2018.12.310.

[100] D. Wan, A. Alvaro, V. Olden, A. Barnoush, Hydrogen-assisted fatigue crack growth in ferritic steels – a fractographic study, MATEC Web of Conferences, 2018, p. 03004.

[101] D. Wan, A. Alvaro, V. Olden, A. Barnoush, Hydrogen-enhanced fatigue crack growth behaviors in a ferritic Fe-3wt%Si steel studied by fractography and dislocation structure analysis, Int. J. Hydrog. Energy 44(10) (2019) 5030-5042, DOI: 10.1016/j.ijhydene.2018.12.190.

[102] S. Zaefferer, N.N. Elhami, Theory and application of electron channelling contrast imaging under controlled diffraction conditions, Acta Mater. 75 (2014) 20-50, DOI: 10.1016/j.actamat.2014.04.018.

[103] I. Gutierrez-Urrutia, Analysis of FIB-induced damage by electron channelling contrast imaging in the SEM, J. Microsc. (2016), DOI: 10.1111/jmi.12462.

[104] I. Gutierrez-Urrutia, Analysis of dislocation configurations in a [0 0 1] fcc single crystal by electron channeling contrast imaging in the SEM, Microscopy (Oxf) 66(2) (2017) 63-67, DOI: 10.1093/jmicro/dfw099.

[105] I. Gutierrez-Urrutia, J.A. del Valle, S. Zaefferer, D. Raabe, Study of internal stresses in a TWIP steel analyzing transient and permanent softening during reverse shear tests, J. Mater. Sci. 45(24) (2010) 6604-6610, DOI: 10.1007/s10853-010-4750-7.

[106] I. Gutierrez-Urrutia, D. Raabe, Microbanding mechanism in an Fe–Mn–C high-Mn twinning-induced plasticity steel, Scripta Mater. 69(1) (2013) 53-56, DOI: 10.1016/j.scriptamat.2013.03.010.

[107] I. Gutierrez-Urrutia, S. Zaefferer, D. Raabe, Electron channeling contrast imaging of twins and dislocations in twinning-induced plasticity steels under controlled diffraction conditions in a scanning electron microscope, Scripta Mater. 61(7) (2009) 737-740, DOI: 10.1016/j.scriptamat.2009.06.018.

[108] I. Gutierrez-Urrutia, S. Zaefferer, D. Raabe, The effect of grain size and grain orientation on deformation twinning in a Fe–22wt.% Mn–0.6wt.% C TWIP steel, Mater. Sci. Eng., A 527(15) (2010) 3552-3560, DOI: 10.1016/j.msea.2010.02.041.

[109] I. Gutierrez-Urrutia, S. Zaefferer, D. Raabe, Coupling of Electron Channeling with EBSD: Toward the Quantitative Characterization of Deformation Structures in the SEM, JOM 65(9) (2013) 1229-1236, DOI: 10.1007/s11837-013-0678-0.

[110] M. Koyama, E. Akiyama, K. Tsuzaki, D. Raabe, Hydrogen-assisted failure in a twinning-induced plasticity steel studied under in situ hydrogen charging by electron channeling contrast imaging, Acta Mater. 61(12) (2013) 4607-4618, DOI: 10.1016/j.actamat.2013.04.030.

[111] J. Nellessen, S. Sandlöbes, D. Raabe, Effects of strain amplitude, cycle number and orientation on low cycle fatigue microstructures in austenitic stainless steel studied by electron channelling contrast imaging, Acta Mater. 87 (2015) 86-99, DOI: 10.1016/j.actamat.2014.12.024.

[112] C. Schayes, J. Bouquerel, J.-B. Vogt, F. Palleschi, S. Zaefferer, A comparison of EBSD based strain indicators for the study of Fe-3Si steel subjected to cyclic loading, Mater. Charact. 115 (2016) 61-70, DOI: 10.1016/j.matchar.2016.03.020.

[113] C. Schayes, J.-B. Vogt, J. Bouquerel, F. Palleschi, S. Zaefferer, Cyclic plasticity mechanism of the M330-35A steel, Int. J. Fatigue 82 (2016) 530-539, DOI: 10.1016/j.ijfatigue.2015.09.008.

[114] C.-C. Shih, N.-J. Ho, H.-L. Huang, Transmission and scanning electron microscope study on the secondary cyclic hardening behavior of interstitial-free steel, Mater. Charact. 60(11) (2009) 1280-1288, DOI: 10.1016/j.matchar.2009.05.013.

[115] C.-C. Shih, N.-J. Ho, H.-L. Huang, Dislocation evolution in interstitial-free steel during constant and variable amplitude testing, J. Mater. Sci. 45(7) (2010) 1809-1816, DOI: 10.1007/s10853-009-4163-7.

[116] C.-C. Shih, N.-J. Ho, H.-L. Huang, The Study of Fatigue Behaviors and Dislocation Structures in Interstitial-Free Steel, Metall. Mater. Trans. A 41(8) (2010) 1995-2001, DOI: 10.1007/s11661-010-0186-6.

[117] E. Breitbarth, S. Zaefferer, F. Archie, M. Besel, D. Raabe, G. Requena, Evolution of dislocation patterns inside the plastic zone introduced by fatigue in an aged aluminium alloy AA2024-T3, Mater. Sci. Eng., A 718 (2018) 345-349, DOI: 10.1016/j.msea.2018.01.068.

[118] D. Wan, Electron channeling contrast imaging (ECCI) analysis on deformed aluminum, Institute of physical metallurgy and metal physics, RWTH Aachen University, Aachen, Germany, 2015, p. 72.

[119] J. Zhang, L. Morsdorf, C.C. Tasan, Multi-probe microstructure tracking during heat treatment without an in-situ setup: Case studies on martensitic steel, dual phase steel and β-Ti alloy, Mater. Charact. 111 (2016) 137-146, DOI: 10.1016/j.matchar.2015.11.019.

[120] S. Kaboli, D. Goldbaum, R.R. Chromik, R. Gauvin, Electron channeling contrast imaging of plastic deformation induced by indentation in polycrystalline nickel, Microsc. Microanal. 19(6) (2013) 1620-31, DOI: 10.1017/S1431927613013469.

[121] F. Ram, Z. Li, S. Zaefferer, S.M. Hafez Haghighat, Z. Zhu, D. Raabe, R.C. Reed, On the origin of creep dislocations in a Ni-base, single-crystal superalloy: an ECCI, EBSD, and dislocation dynamics-based study, Acta Mater. 109 (2016) 151-161, DOI: 10.1016/j.actamat.2016.02.038.

[122] Z.B. Zhang, G. Obasi, R. Morana, M. Preuss, Hydrogen assisted crack initiation and propagation in a nickel-based superalloy, Acta Mater. 113 (2016) 272-283, DOI: 10.1016/j.actamat.2016.05.003.

[123] P.J. Ferreira, I.M. Robertson, H.K. Birnbaum, Hydrogen effects on the interaction between dislocations, Acta Mater. 46(5) (1998) 1749-1757, DOI: 10.1016/s1359-6454(97)00349-2.

[124] D. Xie, S. Li, M. Li, Z. Wang, P. Gumbsch, J. Sun, E. Ma, J. Li, Z. Shan, Hydrogenated vacancies lock dislocations in aluminium, Nat. Commun. 7 (2016) 13341, DOI: 10.1038/ncomms13341.

[125] S. Wang, N. Hashimoto, S. Ohnuki, Effects of hydrogen on activation volume and density of mobile dislocations in iron-based alloy, Mater Sci Eng A 562 (2013) 101-108, DOI: 10.1016/j.msea.2012.10.100.

[126] A. Alvaro, D. Wan, V. Olden, A. Barnoush, Hydrogen enhanced fatigue crack growth rates in a ferritic Fe-3 wt%Si alloy and a X70 pipeline steel, Eng. Fract. Mech. (2019), DOI: 10.1016/j.engfracmech.2019.106641.

[127] A. Alvaro, O.M. Akselsen, X. Ren, P.-A. Kane, Fatigue Properties of a 420 MPa Structural Steel at Low Temperature, The 25th International Ocean and Polar Engineering Conference, Kona, Big Island, Hawaii, USA, 2015, pp. 331-337.

[128] Y. Ogawa, D. Birenis, H. Matsunaga, O. Takakuwa, J. Yamabe, O. Prytz, A. Thogersen, The role of intergranular fracture on hydrogen-assisted fatigue crack propagation in pure iron at a low stress intensity range, Mater Sci Eng A 733 (2018) 316-328, DOI: 10.1016/j.msea.2018.07.014.

Part II

Paper 1

Hydrogen embrittlement effect observed by in-situ hydrogen plasma charging on a ferritic alloy

Di Wan*, Yun Deng, Afrooz Barnoush

Scripta Mater. 151 (2018) 24-27, DOI: 10.1016/j.scriptamat.2018.03.038.

Hydrogen embrittlement effect observed by in-situ hydrogen plasma charging on a ferritic alloy

Di Wan*, Yun Deng, Afrooz Barnoush

Department of Mechanical and Industrial Engineering, Norwegian University of Science and Technology, Richard Birkelands vei 2B, 7491 Trondheim, Norway

Abstract

To study the hydrogen embrittlement (HE) effect, a novel in-situ slow strain rate tensile test together with in-situ hydrogen (H) charging by H-plasma was conducted in an environmental scanning electron microscope (ESEM). The introduction of H-plasma gave a reduction in tensile elongation by about 5% in comparison with a reference test in vacuum. Fractographic observation clearly showed the difference in the resulted features on the fracture surfaces. Electron backscatter diffraction (EBSD) was conducted to elucidate the characteristics of the cracks. Such investigations can help to refresh the existing knowledge in HE study.

Keywords: hydrogen embrittlement; in-situ test; Fe-3wt.%Si; plasma; crack.

Hydrogen embrittlement (HE) is a well-acknowledged phenomenon in metals. It draws much scientists' and engineers' attention because it can lead to catastrophic failure of an industrial structure. Researchers use different methods to charge a test piece with hydrogen (H) and study the behavior of the material during or after charging. A common method is to use H2 gas as the environment, for example Vehoff [1, 2] used gaseous H to study the H effect on the fracture behavior of ferritic steels. More examples can be found in Ref.[3-12]. Furthermore, electrochemical cathodic charging is also commonly used, for example Wang et al. [13] used cathodic charging with an in-situ tensile test to study the effect of H on mobile dislocations, and the H concentrations were also determined. Other examples can be found in Ref.[14-22] as well. There is also a smart method for special materials, for example, Deng et al. [23, 24] and Rogne et al. [25] used water vapor to charge Fe-Al intermetallic alloys since the H_2O molecule can react with Al, producing alumina and H to invade the matrix.

Due to the high diffusivity of H in body-centered cubic (BCC) lattice [13], it is always critical to have H pre-charging on the test piece because H can diffuse out even during a short transferring procedure. Therefore, in-situ H-charging is favored for the HE study of BCC structures.

Currently, in-situ charging of ferritic steel is either done in high pressure hydrogen gas or under electrochemical control by cathodic H-charging. This makes the high-resolution observation of the sample during deformation challenging.

Environmental scanning electron microscopy (ESEM) combined with miniaturized tensile stages provides a unique possibility to test the effect of H on mechanical deformation, however the limited maximum pressure inside the chamber and restrictions on the possible gases at that pressure in the chamber from the manufacturer hinders the HE tests inside the ESEM. At low pressures, the fugacity of H is not enough to have adequate physisorption and dissociation of the H_2 molecules on the surface to observe HE within a reasonable time scale. Converting H_2 gas to H plasma before letting it enter the ESEM chamber will increase the H fugacity in the chamber and provide possibilities to observe the HE processes inside the ESEM.

Narita [26] used H glow charging to study the embrittlement effect in a Fe-Si system with a tensile test on single crystals and concluded that this method is capable of charging the samples with enough H to reveal an embrittlement effect without severe surface damage. Kimura and Birnbaum [27] observed that that H-plasma charging can cause a softening effect in the flow stress of pure iron samples. A recent work from Malitckii et al. [28] used H-rich plasma at elevated temperatures to charge two kinds of steels and successfully revealed the HE effect on them.

In this paper, we show that the introduction of low pressure H-plasma in ESEM chamber can provide a possibility to study the HE of a ferritic alloy with in-situ mechanical testing. The limitation in in-situ investigation has been discussed. Moreover, ex-situ characterization was carried out to study the details of the tested specimen. Such investigations can help us refresh the knowledge in HE.

Simple ferritic Fe-3wt.%Si alloy with the composition shown in Tab. 1 was used in this study. The as-received material has a coarse grain size of 300 µm. This simple microstructure makes the alloy a perfect model material to establish the methodology

(e.g. [1, 2, 29-33]).Tensile specimens were cut from the raw material by electrical discharge machining (EDM) to a dog-bone shape with the gauge geometry of 20 mm × 6 mm × 2 mm. Grinding to #4000 emery paper followed by 3 µm and 1 µm diamond paste polishing plus final electropolishing was adopted to make sure the tested surfaces were flat and smooth without residual deformation. The tensile/ compression module from Kammrath & Weiss GmbH (Germany) was used for mechanical testing inside a Quanta 650 ESEM (Thermo Fisher Scientific Inc., USA). The engineering strain rate was chosen to be 10^{-5} s^{-1} in order to provide enough time for H adsorption and diffusion. After fracture, the half-specimens were taken out for further characterization. For H-charging, an Evactron Model 25 Zephyr Plasma Cleaner (XEI Scientific, USA) was used with gaseous H_2 as a process gas from a hydrogen generator. It should be noted that remote plasma was applied in this cleaner. With this method, the interaction between plasma and material occurs at a location that is remote from the plasma afterglow. In other words, only active plasma would participate in the interactions with the material, such that the specimen surface can prevent from heating, contaminating and damaging effects.

Tab. 1 Chemical composition of the investigated material

Elem.	C	Si	Mn	P	S	Cr	Ni	Mo
wt.%	0.018	3.000	0.055	0.008	0.003	0.010	0.006	0.003
Elem.	Cu	Al	Ti	Nb	V	B	Zr	Fe
wt.%	0.013	0.015	0.001	0.002	0.001	0.0002	0.0010	Bal.

Fig. 1 shows the experimental setup of the SEM chamber. The plasma cleaner was connected to the SEM chamber via a flange, and the hydrogen generator was connected to the working gas inlet of the plasma cleaner. The tensile specimen was installed into the tensile/ compression module connecting to an external controlling unit via another flange. With this setup, in-situ mechanical testing with in-situ H-charging can be realized. In-situ observation by normal SEM mode is limited and we are discussing the possibilities for imaging at low pressure H-plasma with the ESEM manufacturer. To the authors' knowledge, no reports on imaging by high voltage electrons with H-plasma presenting have been found. According to the communications with the company, in-situ imaging with high-voltage in H environment is potentially unsafe. Since H is extremely flammable, there is a likelihood of arcing in the chamber from the detectors and this is extremely likely to cause the H to ignite. For this reason, the investigations

in this study could only be done when the chamber is completely evacuated to high-vacuum state.

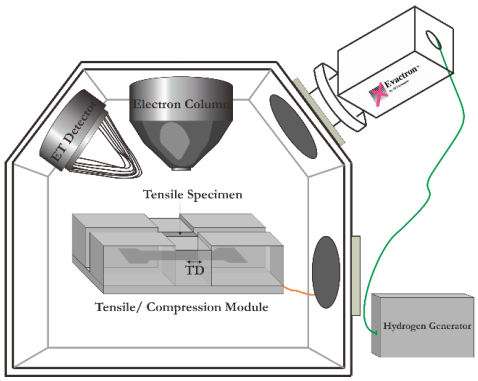

Fig. 1 Experimental setup of the SEM chamber (TD: tensile direction)

The stress-strain curves for the tensile tests are shown in Fig. 2. It should be noted that the stress is calculated by dividing the load over the cross-section area in the gauge range, which was re-measured after preparation since grinding and polishing could change the geometry of the specimen. The tests were denoted as Vac case (tested in vacuum) and H case (tested in H-plasma), respectively. The H test was done by stopping the test at the ultimate tensile strength (UTS) range from the Vac test for one hour to give more time for H uptake into the lattice under enhanced solubility effect of the tensile stress as well as exposure of the oxide free surface. From the curves, the two specimens had similar behaviors in the elastic range and behaved similarly up to the UTS range with a slight hardening effect in the H case. But the H-charged specimen had a reduction in the elongation to fracture by about 5% and the crack propagation procedure was much faster and more unstable. It is difficult to define the crack initiation from the stress-strain curves, but it can be seen qualitatively that the crack was growing in a more stable manner in Vac than in H case, which showed a sudden failure. A supplementary video was attached to this work, showing the relatively stable crack propagation procedure of the Vac case. This procedure corresponds to the part highlighted by blue dash-lines in Fig. 2. For the H case, due to technical limitations, no imaging is possible during the plasma charging and pictures can only be taken after interrupting the plasma and evacuating the chamber from H. We are currently discussing with the ESEM manufacturer for modification to try to make this imaging process possible.

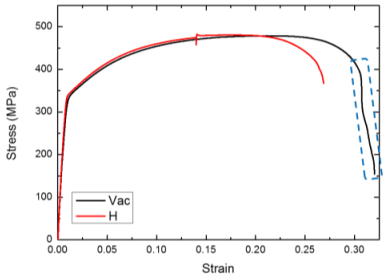

Fig. 2 Stress-strain curves of the investigated specimens (the highlighted part corresponds to the crack propagation procedure, which is shown by a video in supplementary files)

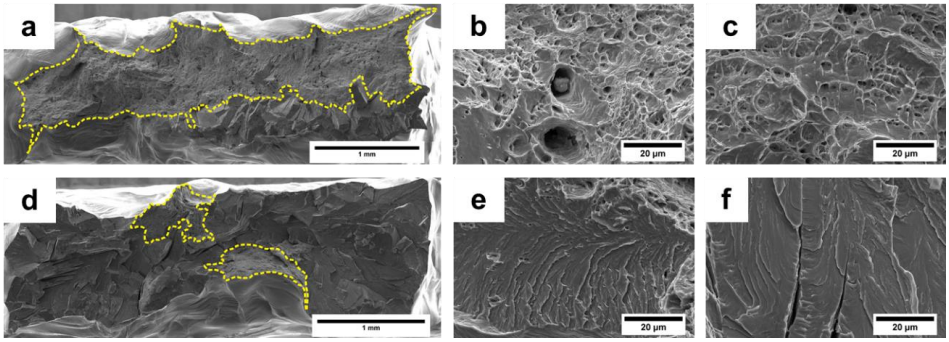

Fig. 3 Fracture surfaces of the fractured tensile specimens (a-c: in vacuum; d-f: with H-plasma charging; b, c and e, f are magnified representative features in a and d, respectively; highlighted areas enclosed by yellow dash-lines are ductile part with an area fraction of 75% for Vac, and 10% for H, respectively; detailed discussion in text)

Fig. 3 shows the fracture surfaces of the specimens after final fracture in Vac and in H case, respectively. The reduction in area from calculation is 61.4% for Vac and 50.1% for H case, respectively. The fracture surfaces showed generally transgranular type, regardless of H-plasma charging. The ductile feature (dimples) is highlighted by yellow dash-lines. A large area fraction (about 75% of the whole fracture surface) of dimples can be found in the Vac case, which indicates the crack growth procedure was in a more ductile manner when H was absent. While in the H case, most of the area shows brittle transgranular cleavage-like features with only a limited area fraction (about 10% of the whole fracture surface) of ductile features. Besides, many secondary cracks are observed on the fracture surface in the H case while these are not seen in the Vac case. Fig. 3b and c show the magnified dimple features in Vac case, with b showing inclusion spots in dimples and c showing pure dimple structure. This indicates a ductile behavior of this specimen in Vac, regardless of the presence of small inclusions. Fig. 3e and f

reveal detailed fracture surface of the H case showing cleavage-like features. Fig. 3e shows typical brittle facets on the fracture surface with microligaments and river-lines. Fig. 3f shows clear river-lines with secondary cracks on the fracture surface. This observation is consistent with previous works on the similar alloy system [2, 32, 34]. The river-patterns are formed from cleavage and are characteristic for brittle fracture mechanism. The appearance of these features indicates a brittle, though plasticity-related cracking process. Mine et al. [35] did a micro-tensile test with H on austenitic steels, and found similar quasi-cleavage fracture features. They concluded that a high H concentration can lead to localized shear and form quasi-cleavage fracture.

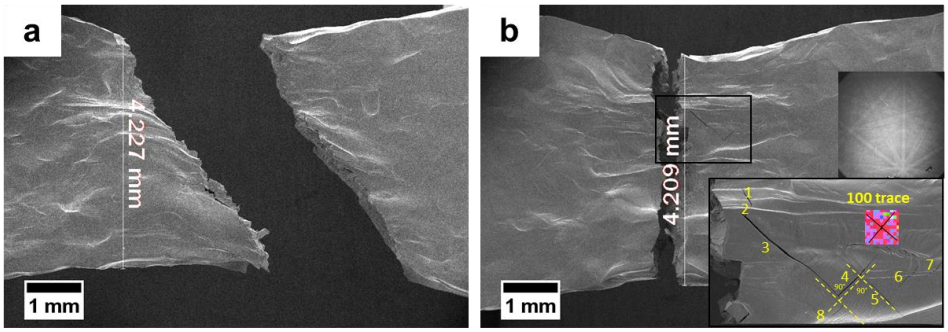

Fig. 4 Top-view on the tensile specimens after final fracture (a: in vacuum; b: in H-plasma; the structure shown in the lower right corner of b is highlighted by the black square, and the {100} traces were measured by EBSD with a representative Kikuchi pattern from the raw data)

Fig. 4 gives the top-view on the specimens after tensile fracture. The magnified zone in the lower right corner of Fig. 4b is from the highlighted area in the middle and the {100} traces are from electron backscatter diffraction (EBSD) analysis on the corresponding cracking grains. The Vac case shows a shear fracture along the direction approximately 45° to the tensile direction. This is not rare for materials that experience ductile fracture failure since 45° is the direction of the principal shear stress during monotonic tensile loading. The H case shows the main crack nearly perpendicular to the tensile direction. The final widths of the specimens were measured with showing no significant difference between the two cases. It is interesting that many secondary cracks (eight as measured in the magnified zone in Fig. 4b) can also be found in this view in the H case, while the Vac case does not show similar features. Thus, the appearance of these secondary cracks can be ascribed to the H effect. The secondary cracks form clearly a relationship of 90° between each other. A further EBSD test was done on the fractured

specimen and confirmed the direction being [100]. This is rational because {100} plane system is the cleavage plane system of BCC lattice, and this implies a possible H-induced cleavage transition mechanism.

It is generally acknowledged that there are two important necessary conditions to cause HE effect, namely high enough stress and adequate H concentration. In the present study, we used a relatively low strength steel. According to the standard, steels with yield strength below 400 MPa are immune against HE. Therefore, the tensile behavior of the H case was the same as the Vac case before the UTS was reached, and deviation of the stress-strain curve happened after the stress level in the steel reached to higher values and close to the UTS (see Fig. 2). When necking happened, the localized deformation led to a localized stress field that can enhance local H uptake and cause embrittlement effect at the necked area. It is assumed that the combination of local high stress condition and high H concentration caused the HE effect. This can be the reason that the stress-strain curve of the H case started to deviate after necking, as seen in Fig. 2. In this case, the HE actually took place in a material that has been hardened up to the UTS level, and the real HE effect should be considered from the critical status. If we define the HE effect in percentage could be calculated by the elongation loss over the full elongation range in the Vac case, the value from the original curves should be about 18%; while if we assume the HE starts from the hardened status, this value changes to about 33%.

An important parameter in HE study is the H content. We used a fixed H2 flow rate of about 250 ml/min from the hydrogen generator. The chamber pressure for plasma excitation is around 40 Pa in this study, and when the plasma is excited, the working pressure can reach an approximately fixed value of 70-80 Pa, with an increment of about 30-40 Pa. Vesel et. al [36] in comparable H-plasma formation condition used fiber-optic catalytic probe and measured a density of H atom in the range of 2.5×1021 atom/m3 [36] which shows that the atomic H is the main expected constituent of the plasma in the vicinity of the source. The fugacity of the dissociated H atoms will be far above 80 Pa as reported by Bond et. al and can reach values as high as several MPa[37]. According to the conclusions in Ref.[38] that HE doesn't occur with insufficient H concentration, the amount of H in this work revealed to be enough to cause HE.

The H-plasma charging procedure gives a minor influence on the strength of the material, which is consistent with the work from Malitckii [28] and Depover [16, 19] on different kinds of steels with other charging methods. Birnbaum [39] reported that H in solid solution increased the mobilities of dislocations and could give a macroscopic softening in the presence of slip localization. In this study, however, no significant proof of slip localization was found yet and neither softening effect when H was present. One possible reason is that the dislocations were motivated by H to contribute to cracks formation rather than forming local slip lines. The results in Fig. 3d-f all show that the cracks were formed inside the matrix of the specimen in a transgranular and brittle manner.

Kimura et al. [38] reported an important effect of H in iron is that H reduces the {100} cleavage stress, which is one of the fundamental mechanisms of HE in iron. From the classical theory of dislocation interactions in BCC lattice [40], a [-1-11] type dislocation and a [111] type dislocation in BCC lattice can meet and produce an immobile [001] type dislocation, and the accumulation of this type of immobile dislocations can lead to a cleavage fracture of (001) planes. This is believed to be a plasticity-related cleavage fracture mechanism. Chen et al. [34] concluded that the cracking induced by external H in Fe-3wt.%Si single crystal is cleavage process accompanied with severe plasticity.

One hypothesis proposed by the work from Ref. [24, 25, 41] is that during deformation, the stress was localized at the necking area when the specimen started to deform unstably. The stress localization activated multi slip systems in the necking region. There, the H-dislocation interaction was strongly intensified and the dislocation motion was further blocked by increasing H pinning effect [24, 42]. A common finding of these works is that when H is absent, the crack tip keeps blunting, while when H is presenting, the principal crack keeps sharp and leads to brittle cleavage fracture. The resulting fracture surfaces are similar to the present study: voids and dimples were found in Vac case and flat, cleavage-like fracture were found in H case. Similar phenomena were found in FeAl[23, 24], Fe3Al[25] and Fe-3wt.%Si[41] by micro-cantilever bending test with in-situ H-charging, and explained schematically and systematically in Ref.[24].

To sum up, the present study used a novel in-situ setup for HE research combining H-charging, mechanical testing and investigation. It is clearly shown that this study reveals the HE effect of a ferritic Fe-3wt.%Si alloy during slow strain rate monotonic tension

under H-plasma charging. The elongation to fracture got a reduction by about 5% as well as the failure procedure shifted to a faster and more brittle manner. The flow stress of the material got a minor influence from H-plasma. The microstructure observation reveals that the H-free specimen has more ductile features than the H-charged one. An ideal outcome would be that the HE effect can be observed during mechanical testing by switching on and off the H-source with showing a shift in the mechanical behavior or microstructure in a well-defined specimen, by which manner the original mechanism of H on the test piece can be directly observed and depicted. However, due to technical limitations, this could not yet be realized in this work and would be the prospect for the next work.

Acknowledgement

This work was supported by the Research Council of Norway through the project HyF-Lex (project number: 244068/E30).

Reference

[1] H. Vehoff, P. Neumann, Acta Metall. 28(3) (1980) 265-272.
[2] H. Vehoff, W. Rothe, Acta Metall. 31(11) (1983) 1781-1793.
[3] M. Koyama, Y. Onishi, H. Noguchi, Int. J. Fract. 206(1) (2017) 123-130.
[4] G. Bilotta, G. Henaff, D. Halm, M. Arzaghi, Int. J. Hydrog. Energy 42(15) (2017) 10568-10578.
[5] Z. Sun, G. Benoit, C. Moriconi, F. Hamon, D. Halm, F. Hamon, G. Hénaff, Int. J. Hydrog. Energy 36(14) (2011) 8641-8644.
[6] M. Dadfarnia, A. Nagao, S. Wang, M.L. Martin, B.P. Somerday, P. Sofronis, Int. J. Fract. 196(1-2) (2015) 223-243.
[7] M. Dadfarnia, P. Sofronis, B.P. Somerday, I.M. Robertson, Int. J. Mat. Res. 99(5) (2008) 557-570.
[8] J.A. Ronevich, B.P. Somerday, C.W. San Marchi, Int. J. Fatigue 82 (2016) 497-504.
[9] B.P. Somerday, P. Sofronis, K.A. Nibur, C. San Marchi, R. Kirchheim, Acta Mater. 61(16) (2013) 6153-6170.
[10] H. Matsunaga, M. Yoshikawa, R. Kondo, J. Yamabe, S. Matsuoka, Int. J. Hydrog. Energy 40(16) (2015) 5739-5748.

[11] Y. Ogawa, D. Birenis, H. Matsunaga, A. Thøgersen, Ø. Prytz, O. Takakuwa, J. Yamabe, Scr. Mater. 140 (2017) 13-17.
[12] J. Yamabe, M. Yoshikawa, H. Matsunaga, S. Matsuoka, Int. J. Fatigue 102 (2017) 202-213.
[13] S. Wang, N. Hashimoto, S. Ohnuki, Mat. Sci. Eng. A 562 (2013) 101-108.
[14] T. Depover, O. Monbaliu, E. Wallaert, K. Verbeken, Int. J. Hydrog. Energy 40(47) (2015) 16977-16984.
[15] T. Depover, D. Pérez Escobar, E. Wallaert, Z. Zermout, K. Verbeken, Int. J. Hydrog. Energy 39(9) (2014) 4647-4656.
[16] T. Depover, K. Verbeken, Int. J. Hydrog. Energy 41(32) (2016) 14310-14329.
[17] T. Depover, K. Verbeken, Mater. Sci. Eng. A 669 (2016) 134-149.
[18] T. Depover, K. Verbeken, Mater. Sci. Eng. A 675 (2016) 299-313.
[19] T. Depover, K. Verbeken, Corros. Sci. 112 (2016) 308-326.
[20] T. Depover, E. Wallaert, K. Verbeken, Mater. Sci. Eng. A 649 (2016) 201-208.
[21] T. Depover, E. Wallaert, K. Verbeken, Mater. Sci. Eng. A 664 (2016) 195-205.
[22] C. Lekbir, J. Creus, R. Sabot, X. Feaugas, Mater. Sci. Eng. A 578 (2013) 24-34.
[23] Y. Deng, T. Hajilou, D. Wan, N. Kheradmand, A. Barnoush, Scr. Mater. 127 (2017) 19-23.
[24] Y. Deng, A. Barnoush, Acta Mater. 142 (2018) 236-247.
[25] B.R.S. Rogne, N. Kheradmand, Y. Deng, A. Barnoush, Acta Mater. 144 (2018) 257-268.
[26] N. Narita, Scr. Metall. 18(9) (1984) 985-988.
[27] A. Kimura, H.K. Birnbaum, Scr. Metall. 21(1) (1987) 53-57.
[28] E. Malitckii, Y. Yagodzinskyy, H. Hänninen, Fusion Eng. Des. 98-99 (2015) 2025-2029.
[29] A. Barnoush, H. Vehoff, Acta Mater. 58(16) (2010) 5274-5285.
[30] A. Barnoush, H. Vehoff, Corros. Sci. 50(1) (2008) 259-267.
[31] H. Vehoff, Rißbildung und Rißausbreitung in Ein- und Bikristallen, VDI-Verlag, Düsseldorf, 1994.
[32] H. Vehoff, Untersuchung der duktilen und quasispröden zyklischen Rißausbreitung in Fe-3%-Si-Einkristallen, PhD thesis, RWTH Aachen, Aachen, 1977.
[33] H. Vehoff, P. Neumann, W. Rothe, Met. Sci. 15(10) (2013) 469-470.
[34] S.H. Chen, Y. Katz, W.W. Gerberich, Philos. Mag. A 63(1) (1991) 131-155.

[35] Y. Mine, K. Koga, O. Kraft, K. Takashima, Scr. Mater. 113 (2016) 176-179.
[36] A. Vesel, A. Drenik, R. Zaplotnik, M. Mozetic, M. Balat-Pichelin, Surf. Interface Anal. 42(6-7) (2010) 1168-1171.
[37] G.M. Bond, I.M. Robertson, H.K. Birnbaum, Scr. Metall. 20(5) (1986) 653-658.
[38] A. Kimura, H. Kimura, Mater. Sci. Eng. 77 (1986) 75-83.
[39] H.K. Birnbaum, Scr. Metall. Mater. 31(2) (1994) 149-153.
[40] D. Hull, D.J. Bacon, Introduction to Dislocations, fifth ed., Elsevier, 2011.
[41] T. Hajilou, Y. Deng, B.R. Rogne, N. Kheradmand, A. Barnoush, Scr. Mater. 132 (2017) 17-21.
[42] J. Song, W.A. Curtin, Nat. Mater. 12(2) (2013) 145-51.

Paper 2

Hydrogen-enhanced fatigue crack growth behaviors in a ferritic Fe-3wt%Si steel studied by fractography and dislocation structure analysis

Di Wan*, Antonio Alvaro, Vigdis Olden, Afrooz Barnoush

Int. J. Hydrog. Energy 44(10) (2019) 5030-5042, DOI:
10.1016/j.ijhydene.2018.12.190.

Hydrogen-enhanced fatigue crack growth behaviors in a ferritic Fe-3wt%Si steel studied by fractography and dislocation structure analysis

Di Wan[a,*], Antonio Alvaro[b], Vigdis Olden[b], Afrooz Barnoush[a]

a. Department of Mechanical and Industrial Engineering, Norwegian University of Science and Technology, Richard Birkelands vei 2B, 7491 Trondheim, Norway

b. SINTEF Industry, 7456 Trondheim, Norway

Abstract

The effect of hydrogen (H) on the fatigue behavior is of significant importance for metallic structures. In this study, the hydrogen-enhanced fatigue crack growth rate (FCGR) tests on in-situ electrochemically H-charged ferritic Fe-3wt%Si steel with coarse grain size were conducted. Results showed strong difference between the H-charged and the non-charged conditions (reference test in laboratory air) and were in good agreement with the results from literature. With H-charging, the fracture morphology changed from transgranular (TG) type to "quasi-cleavage" ("QC"), with a different fraction depending on the loading frequency. With the help of electron channeling contrast imaging (ECCI) inside a scanning electron microscope (SEM), a relatively large area in the failed bulk specimen could be easily observed with high-resolution down to dislocation level. In this work, the dislocation sub-structure immediately under the fracture surfaces were investigated by ECCI to depict the difference in the plasticity evolution during fatigue crack growth (FCG). Based on the analysis, the H-enhanced FCG mechanisms were discussed.

Keywords: hydrogen embrittlement; fractography; Fe-3wt%Si; fatigue crack growth (FCG); SEM; ECCI.

1. Introduction

The hydrogen embrittlement (HE) effect of metallic materials has been intensively studied through the last decades. Several mechanisms have been developed based on the interaction between hydrogen and metals[1] among which hydrogen-enhanced localized plasticity (HELP) [2-7], hydrogen-enhanced decohesion (HEDE) [8-11] and

adsorption-induced dislocation-emission (AIDE) [12] gained the most credibility among the scientific community. The HELP mechanism considers the hydrogen (H) effect on promoting the dislocation motion and generation and thus localized plastic zone and increase in the local stress state, which leads to an early fracture. In the HEDE mechanism H acts towards weakening the interatomic bonds in the material therefore promoting brittle fracture. The AIDE mechanism involves the weakening of interatomic bonding at the crack tips due to adsorbed H, which leads to cleavage-like and intergranular fractures. In practice, there could be several mechanisms simultaneously affecting the fracture behavior of the metallic structures [13] and hence, special attention should be paid when considering different cases.

Metal fatigue is one of the main reasons behind catastrophic failures of modern engineering structures, costing a large amount of economical loss and sometimes even fatality each year [14]. The presence of H in the material can enhance the metallic component's fatigue crack growth rate (FCGR) leading to even earlier dangerous unexpected failures. In other words, the presence of H can ruin the primary fatigue design and life estimation of the structures in service. Oil platforms, for example, experience continuously oscillatory environmental loads with the presence of H. Degradation by H under such conditions would obviously lead to a reduction of the fatigue life of the structures. Hence, it is a critical issue to investigate and analyze the fatigue failure under H environments, which can help to improve the understanding of the mechanical behaviors and improve the fatigue design.

Classically, the fatigue crack growth (FCG) behavior of materials is characterized by three stages, namely crack initiation and slow growth (stage I), stable crack propagation (stage II) and a strongly accelerated crack growth rate which lead to unstable sudden fracture (stage III). Among these three regions, the stage II FCG behavior is usually described by the Paris' (also known as Paris-Erdogan) law as a mathematical relation, of which the basic equation reads as Eq. 1:

$$\frac{da}{dN} = C \cdot \Delta K^m \qquad \text{Eq. 1}$$

where a is the crack length and N is the number of the cycles, giving da/dN the discrete crack extension/growth per cycle. C and m on the right-hand side of the equation are

constants that depend on the material and the testing conditions, while ΔK is the range of the stress intensity factor experienced by the cracked material during the fatigue cycles. By taking logarithms for both sides, it yields Eq. 2:

$$\log\left(\frac{da}{dN}\right) = m \cdot \log(\Delta K) + C' \qquad \text{Eq. 2}$$

in which the C' is the constant after the logarithmic operation referring to the C in Eq. 1. Engineers strongly rely on this relation when it comes to the repair time schedule planning and the lifetime estimations of components and welded structures since it is possible to relate the expected lifetime with the limits of the available crack detection with nondestructive testing techniques.

Steels are commonly used structural materials that may be affected by HE [15-18]. There are mainly two different crystal structures in steels, namely face-centered cubic (FCC) and body-centered cubic (BCC). Generally, FCC lattice can contain more H atoms while having a slower diffusion rate (approx. 10-11 cm2/s in some austenitic steels [19]), while BCC lattice has a lower H solubility but a faster diffusion rate of H (approx. 10^{-5}~10^{-4} cm^2/s [20-23]). In FCC materials, up to 12 slip systems could be found, which made the deformation analysis relatively easier, and a lot of works can be found with deep understanding on the failure behaviors, for example austenitic steels [24-26], Ni alloys [27-30] and some high-entropy alloys [31-33]. However, due to the intrinsic structure of the BCC lattice, up to 48 slip systems can be found in the deformation structure, which made the analysis much more difficult than the FCC materials. Furthermore, the non-Schmid behaviors[34, 35] as well as the non-planar nature of the screw dislocations[36] makes the deformation analysis in BCC materials complicated. To understand the basic mechanisms in BCC materials, simple model materials with well-defined materials parameters should be studied.

Fe-Si alloys contain normally several weight percent of Si in iron matrix, giving a simple ferritic structure with BCC lattice, and this material could be used as model material for different studies. There are several reasons for choosing this alloy as a model material. First of all, Si is a ferrite stabilizing element which can ensure the material contain fully ferritic structure. Secondly, Fe-Si alloys have a higher strength than pure iron, which makes the HE effect more significant since the HE effect is in

general more sensitive at higher stress levels. Thirdly, the grain size of this type of alloy can be easily controlled thanks to the adequate data of the heat treatment processes. Vehoff [37-42] did intensive work on Fe-Si alloys regarding fracture, fatigue failure and HE since 1970s. It was proposed that under H_2 gaseous environment, a crack in Fe-Si single crystal can grow stably by a combined micro-cleavage and crack-tip dislocation emissions. However, due to technical limitations in the previous decades, the resolution of their observation was rather low, though giving solid background. With the modern high-resolution techniques, more studies could be done to deepen the knowledge of these topics.

This work aims at investigating the FCGR behavior of BCC metals under electrochemical H charging conditions. Fe-3wt%Si was used as model material to reveal the role that H plays during FCG and how this extrinsicates into variations of the FCGR curves. Fractographic analysis was done by scanning electron microscopy (SEM) to investigate the microscale features of the fatigue fractured specimens. The validity of the conventional Paris' law was checked both with the mechanical data and the fractography. Statistical analysis on the small-scale features was conducted to study the H effect on the fracture modes. In addition, electron channeling contrast imaging (ECCI) was conducted to investigate the dislocation structures beneath the fracture surface. These results helped to gain a better understanding of the mechanisms of H-accelerated FCG procedure in ferritic alloys.

2. Experimental

2.1 Materials and specimens

The material used in this study is Fe-3wt%Si with simple ferritic structure. The detailed chemical composition is shown in Table 1. The raw plates were rolled from three forged blocks (approx. 80 × 160 × 470 mm each) followed by 10% cold rolling plus annealing at 800 °C for three times with the last time annealing at 1050 °C and straightening. The material has a large grain size of about 300 μm to make the test condition as simple as possible. The microstructure of the investigated material is shown in Figure 2. Compact Tension (CT) specimens were cut by electron discharge machining (EDM) from the raw materials and used for the fatigue crack growth rate testing. Figure 1 shows the geometry of the specimens (as per ASTM E647 standard), with the indicated characterizations performed after the tests.

Table 1 Chemical composition of the investigated Fe-3wt%Si steel.

Element	C	Si	Mn	P	S	Cr	Ni	Mo
wt%	0.018	3.000	0.055	0.008	0.003	0.010	0.006	0.003
Element	Cu	Al	Ti	Nb	V	B	Zr	Fe
wt%	0.013	0.015	0.001	0.002	0.001	0.0002	0.0010	balance

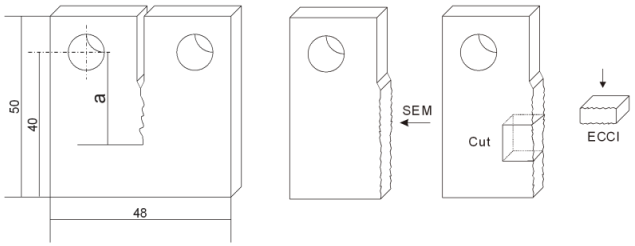

Figure 1 Geometry of the CT specimen and the microstructure of the investigated material, the crack length a is calculated from the center-line of the holes to the front of the crack tip (thickness = 8 mm). Fractography was done on the fracture surface and ECCI was done on the cross-section below the fracture surface, as indicated by the arrows.

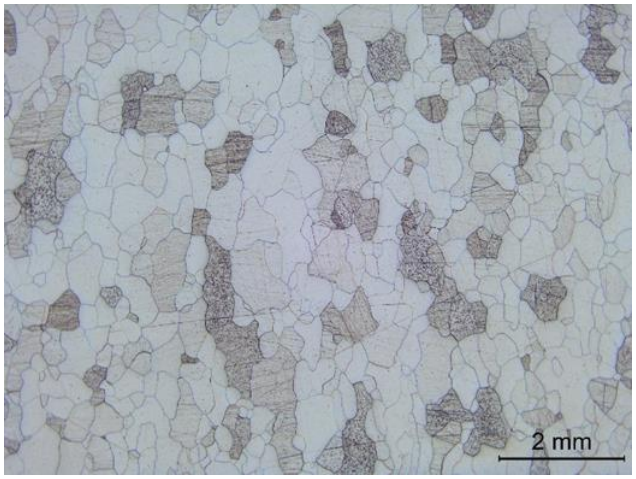

Figure 2 Microstructure of the investigated Fe-3wt%Si steel: pure ferritic structure with a grain size of about 300 µm.

2.2 Fatigue Crack Growth Rate test

The FCGR tests were carried out both in air and under in-situ electrochemical charging conditions at room temperature. The specimens were cathodically charged in a 0.1M

Na2SO4 electrolyte with a constant potential of -1400 mV_{SCE}. Multimeters were used during the whole test in order to check the values and keep the circuit run as designed. In the electrochemical system, the specimens were used as working electrode, Pt was used as counter electrode and the reference electrode was chosen to be the saturated calomel electrode (SCE, $Hg/HgCl_2$). The FCGR test was started as soon as the electrochemistry system started running and no pre-charging was applied. Based on the classical diffusion model [43], the H can diffuse over a distance of about 10 μm (the estimated deformation zone size) within 10^{-2} s due to the relatively high diffusivity in BCC (assumed as 10^{-5} ~10^{-4} cm^2/s). It is thus assumed that the H was saturated in the plastic deformation zone ahead of the crack-tip during the whole test. The experimental setup is schematically shown in Figure 3.

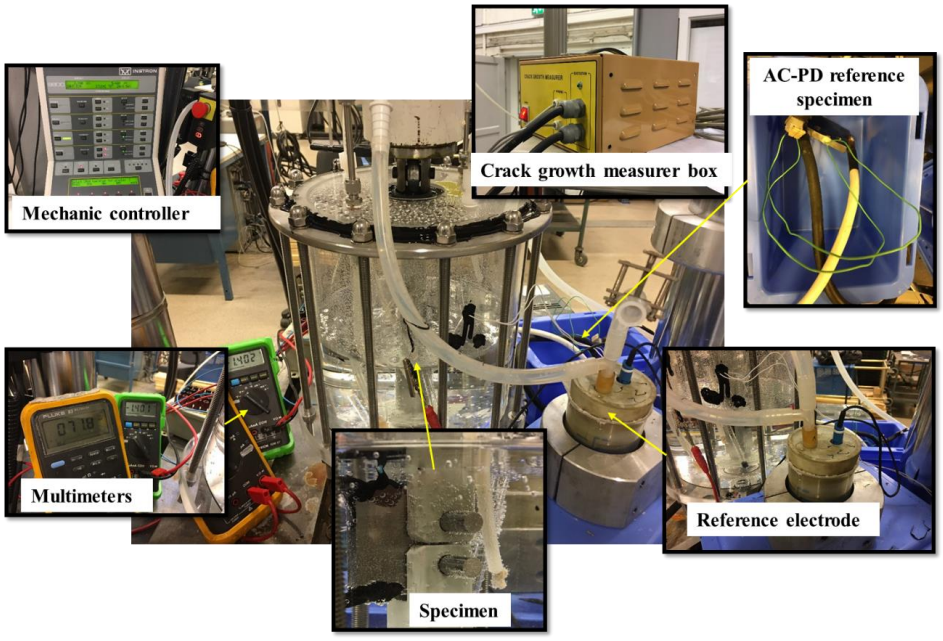

Figure 3 A schematic of the experimental setup. The key parts are pointed out.

The test frequency f was chosen to be 0.1 Hz, 1 Hz and 10 Hz. The load ration R = 0.5 was adopted to reduce the crack closure effect. The crack length a was measured from the center of the holes (where the load was applied) to the crack tip, as shown in Figure 1. Before tests, a pre-crack was produced by fatigue according to the procedure described in Ref.[44]. First, a lower bound threshold stress intensity factor, i.e. ΔK_{th}, ranging from 10-12 MPa √m was used to initiate the crack from the notch. Then a

reduction in the ΔK value of 5% was adopted stepwise until the target K-value was reached, and the crack growth stabilized. Typically, these pre-cracks were in the range of 2~4 mm after approximately 500 000 cycles for this material. It should be noted that after pre-cracking, most of the specimens presented the typical "fingernail" shapes in the fracture surface inherent to the different stress state and stress triaxiality through the specimen's thickness. The start and stop position measurements were therefore obtained by averaging nine points taken along the crack front. To get the crack further growing, a 5% increase in the ΔK from the last step of pre-cracking procedure was used in order to minimize the effect of the plastic zone from the pre-cracking procedure present ahead of the crack. An alternate current-potential drop (AC-PD) crack growth rate measure box was used during the whole test to record the crack growth. At the end of the test the specimens were cracked in liquid nitrogen and the da/dN vs ΔK curves were obtained from start/stop surface measurements. By integrating the crack growth data from the AC-PD measurement over the number of cycles, the crack length can be correlated to the number of cycles, which in turn, provides the ΔK information along the crack path.

2.3 Characterization

Post-mortem SEM fractographic characterization was performed on all the fractured specimens. The FEG Quanta 650 SEM (Thermo Fisher Scientific Inc., USA) was operated at 20 kV acceleration voltage with an aperture size of 50 µm. Measurements on the fracture surfaces were done by using the in-built software. In addition, to investigate the dislocation structures below the fracture surface, Electron Channeling Contrast Imaging (ECCI) was conducted with a solid-state four-quadrant Back-Scatter Electron (BSE) detector in the same SEM on the cross-section of the specimen, as indicated by the arrows in Figure 1. It is worth noting that the observation surface of the ECCI characterization was from the mid-thickness cross-section of the broken specimen, which was experiencing more plane-strain condition during the tests. The ECCI technique adopts the backscatter electron signal and forms contrast based on the local orientation. When the grain matrix is in the channeling condition (dark contrast), the crystal defects such as dislocations, twins and stacking faults can appear as bright contrast due to the local orientation change. The resulting images look similar as the micrographs from dark-field imaging in transmission electron microscopy (TEM). This

technique has shown its capability in studying HE related deformation information in a variety of materials with satisfying results [25, 45-49]. The theoretical and practical details of the ECCI technique can be found in Ref [50].

3. Results

3.1 Fatigue crack growth rate test

Fatigue crack growth rate testing on the Fe-3wt%Si were performed in air (R=0.5; f=10 Hz) and under in-situ cathodic charging conditions (R=0.5; f=0.1, 1 and 10 Hz). The resulting FCGR curves are shown in Figure 4. Additionally, some data on gaseous H_2 charged FCGR tests of pure Fe were added from Ogawa et al. [51] for reference, and this reference showed a similar mechanical performance range between these two different materials and therefore could give a validation of the tests presented in this work. However, since the charging conditions as well as the loading conditions are not exactly the same, no direct comparison between the behaviors could be made to predict the behaviors of these two different materials, and this reference is only used to show the similar degradation tendency in the mechanical performance of these two similar materials in H environment. The Fe-3wt%Si specimens tested under cathodic H-charging conditions exhibited a higher FCGR than the one tested in air. The H-enhanced acceleration featured a strong dependency with respect to the test frequency: the lower the frequency was, the more pronounced acceleration in the FCGR. The Paris' law parameters obtained from the curves were summarized in Table 2. The presence of H induced an acceleration in crack growth of about 1000 times while the low variation in m values indicated rather a shifting of the curves, i.e. the effect of H was independent on the ΔK level when focusing on the Paris' domain. It should be noted that the 1000 times acceleration was based on the frequency dependency when we compared the test with 0.1 Hz under cathodic H-charging and the reference test in air. However, if we focus on the test with 1 Hz loading frequency, the acceleration factor was about 30 times, which is approximately the same as the tests on pure Fe by Ogawa et al. [51].

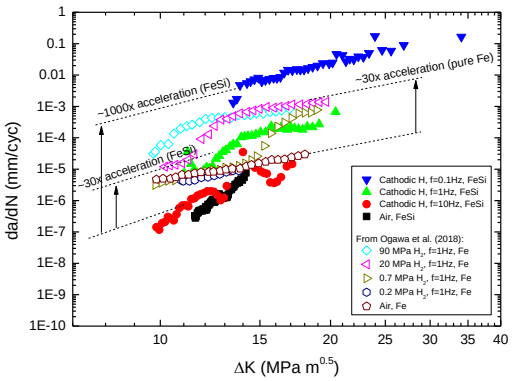

Figure 4 da/d*N* - Δ*K curves of the investigated Fe-3wt%Si steel under different environments. The pure Fe data under gaseous H_2 charging conditions were adopted from Ogawa et al. [128] for comparison.*

Table 2 The fitted Paris' parameters of the investigated Fe-3wt%Si steel.

Test condition	*C'*	*m*
Air, *R*=0.5, *f*=10 Hz	3E-17	7.890
H, *R*=0.5, *f*=10 Hz	3E-15	7.898
H, *R*=0.5, *f*=1 Hz	5E-13	6.986
H, *R*=0.5, *f*=0.1 Hz	7E-9	5.048

3.2 Statistical analysis on fractography

When it came to the fractography analysis, three different regions were identified for each specimen (see Figure 5a): the EDM region, the fatigue pre-cracked region and the stable FCG region. In order to have a consistent and reliable measurement methodology, 1 mm from the measured "start" and "stop" line was removed as well as from the specimen flanks: only the central part enclosed by yellow dashed lines was considered for detailed fractography analysis. This region was schematized through a 0.6 mm grid and the features at the nodes were considered as representative of the mechanism and taken into statistics by their area fraction. The fractographic features were, according to their main appearances, divided in three different categories: transgranular (TG), intergranular (IG) and "quasi-cleavage" (QC) features. TG zones are characterized by the traditional ductile striation whose main directions are mostly aligned with the global crack growth testing direction (see Figure 5b). IG features reveal grain-boundary-like surfaces (see Figure 5c) while "QC" features are normally showing facets and smooth

area between striations, sometimes accompanied by river-marks (Figure 5d). It is worth noting that the "QC" features are different than the pure cleavage fracture features. Cleavage features are normally flat and featureless fracture surfaces or contain some river-marks. And the cleavage features are always strictly along some specific crystallographic planes (in the case of BCC materials, along {100} planes). The "QC" features, however, are not strictly along such planes.

The statistical distribution of the aforementioned fracture zones within the specimens tested under H-charging conditions were plotted in Figure 6 against the ΔK level over the whole tested area (Figure 6a) and focusing at a common ΔK range for all three specimens (Figure 6b) to ease a direct comparison. It is evident that the fracture modes are quantitatively strongly dependent on the test frequency and the ΔK level. When the ΔK level increased, the fracture mode changed from TG to "QC", while IG type fracture took only a small fraction and did not change significantly. The same trend could be observed when the load frequency became lower. When focusing at the same ΔK level, a lower frequency gave a higher fraction of "QC" fracture and a smaller fraction of TG fracture, but IG type fracture remained similar for all frequencies by a minor fraction.

The analysis of the striation morphology exhibited in the different specimens indicates a different striation appearance in relation to the different fracture modes and depending on the environmental conditions. Striations from TG zones are denser and deeper (Figure 7) indicating a strong plastic development in front of the crack during the load cycle and the crack advance while the ones featured in the "QC" fracture zones are sparser (Figure 8), and with much smaller crests. In IG zones, no striations were observed (Figure 9).

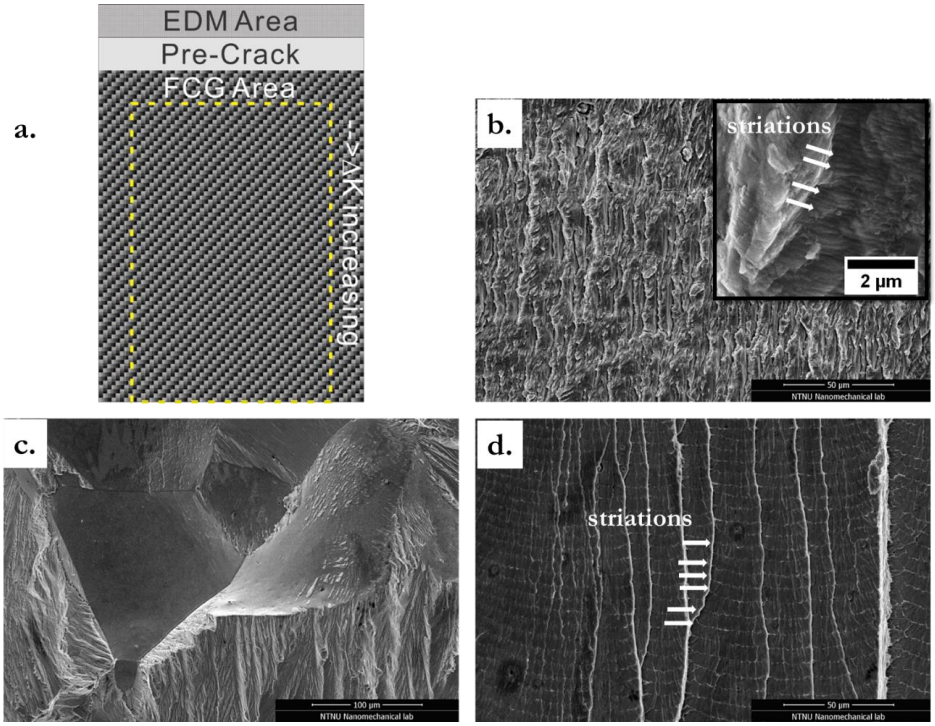

Figure 5 ***a****. schematic description of the statistical analysis;* ***b****. typical TG fracture surface with a close-up sub-figure;* ***c****. typical IG fracture surface;* ***d****. typical "QC" fracture surface. The striations are highlighted by white arrows.*

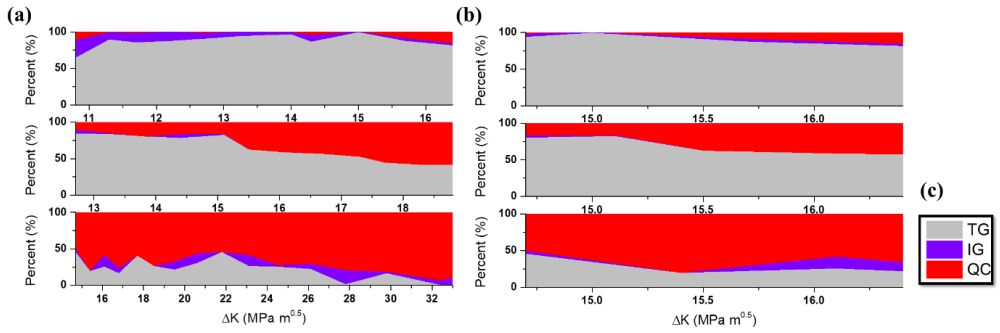

Figure 6 Fracture mode statistical distribution vs. ΔK level (a) over the whole tested area and (b) focusing at the same ΔK range. (c) is the legend for all plots.

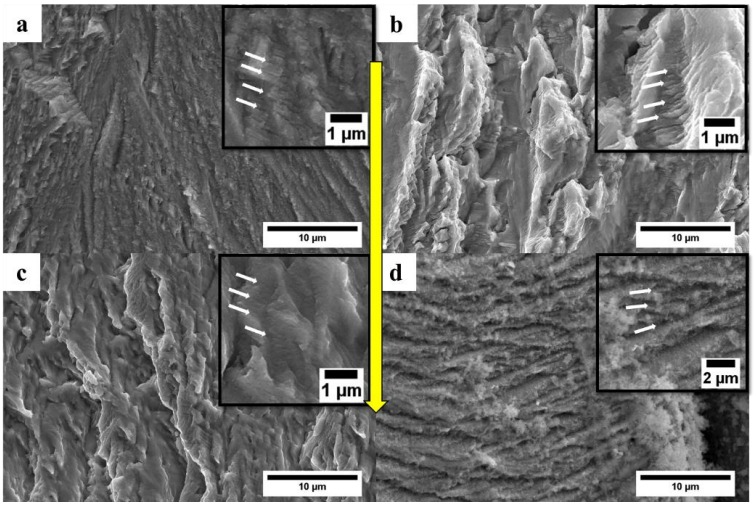

*Figure 7 Fatigue striations in TG fracture zones with corresponding magnified subsets (**a**. in Air; **b**. in H, f = 10 Hz; **c**. in H, f = 1 Hz; **d**. in H, f = 0.1 Hz). The yellow arrow shows the global fatigue crack growth direction. White arrows show the striations.*

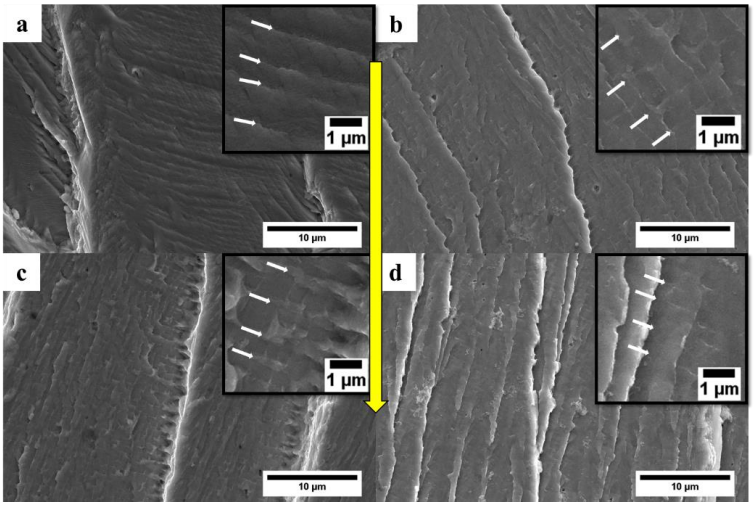

*Figure 8 Fatigue striations in "QC" fracture zones with corresponding magnified subsets (**a**. in Air; **b**. in H, f = 10 Hz; **c**. in H, f = 1 Hz; **d**. in H, f = 0.1 Hz). The yellow arrow shows the global fatigue crack growth direction. White arrows show the striations.*

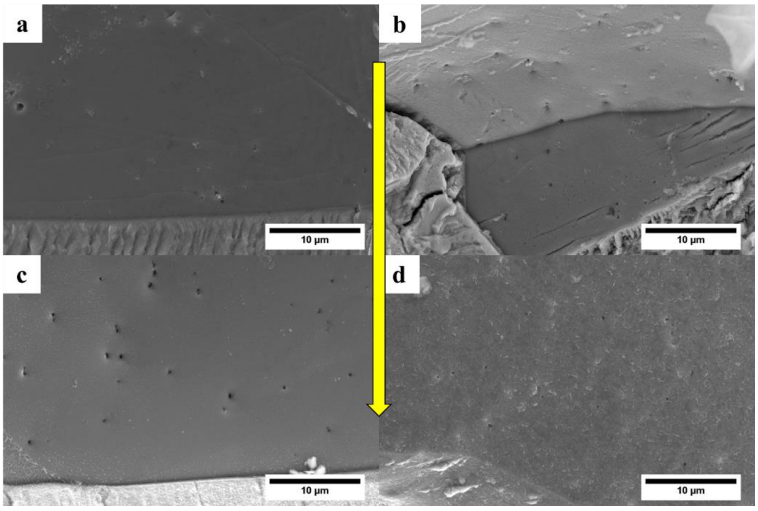

*Figure 9 IG fracture zones (**a**. in Air; **b**. in H, f = 10 Hz; **c**. in H, f = 1 Hz; **d**. in H, f = 0.1 Hz). The arrow shows the global fatigue crack growth direction.*

3.3 Dislocation structures

ECCI investigations were performed for both H-free (reference air test) and H-charged (the most significantly accelerated condition at f=0.1 Hz) conditions at similar ΔK levels in order to unveil the dislocation structures below the fracture surface. The H-free cases consist of fracture features only in TG manner, thus the area below the TG feature in the H-charged case which experienced the same K level were also subjected to investigation for the sake of comparison. The preliminary results are shown in Figure 10. Clearly, a plastic zone can always be observed under the fracture surface, meaning the FCG procedure was accompanied by plastic deformation mechanisms, but the plastic zone has a different appearance between the specimens with and without H-charging. At the investigated common ΔK level (14~17 MPa √ m), the air tested specimen always shows dislocation cells that were emanated from the fracture surface. The dislocation density became lower when it goes further from the fracture surface, but the majority of dislocations tend to form highly-densed dislocation walls (HDDWs) in the investigated areas. On the contrary, although a plastic zone was also observed under the fracture surface of the H-charged specimen, the dislocations did not prefer to form well-structured walls but rather distributed individually or at least less organized. At the highest ΔK level investigated (17 MPa √ m), the dislocations in the H-charged

specimen started to organize, but only a single tangling direction could be seen, as shown in Figure 10f, and no complete dislocation cells could be observed. These results showed a convincing proof of the H effect on the dislocation activities during FCG.

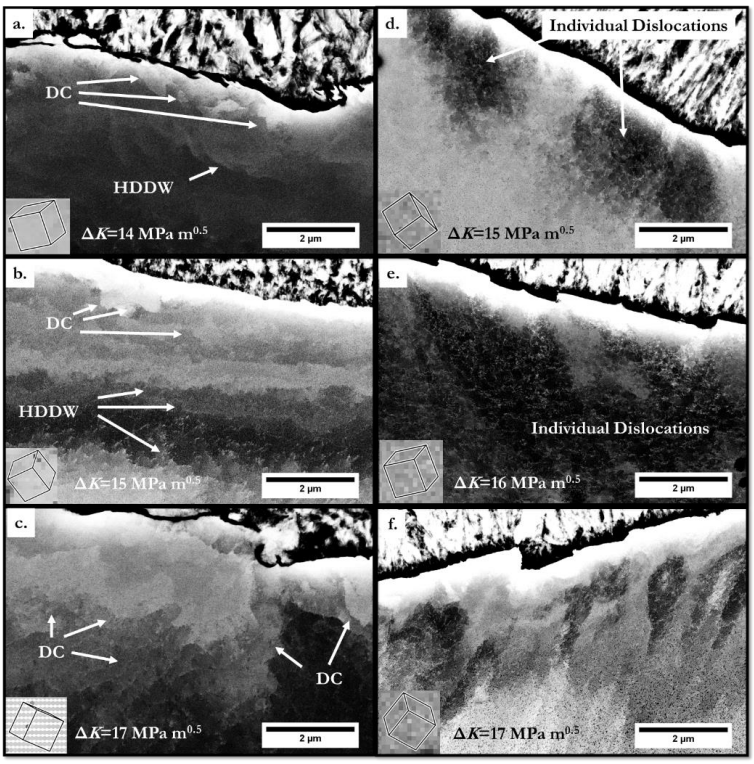

*Figure 6 Dislocation structures below the fracture surface after FCGR testing with features highlighted (**a-c**. reference test in air; **d-f**. with cathodic H-charging, R=0.5, f=0.1 Hz). DC: dislocation cell. HDDW: highly densed dislocation wall. The global FCG direction is from left to right. The ΔK levels and representative unit cells are indicated in each sub-figure.*

4. Discussion

4.1 Paris' law

The Paris' relation was used to describe the FCG behavior at macroscale viewpoint in coincidence with the linear regime or stable crack growth regime, just as shown in Figure 4. A general phenomenon is that "QC" type fracture gave a faster crack growth rate (higher d*a*/d*N* value) while that for TG type fracture was slower (lower d*a*/d*N* value). The shift from a TG to "QC" mechanism determined the enhanced FCGR in presence of H as the testing frequency was decreased from 10 Hz to 0.1 Hz.

For FCG tests in Air, the fracture mode could remain similar all over the specimen without strong change in mechanism, and the parameters in the Paris' relation could be linked more easily to the fracture feature (da/dN). Therefore, the Paris' law holds the mathematically simple linear relation for most of the crack path. However, when tested in H environment, the fracture mode was changed by the effect of H, which determined the local fracture mechanism and consequently the appearance of the fracture surface, and thus, it cannot be simply described by the single mathematical relation. That is to say, it is difficult to link the microstructural features to the Paris' parameters. To the authors' knowledge, there is no report correlating the Paris' parameters to the dislocation activities, especially with H influence. However, since the global FCGR is an averaged value over a large area comparing to single striations, the Paris' law still holds at the continuum level.

Hence, it can be concluded that the Paris' law can describe the global mechanical FCG data in a satisfactory manner, but it is difficult to describe the local FCG behavior at microscale, especially when special environmental conditions apply.

4.2 FCGR behavior in air

The da/dN - ΔK curve showed a typical Paris' regime of the specimen tested in Air environment. The general features in the fracture surface are mainly TG type, revealing good ductility of this material. These findings are consistent with most other studies on the similar Fe-Si alloy system [37-41, 52-54]. A rather limited fraction of IG type fracture indicated that grain boundaries (GBs) were not significant vulnerable places for this material when subjected to H environment. This was confirmed in a previous work by Hajilou et al. [55] that the GB in Fe-3wt%Si was not a favored path for crack growth after their test of bending a micro-cantilever with a notch on a GB. They found that the crack generated from the notch would rather propagate along the direction with the highest degree of stress concentration rather than along the GB, whether in vacuum or in H environment. When the GB was placed beneath the notch (technically, it was the notch fabricated above the GB), the position of stress concentration could be influenced by the GB, while the crack still extended following the concentration direction but not exactly the GB direction. From this investigation, it can be concluded that the GB of this material is not the preferred cracking path under monotonic loading and is not sensitively susceptible to HE, such that the crack cannot propagate via the

interface opening mechanism. Since fatigue crack generally grows via ductile mechanisms even along a microstructural interface, it is reasonable to think that IG fracture is even more difficult in the FCGR testing. Furthermore, the dimension of the micro-cantilever testing in [55] can roughly present the case of a single cycle in the present FCGR testing. From these aspects, it is assumed that the GB in the investigated material has a relatively good resistance against IG cracking both in H-free and in H-charged environments. This assumption agrees well with the fractography analysis that the IG feature fraction was not changed significant with different H-charging conditions.

4.3 H-affected fatigue crack growth rate

In the H-charged specimens, the distance between fatigue striations was measured and verified with the global da/dN data from the FCGR test. When measuring the distances, a specific area with a certain ΔK value was located, and a line was drawn along the direction perpendicular to the striations (referring to the local crack growth direction). The distance between striations was then calculated to be the length of the line over the number of striations (normally around 20 striations were counted per measurement). For each specific ΔK value, at least five different areas with clear striations were measured to reduce the occasional error. It is found that the distance between striations (considered as the local crack extension per cycle, da/dN) in the "QC" fracture zones is always several times higher than the globally measured da/dN data, while that in the TG fracture zones is approximately the same or a little bit smaller than the measured global da/dN data, independent of the testing frequency. The measurement was subjected to the same ΔK range and the result is shown in Figure 11. It suggests that the different fraction of the "QC" feature should be responsible for the global enhancement of the FCGR. And the fraction of the "QC" has a dependency on the loading frequency. In the studied loading frequency range (0.1 ~ 10 Hz), a lower frequency gives a larger fraction of the "QC" features. IG type fracture was also not so common in H-charged specimens, suggesting that GB is not the most critical material feature with respect to HE in this material.

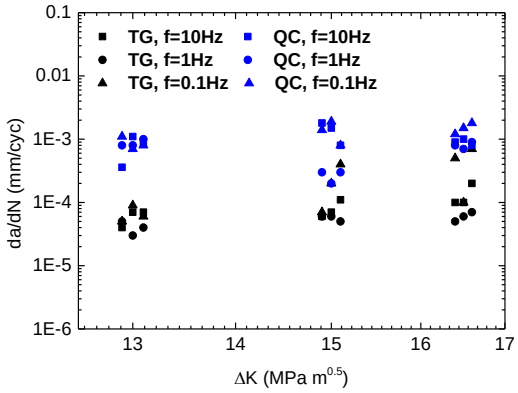

Figure 11 Striation distance vs. ΔK level in different fracture modes.

It has been observed in other works that H can change the fatigue fracture mode from ductile striations to brittle cleavage facets. Marrow et al. [56] discussed this phenomenon intensively in 1992. They proposed that H can be trapped to the intensive stress field ahead of the crack tip, arresting the sharp cleavage crack and blunting the crack. This procedure will be repeated during cyclic loading and make the cleavage fracture surface shown as facets. Vehoff [40] observed similar structures in Fe-2.6%Si single crystals. It is considered that under gaseous H2 environment, the crack grows stably in a stepwise micro-cleavage manner as well as through enhanced dislocations emission from the crack tip. This was proposed to explain the sharp cleavage fracture structure. Several works have observed similar features in low carbon steels [57-59] and Fe-Si alloys [60], subjected FCG tests in H_2 gaseous environments. Most of these proposals were based on the cleavage fracture behavior. In this work, however, no solid proof showed the cleavage fracture manner. According to the grain orientation information shown in Figure 10, the fracture surfaces were not consistently parallel to the cleavage {100} planes of the grains. One reason could be that the H concentration produced by the in-situ cathodic charging was not high enough to activate the cleavage fracture manner of this material. To prove this hypothesis, the diffusion condition and electrochemical processes should be analyzed in detail, and this analysis will be conducted in a future work.

Similar tests on pure iron and low carbon steels were done recently in a similar manner subjected to gaseous H2 environment [61, 62]. The fracture behaviors were identical to

what was observed in the present study. It was explained that H can be transported by mobile dislocations based on the hypothesis of the HELP mechanism [5, 63], and the formation of dislocation tangles can give a local enhancement of the H concentration, leading to H-assisted cracking. This description seemed to be a "black box" in explaining the formation of the "QC" fracture feature. Basically, they linked the more brittle "QC" fracture feature directly to the local H concentration. Under this assumption, more "QC" fracture should be observed along the dislocation cell boundaries since more H was trapped there. According to the dislocation structure characterization results in the present work (Figure 10), the dislocations became less tangled when H was charged, meaning that H did affect the deformation structures during FCG. This effect of H agreed with a previous report on Ni [3]: when H was introduced to the Ni specimen, the dislocations moved out of the cell wall into the cell matrix within two seconds upon 150 torr gaseous H2 charging. One possible mechanism could be that H tried to stop the dislocation sub-structure evolution during deformation, and the crack blunting by dislocation motion was suppressed and thus the crack became sharper. According to the basic linear elastic fracture mechanics theory, sharper cracks could make the local stress intensity higher and consequently, a faster crack growth could be expected.

Now attention should be paid to why the dislocation structure was changed by H. One possible explanation put forward by Wang et al. [4] was that the presence of H would enhance the velocity of dislocations, as already confirmed in some previous works by means of in-situ TEM with the help of environmental cells [7]. The attachment of H atoms to the dislocations would change the local stress field of the dislocations, resulting in the enhancement of dislocation mobility in some directions while suppressing the motion in other directions. Consequently, the dislocation celling procedure could not be realized but instead, more isolated dislocations in specific directions should be observed. This explanation agreed with the present results in Figure 10. However, the present results could not give a comprehensive understanding on the influence of H on the specific dislocation motion directions due to several reasons. Firstly, the investigated material was a large-grained polycrystalline material so that the local stress state could be different from place to place at grain scale. Secondly, the tested specimen experienced different stress state through the thickness direction. The investigated results were from the mid-thickness cross-section that

experienced more plane-strain condition, which might give some difference to other works since most researches were focusing on the surface area which had more plane-stress condition. Thirdly, the diffraction condition of the ECCI investigations in this work was not under fully control, and some crystallographic directions in the images were not indexed. To solve these problems, new study by using single crystalline specimens with defined stress condition combined with high-resolution TEM technique was encouraged. Due to technical limitations, this could not be realized in this work.

It is interesting to note that although a similar mechanical performance (c.f. Figure 4) was observed on pure Fe [51], the dislocation structures, however, showed strongly different appearances as to the present study. The major dislocation structures in pure Fe in Ref. [51] were dislocation cells independent on the H-charging conditions, while in the investigated Fe-3wt%Si steel, dislocation cells appeared only in the air tested specimen. Several reasons could contribute to this difference. Firstly, pure Fe is mechanically softer than Fe-3wt%Si since the Si, as a substitutional element, hardens the matrix by solid solution hardening mechanism [64]. Under the same load, the dislocations in the softer pure Fe could be organized into cells more easily than in the harder Fe-3wt%Si steel since the dislocation motion in softer materials is more pronounced than in harder materials. When H was charged into the system, the matrix could further be hardened by H atom since this element could serve as interstitial element and cause solid solution strengthening. As a result, the H-charged specimen might have less possibility in the dislocation cell formation. Secondly, the dislocation cell formation is strongly associated with dislocation activities that depend on the stacking fault energy (SFE), for example the cross-slip and climbing procedures. A general rule is that when the SFE is high, dislocations are easily remained as full dislocations during deformation and the cross-slip and climbing procedures are more pronounced. As a result, dislocations cells could be formed more easily [43]. Regarding the present study, the SFE of ferrite was reduced by adding Si [65]. Therefore, the Fe-3wt%Si steel was expected to have less cell formation than the pure Fe due to this SFE difference. If we focus on the H-free case for both of these two works, the present Fe-3wt%Si showed the cell formation up to about 5 μm under the fracture surface, while the pure Fe in [51] showed all features as dislocation cells through the investigation range of more than 10 μm. From this comparison, it might be inferred that the SFE played a role in the dislocation structure formation. By simply adding Si or H into the

system, the dislocation sub-structure did not change significantly. Nevertheless, when both Si and H were introduced, the dislocation cells disappeared. Since both Si and H have the effect of decreasing the SFE of the system, this could be considered as a reason for this evolution. To prove this proposal, researchers working in the numerical methods are encouraged to give a contribution since it is technically challenging for the experimentalists. Thirdly, we showed the results with respect to the loading frequency change while the results in [51] mainly focused on the amount of H by changing the H2 gas pressure. Although both cases could give the dependency on the H amount, the mechanisms of H-uptake were different. Furthermore, the results of H-charged specimen in Figure 10 were from the test at f=0.1 Hz, while the results in [51] were mainly from the tests at f=1 Hz, by which comparison it could make the H-uptake difference even more significant. From the mechanical behavior, the Fe-3wt%Si in the present work showed a more pronounced acceleration in the FCGR (up to 1000x) than the pure Fe in [51] (up to 30x), and this might indicate that the H was influencing the Fe-3wt%Si more severely than the pure Fe in Ref [51] under the tested conditions. Hence, it could be inferred that the different dislocation structures came from the different H amount: a more significant H influence could lead to less dislocation cell formation. In summary, the dislocation structure difference between Fe-3wt%Si and pure Fe could be reasoned as the influence from strength, SFE and H-charging. Nevertheless, the difference in the H fugacity in different materials as well as under different charging conditions could give contribution to the deformation structure evolution and due to limitations in the techniques and time, only qualitative comparisons could be provided in the present work. For more detailed quantitative analysis, researchers in the field of numerical methods and with more advanced devices are encouraged to shed some light on this topic.

4.4 Frequency effect

The fracture modes as a function of ΔK level and crack propagation for different frequencies were measured as described in 3.2 and the resulting map is shown in Figure 6. It is clearly shown in this map that the frequency of the fatigue test yields strong change in the fracture modes. When a low frequency (0.1 Hz) was applied, the “QC” type dominated in the fracture surface, and when a high frequency (10 Hz) was applied, the TG type dominated, while an intermediate frequency (1 Hz) gives the result in

between. In other words, the lower the test frequency, the more the time for H to diffuse toward the highly stressed zone at the crack tip, the more pronounced is the measured acceleration in the FCGR. Since the diffusivity of H in BCC structure is commonly considered as high (diffusion coefficient of H in α-Fe is about 10^{-5}~10^{-4} cm^2/s, according to Refs [20-23]), such that the time for H diffusion into the deformation structure is short enough to be neglected, the procedure of H interaction with deformation structure is considered as a time-dependent process.

5. Conclusions

The effect of H on fatigue crack growth behavior in a Fe-3wt%Si alloy under in-situ electro-chemical H charging condition was studied. The fracture modes distribution was statistically summarized along the crack growth path and the effect of testing frequency on the fracture mode transition was discussed. Some conclusions are drawn as follows:

- The H-assisted FCGR was revealed by means of in-situ cathodic charging on a Fe-3wt%Si steel. The H-charging could enhance the FCGR by up to 1000 times compared to the reference test in lab air, depending on the test frequency.
- The Paris' law could satisfactorily describe the FCGR behavior of a specimen at continuum level but cannot precisely describe the local behavior at microstructure level, especially when special environmental conditions applied.
- Post-mortem fractography clearly showed a shift in crack growth mechanisms: the FCG mode of the investigated material changed from TG to "QC" type; IG type fracture was not common in this material, indicating that the GB in this material was not the preferred path for crack propagation.
- The investigated dislocation structures below the fracture surface suggested that H can give a negative effect on the dislocation cell formation. This phenomenon was explained by the enhancement of dislocation mobility in specific directions.
- The test results confirmed the time-dependent nature of the H-deformation interaction: in the tested frequency range (0.1 Hz – 10 Hz) in H environment, a lower frequency would lead to more significant enhancement of the FCGR.

An ideal prospect would be an in-situ investigation on a specimen with most parameters well-defined. This has been planned by the present authors and would be realized in a future work.

Acknowledgement

This work was financially supported by the Research Council of Norway (Petromaks2 Program, Project No. 244068/E30, HyF-Lex).

Reference

[1] Hirth JP. 1980 Institute of Metals Lecture the Metallurgical-Society-of-Aime - Effects of Hydrogen on the Properties of Iron and Steel. Metallurgical Transactions a-Physical Metallurgy and Materials Science. 1980;11:861-90.

[2] Robertson IM, Birnbaum HK, Sofronis P. Hydrogen Effects on Plasticity. In: Hirth JP, Kubin L, editors. Dislocations in Solids. first ed. Amsterdam: Elsevier; 2010. p. 249-93.

[3] Robertson IM, Birnbaum HK. An Hvem Study of Hydrogen Effects on the Deformation and Fracture of Nickel. Acta Metall. 1986;34:353-66.

[4] Wang S, Nagao A, Sofronis P, Robertson IM. Hydrogen-modified dislocation structures in a cyclically deformed ferritic-pearlitic low carbon steel. Acta Mater. 2018;144:164-76.

[5] Beachem CD. A new model for hydrogen-assisted cracking (hydrogen "embrittlement"). Metall Mater Trans B. 1972;3:441-55.

[6] Birnbaum HK, Sofronis P. Hydrogen-enhanced localized plasticity—a mechanism for hydrogen-related fracture. Mater Sci Eng, A. 1994;176:191-202.

[7] Robertson IM. The effect of hydrogen on dislocation dynamics. Eng Fract Mech. 1999;64:649-73.

[8] Gangloff RP. Critical issues in hydrogen assisted cracking of structural alloys. In: Shipilov SA, Jones RH, Olive J-M, Rebak RB, editors. Environment-Induced Cracking of Materials. Amsterdam: Elsevier; 2008. p. 141-65.

[9] Gerberich WW, Marsh PG, Hoehn JW. Hydrogen Induced Cracking Mechanisms - Are There Critical Experiments? In: Thompson AW, Moody NR, editors. Hydrogen

Effects in Materials. Warrendale, Pennsylvania, USA: Minerals, Metals & Materials Society (TMS); 1996. p. 539-54.

[10] Oriani RA. Whitney Award Lecture—1987:Hydrogen—The Versatile Embrittler. Corrosion. 1987;43:390-7.

[11] Oriani RA, Josephic PH. Equilibrium and kinetic studies of the hydrogen-assisted cracking of steel. Acta Metall. 1977;25:979-88.

[12] Lynch SP. Environmentally Assisted Cracking - Overview of Evidence for an Adsorption-Induced Localized-Slip Process. Acta Metall. 1988;36:2639-61.

[13] Bilotta G, Henaff G, Halm D, Arzaghi M. Experimental measurement of out-of-plane displacement in crack propagation under gaseous hydrogen. Int J Hydrog Energy. 2017;42:10568-78.

[14] Peralta P, Laird C. Fatigue of Metals. In: Laughlin DE, Hono K, editors. Physical Metallurgy (Fifth Edition). Amsterdam: Elsevier; 2014. p. 1765-880.

[15] Depover T, Laureys A, Perez Escobar D, Van den Eeckhout E, Wallaert E, Verbeken K. Understanding the Interaction between a Steel Microstructure and Hydrogen. Materials (Basel). 2018;11.

[16] Depover T, Pérez Escobar D, Wallaert E, Zermout Z, Verbeken K. Effect of hydrogen charging on the mechanical properties of advanced high strength steels. Int J Hydrog Energy. 2014;39:4647-56.

[17] Depover T, Verbeken K. Evaluation of the role of Mo2C in hydrogen induced ductility loss in Q&T FeCMo alloys. Int J Hydrog Energy. 2016;41:14310-29.

[18] Depover T, Verbeken K. Hydrogen trapping and hydrogen induced mechanical degradation in lab cast Fe-C-Cr alloys. Mater Sci Eng, A. 2016;669:134-49.

[19] Kanezaki T, Narazaki C, Mine Y, Matsuoka S, Murakami Y. Effects of hydrogen on fatigue crack growth behavior of austenitic stainless steels. Int J Hydrog Energy. 2008;33:2604-19.

[20] Wang S, Hashimoto N, Ohnuki S. Effects of hydrogen on activation volume and density of mobile dislocations in iron-based alloy. Mater Sci Eng A. 2013;562:101-8.

[21] Araújo DF, Vilar EO, Palma Carrasco J. A critical review of mathematical models used to determine the density of hydrogen trapping sites in steels and alloys. Int J Hydrog Energy. 2014;39:12194-200.

[22] Lynch S. Hydrogen embrittlement phenomena and mechanisms. Corros Rev. 2012;30:105-23.

[23] Bruzzoni P, Carranza RM, Collet Lacoste JR, Crespo EA. Hydrogen diffusion in α-iron studied using an electrochemical permeation transfer function. Electrochim Acta. 1999;44:2693-704.

[24] Koyama M, Akiyama E, Sawaguchi T, Ogawa K, Kireeva IV, Chumlyakov YI, et al. Hydrogen-assisted quasi-cleavage fracture in a single crystalline type 316 austenitic stainless steel. Corros Sci. 2013;75:345-53.

[25] Koyama M, Springer H, Merzlikin SV, Tsuzaki K, Akiyama E, Raabe D. Hydrogen embrittlement associated with strain localization in a precipitation-hardened Fe-Mn-Al-C light weight austenitic steel. Int J Hydrog Energy. 2014;39:4634-46.

[26] Koyama M, Yamamura Y, Che RQ, Sawaguchi T, Tsuzaki K, Noguchi H. Comparative study on small fatigue crack propagation between Fe-30Mn-3Si-3Al and Fe-23Mn-0.5C twinning-induced plasticity steels: Aspects of non-propagation of small fatigue cracks. Int J Fatigue. 2017;94:1-5.

[27] Demetriou V, Robson JD, Preuss M, Morana R. Study of the effect of hydrogen charging on the tensile properties and microstructure of four variant heat treatments of nickel alloy 718. Int J Hydrog Energy. 2017;42:23856-70.

[28] Yu HY, Olsen JS, Olden V, Alvaro A, He JY, Zhang ZL. Cohesive zone simulation of grain size and misorientation effects on hydrogen embrittlement in nickel. Eng Fail Anal. 2017;81:79-93.

[29] Zhang ZB, Obasi G, Morana R, Preuss M. Hydrogen assisted crack initiation and propagation in a nickel-based superalloy. Acta Mater. 2016;113:272-83.

[30] Carroll MC, Carroll LJ. Developing Dislocation Subgrain Structures and Cyclic Softening During High-Temperature Creep–Fatigue of a Nickel Alloy. Metall Mater Trans A. 2013;44:3592-607.

[31] Luo H, Li Z, Lu W, Ponge D, Raabe D. Hydrogen embrittlement of an interstitial equimolar high-entropy alloy. Corros Sci. 2018;136:403-8.

[32] Zhao Y, Lee D-H, Lee J-A, Kim W-J, Han HN, Ramamurty U, et al. Hydrogen-induced nanohardness variations in a CoCrFeMnNi high-entropy alloy. Int J Hydrog Energy. 2017;42:12015-21.

[33] Li Z, Raabe D. Influence of compositional inhomogeneity on mechanical behavior of an interstitial dual-phase high-entropy alloy. Mater Chem Phys. 2017.

[34] Taylor GI, Elam CF. The Distortion of Iron Crystals. Proc R Soc London, Ser A. 1926;112:337-61.

[35] Christian JW. Some surprising features of the plastic deformation of body-centered cubic metals and alloys. Metall Mater Trans A. 1983;14:1237-56.

[36] Vitek V, Mrovec M, Bassani JL. Influence of non-glide stresses on plastic flow: from atomistic to continuum modeling. Mater Sci Eng, A. 2004;365:31-7.

[37] Vehoff H. Untersuchung der duktilen und quasispröden zyklischen Rißausbreitung in Fe-3%-Si-Einkristallen. Aachen: RWTH Aachen; 1977.

[38] Vehoff H, Neumann P. In situ sem experiments concerning the mechanism of ductile crack growth. Acta Metall. 1979;27:915-20.

[39] Vehoff H, Neumann P. Crack propagation and cleavage initiation in Fe-2.6%-Si single crystals under controlled plastic crack tip opening rate in various gaseous environments. Acta Metall. 1980;28:265-72.

[40] Vehoff H, Rothe W. Overview .30. Gaseous-Hydrogen Embrittlement in Fesi-Single and Ni-Single Crystals. Acta Metall. 1983;31:1781-93.

[41] Vehoff H. Rißbildung und Rißausbreitung in Ein- und Bikristallen. Düsseldorf1994.

[42] Vehoff H, Nykyforchyn A. Fatigue crack nucleation at grain boundaries – experiment and simulation. Z Metallk. 2003;94:682-6.

[43] Gottstein G. Physical Foundations of Materials Science: Springer-Verlag Berlin Heidelberg; 2004.

[44] Alvaro A, Akselsen OM, Ren X, Kane P-A. Fatigue Properties of a 420 MPa Structural Steel at Low Temperature. The 25th International Ocean and Polar Engineering Conference. Kona, Big Island, Hawaii, USA2015. p. 331-7.

[45] Koyama M, Akiyama E, Tsuzaki K, Raabe D. Hydrogen-assisted failure in a twinning-induced plasticity steel studied under in situ hydrogen charging by electron channeling contrast imaging. Acta Mater. 2013;61:4607-18.

[46] Habib K, Koyama M, Tsuchiyama T, Noguchi H. Fatigue crack non-propagation assisted by nitrogen-enhanced dislocation planarity in austenitic stainless steels. Int J Fatigue. 2017;104:158-70.

[47] Koyama M, Akiyama E, Lee Y-K, Raabe D, Tsuzaki K. Overview of hydrogen embrittlement in high-Mn steels. Int J Hydrog Energy. 2017;42:12706-23.

[48] Habib K, Koyama M, Tsuchiyama T, Noguchi H. Visualization of dislocations through electron channeling contrast imaging at fatigue crack tip, interacting with pre-existing dislocations. Materials Research Letters. 2017;6:61-6.

[49] Koyama M, Akiyama E, Sawaguchi T, Raabe D, Tsuzaki K. Hydrogen-induced cracking at grain and twin boundaries in an Fe-Mn-C austenitic steel. Scr Mater. 2012;66:459-62.

[50] Zaefferer S, Elhami NN. Theory and application of electron channelling contrast imaging under controlled diffraction conditions. Acta Mater. 2014;75:20-50.

[51] Ogawa Y, Birenis D, Matsunaga H, Takakuwa O, Yamabe J, Prytz O, et al. The role of intergranular fracture on hydrogen-assisted fatigue crack propagation in pure iron at a low stress intensity range. Mater Sci Eng A. 2018;733:316-28.

[52] Yu W, Esaklul K, Gerberich WW. Fatigue threshold studies in Fe, Fe-Si, and HSLA steel: Part II. thermally activated behavior of the effective stress intensity at threshold. Metall Trans A. 1984;15:889-900.

[53] Gerberich WW, Yu W, Esaklul K. Fatigue threshold studies in Fe, Fe-Si, and HSLA steel: Part I. Effect of strength and surface asperities on closure. Metall Trans A. 1984;15:875-88.

[54] Vehoff H, Neumann P, Rothe W. Quasibrittle fracture and cleavage initiation in Fe–2·6Si single crystals in different environments. Metal Science. 2013;15:469-70.

[55] Hajilou T, Deng Y, Kheradmand N, Barnoush A. Hydrogen enhanced cracking studies on Fe-3wt%Si single and bi-crystal microcantilevers. Philos Trans A Math Phys Eng Sci. 2017;375.

[56] Marrow TJ, Cotterill PJ, King JE. Temperature Effects on the Mechanism of Time Independent Hydrogen Assisted Fatigue Crack-Propagation in Steels. Acta Metall Mater. 1992;40:2059-68.

[57] Takahashi Y, Nishikawa H, Oda Y, Noguchi H. Microscopic characterization of hydrogen-induced quasi-brittle fatigue fracture in low-strength carbon steel. Mater Lett. 2010;64:2416-9.

[58] Nishikawa H-a, Oda Y, Takahashi Y, Noguchi H. Microscopic Observation of the Brittle-Striation Formation Mechanism in Low Carbon Steel Fatigued in Hydrogen Gas. J Solid Mech Mater Eng. 2011;5:179-90.

[59] Nishikawa H-a, Oda Y, Noguchi H. Investigation of the Mechanism for Brittle-Striation Formation in Low Carbon Steel Fatigued in Hydrogen Gas. J Solid Mech Mater Eng. 2011;5:370-85.

[60] Takahashi Y, Tanaka M, Higashida K, Yamaguchi K, Noguchi H. An intrinsic effect of hydrogen on cyclic slip deformation around a {110} fatigue crack in Fe–3.2wt.% Si alloy. Acta Mater. 2010;58:1972-81.

[61] Ogawa Y, Birenis D, Matsunaga H, Thogersen A, Prytz O, Takakuwa O, et al. Multi-scale observation of hydrogen-induced, localized plastic deformation in fatigue-crack propagation in a pure iron. Scr Mater. 2017;140:13-7.

[62] Ogawa Y, Matsunaga H, Yamabe J, Yoshikawa M, Matsuoka S. Unified evaluation of hydrogen-induced crack growth in fatigue tests and fracture toughness tests of a carbon steel. Int J Fatigue. 2017;103:223-33.

[63] Robertson IM, Sofronis P, Nagao A, Martin ML, Wang S, Gross DW, et al. Hydrogen Embrittlement Understood. Metall Mater Trans B. 2015;46:1085-103.

[64] Caillard D. A TEM in situ study of alloying effects in iron. II—Solid solution hardening caused by high concentrations of Si and Cr. Acta Mater. 2013;61:2808-27.

[65] Das A. Revisiting Stacking Fault Energy of Steels. Metall Mater Trans A. 2015;47:748-68.

Paper 3

Hydrogen-enhanced fatigue crack growth in a single-edge notched tensile specimen under in-situ hydrogen charging inside an environmental scanning electron microscope

Di Wan*, Yun Deng, Jan Inge Hammer Meling, Antonio Alvaro, Afrooz Barnoush

Acta Mater. 170 (2019) 87-99, DOI: 10.1016/j.actamat.2019.03.032.

Hydrogen-enhanced fatigue crack growth in a single-edge notched tensile specimen under in-situ hydrogen charging inside an environmental scanning electron microscope

Di Wan[1,*], Yun Deng[1], Jan Inge Hammer Meling[1], Antonio Alvaro[2], Afrooz Barnoush[1]

1. Department of Mechanical and Industrial Engineering, Norwegian University of Science and Technology, Richard Birkelands vei 2B, 7491 Trondheim, Norway.

2. SINTEF Industry, 7456 Trondheim, Norway.

Abstract

Fatigue crack growth (FCG) test was done on a pre-cracked single-edge notched tensile (SENT) specimen with oligocrystalline ferritic structure. Innovative in-situ hydrogen (H)- charging by plasma inside an environmental scanning electron microscope (ESEM) was adopted to directly observe the H influence on the FCG behavior of this material. Diverse in-situ and post-mortem characterization methods including secondary electron imaging, backscatter electron imaging, electron backscatter diffraction (EBSD) and scanning probe microscopy (SPM) were used to investigate the material's behavior. It was observed that the crack growth rate was enhanced by about one magnitude when H was charged, in comparison with the reference test in vacuum (Vac). The FCG procedure was concluded as strongly associated with the plasticity evolution in the vicinity of the crack-tip. A simple model based on the restricted plasticity was proposed for the H-enhanced FCG behavior. A peculiar frequency dependency of the H-enhanced FCG behavior was observed at low loading frequencies (0.015 Hz ~ 0.15 Hz): under the same in-situ H-charging condition, a lower frequency gave a slower crack growth rate and vice versa. This behavior was explained by the thermally activated dislocation motion correlated with the plasticity shielding effect during crack growth.

Keywords: fatigue crack growth (FCG); hydrogen embrittlement; SENT specimen; EBSD; SEM.

1. Introduction

Hydrogen embrittlement (HE) has been discussed intensively for more than a century since the first document about the hydrogen (H) damage in iron and steels by Johnson in 1875 [1]. Several different mechanisms regarding various scales and aspects have been proposed, such as hydrogen-enhanced localized plasticity (HELP) [2-7], hydrogen-enhanced decohesion (HEDE) [8-11], adsorption-induced decohesion (AIDE) [12-15], hydrogen-enhanced vacancy production [16, 17] and hydrogen-induced phase transformation [18-21]. Among these mechanisms, the HELP and HEDE mechanisms gained the most attention based on diverse experimental proofs.

Another failure mechanism for engineering structures comes from cyclic loading which could lead to fatigue failure. This type of engineering failure was strongly linked to economic loss. According to statistics in 1983, the fatigue failures costed $119 billion per year from the US industry, and this number seemed to be meaningfully increasing in the recent years [22]. It is even worse when environmental conditions applied. For some large industrial structures, such as oil platforms in the sea, a combined effect of vibrational loading and extreme environmental conditions should be taken seriously. In some cases, small cracks could be formed in the structures, which lead to premature failure. As for engineers' prospect, it is of great importance to know how long the structure could still serve in such conditions without further repairing, and in academic point of view, the fatigue crack growth (FCG) behavior should be studied.

The combined effect from HE and cyclic loading has been intensively studied by a group of scientists from Kyushu University [23-28] using high pressure H2 gas on various metals. Most of the embrittled specimens showed localized deformation at the crack-tips, and based on these investigations, a model called "hydrogen-induced successive crack growth (HISCG)" has been proposed [29]. This model adopted the slip deformation localization at the crack-tip, which was in accordance with the HELP mechanism, yielding suppressed crack-tip blunting and a faster crack propagation rate. Even though this model could explain some cases, important evidences are still missing [24]. One reason is that most of the investigation results were on materials with complex structures such as mixed phases, different grain sizes, various precipitates, etc. All the impurities in the materials could make the H-effect more difficult to be interpreted. A

clear setup on clean and simple model material with least possible complexity should be proposed to support this model.

In the present study, a single-edge notched tensile (SENT) specimen was produced from an oligocrystalline ferritic Fe-3wt%Si steel and tested under low frequency cyclic loading in an environmental scanning electron microscope (ESEM) in both vacuum (Vac) condition and H-plasma charging condition. Oligocrystals are coarse-grained materials with only one grain existing through the thickness direction. By using oligocrystal, the behavior of material could be localized in a single grain and some complicated influence from crystal orientation or grain boundaries could be eliminated in certain extent. The FCG behavior was observed by the ESEM and analyzed with other scanning electron microscopy (SEM) techniques. The testing results gave a convincing proof of the HE effect from H-plasma charging and the possible mechanisms of H-enhanced FCG were discussed.

2. Materials and Experimental

The material used in this study was a Fe-3wt%Si ferritic steel. The chemical composition by weight percent is shown in Tab. 1. The raw materials were annealed at 1250 °C for four weeks followed by furnace cooling to facilitate the grain growth. The resulting material has pure ferritic structure and the final grain size is about 1~2 mm.

Tab. 1 Chemical composition of the investigated material.

Elem.	**C**	**Si**	**Mn**	**P**	**S**	**Cr**	**Ni**	**Mo**
wt.%	0.018	3.000	0.055	0.008	0.003	0.010	0.006	0.003
Elem.	**Cu**	**Al**	**Ti**	**Nb**	**V**	**B**	**Zr**	**Fe**
wt.%	0.013	0.015	0.001	0.002	0.001	0.0002	0.0010	Bal.

SENT specimens were cut from the heat-treated materials by electron discharge machining (EDM). The shape of the specimens is shown in Fig. 1. The specimen has the dimension of thickness B = 1 mm, width W = 6 mm and the gauge length L = 20 mm. A pre-crack (PC) with 1 mm length was introduced by cyclic three-point bending. Since the grain size is relatively large, only one grain exists through the thickness direction (oligocrystal). It should be noted that the tests and characterizations shown in the present paper were from a single exemplary specimen for the sake of keeping the constraints identical along the crack.

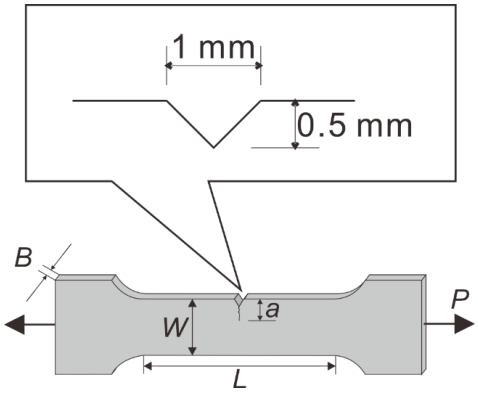

Fig. 1 The SENT specimen geometry and notch dimension.

Before testing, the specimen was characterized by electron backscatter diffraction (EBSD, Nordif EBSD system) in a Quanta 650 ESEM (Thermo Fisher Scientific Inc., USA) with an acceleration voltage of 20 kV at a working distance of about 10 mm. The normal direction inverse pole figure (ND-IPF) maps, kernel average misorientation (KAM) maps, and grain reference orientation deviation (GROD) maps were plotted over the region of interest (ROI). The results are shown in Fig. 2.

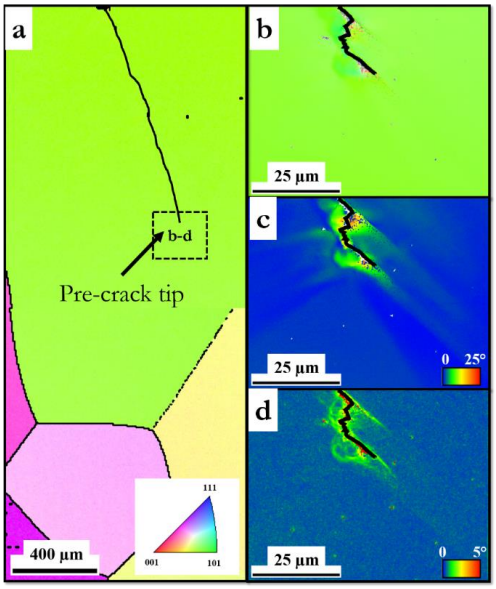

Fig. 2 EBSD maps of the investigated SENT specimen: a. ND-IPF map over the area near the PC; b. ND-IPF map over the PC tip; c. KAM map over the PC tip; d. GROD

map over the PC tip. IPF maps have the legend shown in the orientation triangle. The color scale for a and b is the same.

The FCG test was done by a tensile/ compression module (Kammrath & Weiss GmbH, Germany) inside the ESEM. The specimen was loaded at load ratio $R = 0.5$. The tensile/ compression module was operated in a load-controlled mode with an intrinsic displacement-control nature of the device. The load range was chosen such that the stress intensity factor range (ΔK) was above the empirical threshold value (ΔK_{th}) obtained from preliminary tests and increased following the stage II according to Paris' law. The cyclic loading frequencies were 0.15 Hz and 0.015 Hz, which were denoted as low frequency (LF) and ultra-low frequency (ULF), respectively, in the following text. After every 100 cycles, the specimen was unloaded to 0 N for imaging to avoid possible elastic strain influence on the image. The ESEM was operated at 30 kV accelerating voltage. Both secondary electron (SE) images and backscatter electron (BSE) images were taken. The SE images were used to check the crack length and the topography near the crack, and the BSE images were controlled to an optimum channeling contrast to reveal the plastic deformation near the crack-tip. The crack growth rate was calculated from the measured crack length over the cycles interval (100 cycles).

For simplification, the ΔK during cyclic loading was calculated based on the SENT specimen described in Ref.[30]. It was assumed the crack in this test was a type I crack (opening mode), and the stress intensity could be calculated by Eq. 1:

$$K_I = \frac{P}{B\sqrt{W}} f\left(\frac{a}{W}\right) \qquad \text{Eq. 1}$$

in which f is a dimensionless function and reads as Eq. 2.

$$f\left(\frac{a}{W}\right) = \frac{\sqrt{2\tan\frac{\pi a}{2W}}}{\cos\frac{\pi a}{2W}}\left[0.752 + 2.02\left(\frac{a}{W}\right) + 0.37\left(1-\sin\frac{\pi a}{2W}\right)^3\right] \qquad \text{Eq. 2}$$

where W is the width of the specimen, B is the specimen thickness, a is the crack length and P is the applied tensile load, as already indicated in Fig. 1.

The ΔK value is thus calculated by the following Eq. 3:

$$\Delta K = K_{max} - K_{min} \quad \text{Eq. 3}$$

where K_{max} and K_{min} are the maximum and minimum K_I values, respectively, during one loading cycle.

H-plasma charging technique was applied to study the HE effect during FCG of the studied material. An Evactron plasma source (XEI Scientific, Inc., USA) was used to ignite and inject the plasma phase into the Vac chamber from a hydrogen gas source. The source hydrogen gas was produced by a hydrogen generator using electrolysis principle from pure water. The gas flow rate was 250 ml/min. The H-charging method was the same as described in Ref. [31]. According to the report from XEI Scientific Inc. [32], the H radicals created by the plasma source contained both H atoms and excited hydrogen gas molecules. During charging, the plasma phase was not injected directly on to the specimen surface, but only the active particles could still take part in the reaction. By this means, the specimen surface would have least possible damage from exposure to plasma. The charging conditions were kept constant during the whole test, and the loading condition could be measured and controlled precisely by the miniature testing module, indicating a well-constrained setup for the H-uptake. According to a previous work from the authors' research group [31], the fugacity of the dissociated H atoms can reach a value larger than 80 Pa in the vacuum chamber, and can even reach several MPa locally [33]. However, due to limited thermodynamics data in the plasma phase and the missing physics in the H uptake mechanism from plasma phase, only indirect values of the H concentration could be assumed.

Since the studied specimen has an oligocrystalline structure, the crack could grow a relative long distance with well-defined loading conditions. Furthermore, the relative stress conditions with respect to the neighboring grains could be kept almost unaffected during crack growth. Hence, we changed the environment during the test with keeping all other parameters unbothered to reveal the "pure" environmental influence. This means, both the reference test and the control test were done in the same grain under the same mechanical loading with only alteration in the environment.

The "in-situ" tests were done with in-situ loading and in-situ H-charging. In-situ imaging was partially possible when the H-plasma was switched off and the chamber was pumped to high Vac again. This was due to the technical limitations of the SEM detector. Normally about 10 s was required for the chamber to reach the high Vac state.

Hence, the “in-situ imaging” here was limited to “in-situ in position” but “ex-situ in environment”.

After loading, the specimen was taken out and characterized by SEM including secondary electron imaging and EBSD to check the plastic deformation zone near the crack. Scanning probe microscopy (SPM) in a TI 950 Nanoindentation system (Hysitron Inc., USA) using a Berkovich tip was adopted to check the topography of the region near the propagated fatigue crack. The ROIs were in 8 μm x 8 μm squares and were from the representative characteristic regions near the main fatigue crack. The SPM images were processed by the open source software Gwyddion.

3. Results

3.1 Fatigue crack growth behavior

The crack length data were measured from the SEM images taken between loading cycles, and the ΔK values were calculated based on the SENT specimen assumption as described in the experimental section. The fatigue crack growth rate (FCGR, denoted as da/dN) vs. ΔK results were plotted on a logarithmic scale and shown in Fig. 3 as different comparisons. It is worth noting that the starting ΔK value was controlled to a value that was a little bit higher than the empirical ΔK_{th} from preliminary tests for this material and the FCG behavior in the Paris’ regime was expected from the present test. Fig. 3a shows the comparison between the Vac and H cases under ULF loading condition. The FCGR was slightly enhanced by H, but the enhancement was not very significant. While Fig. 3b shows the comparison under LF loading condition, and the FCGR was increased by about one magnitude when H was charged into the chamber. The comparison in Fig. 3c shows the frequency dependency of the H-enhanced FCGR. The LF loading condition gives a more significant FCGR enhancement by H.

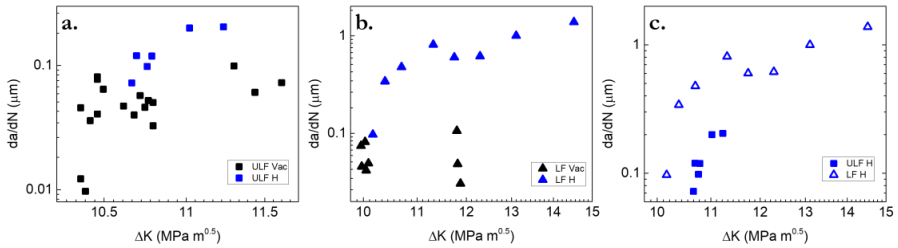

Fig. 3 Fatigue crack growth data of the investigated specimen: a. Vac and H cases under ULF; b. Vac and H cases under LF; c. H cases under ULF and LF.

3.2 Crack-tip characterization

The crack-tip during cyclic loading was characterized by SEM, including secondary electron (SE) imaging and backscatter electron (BSE) imaging. The results are shown in Fig. 4. The crack length increment (Δa) after the loading intervals of each 100 cycles was measured by comparing the present image with the image from the last loading step (not shown in the figures), which is shown by the yellow double-arrow lines in the SE images of Fig. 4. The ΔK range was calculated for each status based on the SENT specimen approach. The images showed the microstructure in the vicinity of the crack-tip resulted from the same ΔK range but under different environmental conditions. For both ULF and LF, the H-charged case had an accelerated FCGR of about 10 μm per 100 cycles, while the Vac case had the FCGR of only 3.3 μm and 4.9 μm per 100 cycles, respectively. The SE images mainly showed the topography near the crack-tip, which revealed the differences mainly in the deformation pile-ups. The crack grown in Vac was normally associated with more severe pile-ups near the crack-tip, and the lines from deformation were normally curves; while the crack grown in H had less pile-ups and the lines were straighter, when present. Moreover, the BSE images showed a stark contrast as contour lines in the vicinity of the crack-tip in Vac case (see the highlighted area in Fig. 4), but in contrast, the H case did not show such contrast. The BSE contrast is normally associated with atomic number contrast and crystal orientation contrast. In this large single-phase ferritic grain, atomic number contrast was almost uniform over the whole grain, and only orientation contrast should be considered from the BSE images. In the present study, these images could be used to evaluate the plasticity near the crack-tips.

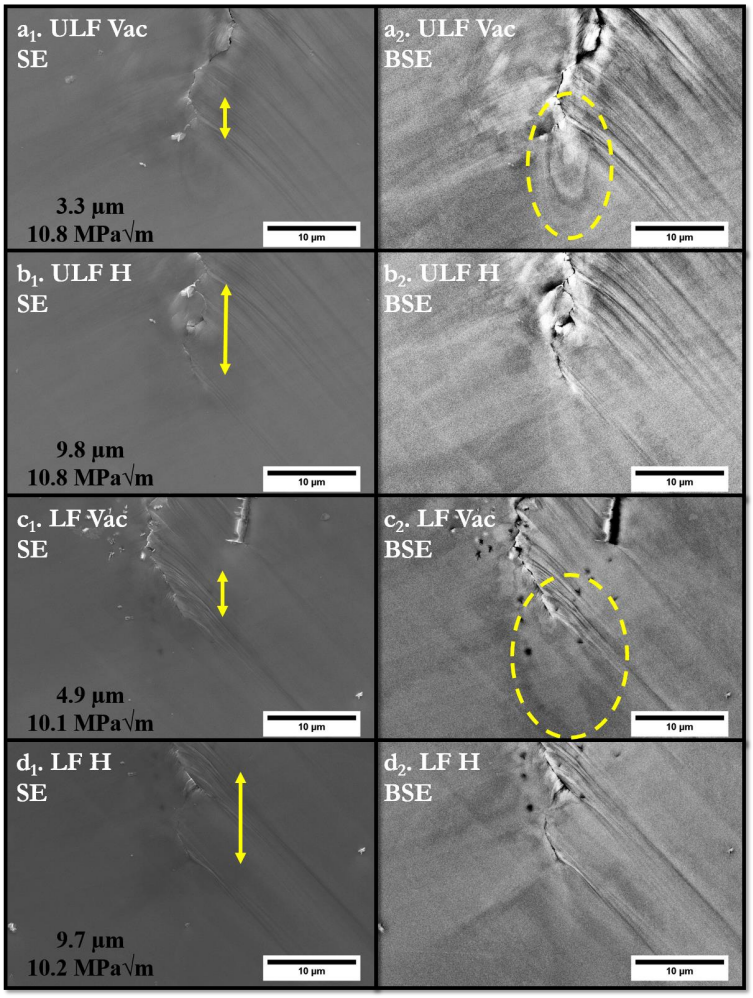

Fig. 4 Crack-tip characterization in different conditions as marked in each subfigure. The double-arrow lines indicate the crack advance during the loading segment of 100 cycles. The corresponding crack growth and ΔK level are marked in each subfigure. The left column (a_1 to d_1) shows the SE images and the right column (a_2 to d_2) shows the BSE images. The global FCG direction is from top to bottom for all subfigures.

3.3 EBSD post-characterization

The area near the fatigue crack was characterized by EBSD technique on the post-mortem specimen after loading. The resulting GROD maps were plotted for both ULF and LF loading conditions, respectively, and were shown in Fig. 5a and b. Different environmental conditions were separated by yellow dash-lines. Magnified representative featured areas on the left part of the crack were plotted in Fig. 5a1, a2 and b1, b2 with the same coloring scale. Since the GROD values were calculated based on the orientation deviation with respect to a reference orientation, this map was commonly used to evaluate the plasticity assuming the orientation change came from plastic deformation [24, 34, 35]. It is worth noting that the large plastic field in the top left corner of Fig. 5a came from the pre-cracking procedure, which was strongly associated with the crack initiation procedure, and this was not an area of interest regarding the present study. From Fig. 5, it was clearly shown that the fatigue fracture was associated with plasticity near the crack. The magnified views in Fig. 5 (a1, a2, b1, b2) were acquired with higher resolution on the plastic zones and showed that the patterns were periodic along the crack growth path. The regular patterns were extending along two different <110> directions on both sides of the crack, and the directions were the same for all conditions. When loaded with ULF, the material had a plastic extension of about 18~20 μm in Vac and 8~10 μm in H, respectively, away from the crack. While when loaded with LF, the plastic extension ranged from 22~25 μm in Vac and 4~8 μm in H, respectively. Fig. 6 showed the misorientation distribution versus the distance away from the crack in different conditions. The distributions along the highlighted lines in Fig. 6a1 (ULF) and b1 (LF) were plotted in a2 and b2, respectively. For both frequencies, one line-profile in Vac and two line-profiles in H were presented. The misorientation of the area loaded in Vac (about 25~30°) was much larger than that in H (up to 5° in LF and up to 15° in ULF). The red triangle in Fig. 6a1 showed the peak misorientation in the H condition after ULF loading, which read about 15° from Fig. 6a2. In the ROI of the LF case, no such strong peaks were found in the misorientation profile, and the maximum value was less than 5° from the data. The size of the plastic zone (considering high misorientation values) could also be evaluated from the profiles, which corresponded to the results mentioned in the above sentences.

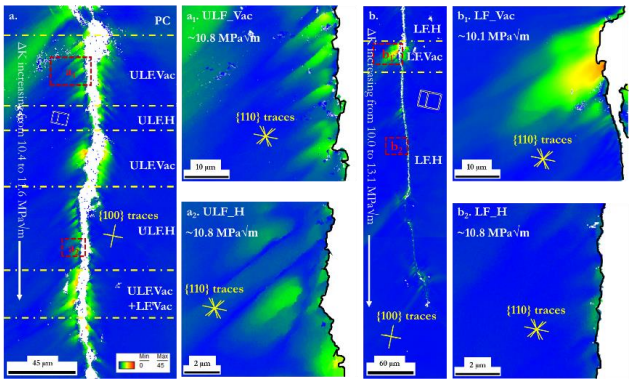

Fig. 5 GROD maps near the fatigue crack after loading with a. ULF (magnified ROIs: a_1. in Vac and a_2. in H) and b. LF conditions (magnified ROIs: b_1. in Vac and b_2. in H). The ΔK range for a is from 10.4 to 11.6 MPa√m, and that for b is from 10.0 to 13.1 MPa√m. The global FCG direction is from top to bottom. The color scale is the same for all sub-plots.

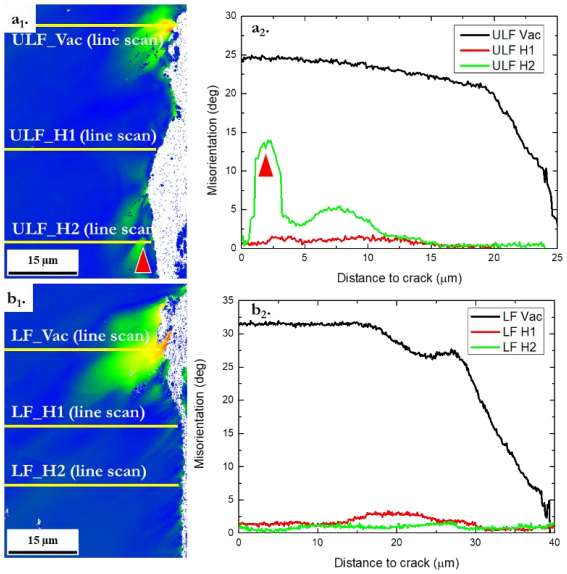

Fig. 6 GROD maps and misorientation distribution focusing on a. ULF loading and b. LF loading; a_2 and b_2 are the misorientation distribution profiles showing the highlighted lines in a_1 and b_1, respectively. The red triangles in a_1 and a_2 are indicating the same misorientation peak. The global FCG direction is from top to bottom. The color scale of the EBSD maps is the same as in Fig. 5.

3.4 Topography near the fatigue crack

The SPM technique was adopted to check the topography of the area near the fatigue crack. Fig. 7 showed the constructed 3D images of the representative areas under different loading conditions. The two areas were taken from the area next to both sides of the fatigue crack. It is clear that the material near the crack formed a topographical roughness with different heights ranging from 10~30 nm in the ROIs from different loading conditions. The roughness is the result from the dislocation slipping, as noted by Vehoff and Neumann [36] in the similar Fe-Si system. The slip lines resulted from loading in Vac (Fig. 7a and b) were generally higher than that resulted from loading in H (Fig. 7c and d). The Vac conditions with both frequencies gave a final roughness in the range of 30 nm while the H conditions gave a less pronounced roughness of about 10~20 nm. The slip lines were denser in LF conditions than in ULF conditions. Considering the distance between the grooves of the roughness in the Vac cases, the ULF case had a larger value of about 3~4 μm while the LF case had only 1~2 μm between each slip line. In the H cases, the slip lines were not extending over the scanned area, and this parameter could not be compared directly. However, the slip lines localized near the crack (Fig. 7c and d) gave a value of about 1 μm for both ULF and LF cases.

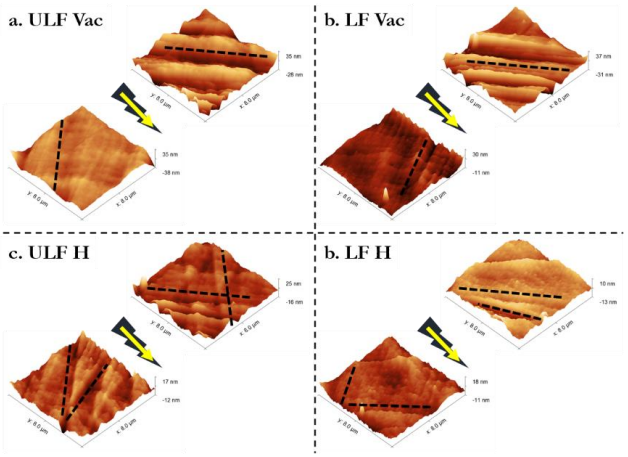

Fig. 7 SPM images on characteristic regions near the main fatigue crack a. ULF Vac, b. LF Vac, c. ULF H, d. LF H. The arrows represent the global FCG direction and the relative position of the crack. The dash lines in the sub-plots denote the directions of the slip lines.

3.5 Fractography

After the specimen has been completely fractured, the fracture surface was investigated by SEM. The fracture features were in general the same along the thickness direction of the SENT specimen, which means the test could be considered as done on a two-dimensional oligocrystal. Thus, some loading complexities could be constrained. In the present results, the crack length data could be correlated to the fracture surface features thanks to the accurate measurement at each loading step. Consequently, the loading parameters as well as the environmental conditions could also be correlated. It could be seen from Fig. 8a that the overall fracture features looked differently regarding different loading and environmental conditions. The whole grain was fractured transgranularly, however, essential differences in the fracture surface that was subjected to different testing conditions could be clearly discerned, as shown in Fig. 8. The striations formed in Vac were densely arranged perpendicular to the FCG direction with the protuberances smooth and round, as illustrated in Fig. 8b and c. While the striations formed in H environment were sparsely distributed and form some brittle-like facets, as shown in Fig. 8d and e. Furthermore, the directions of the striations in general were forming a roughly 45° to the global FCG direction, according to the measurement in the figures. The protuberances look sharper than the Vac case, and the overall surface looked flatter than that of the Vac case. The spacing between the major striations were measured from the magnified fractographs in Fig. 8. Under ULF loading, an average spacing of 0.09 µm and 0.74 µm were obtained for the Vac and H cases, respectively. While for LF loading, the value of 0.10 µm and 0.84 µm were obtained for the Vac and H cases, respectively. These values fit well with the data in Fig. 3 except the ULF H case. However, one could also see some denser striations in the ULF H case besides the characteristic “quasi-cleavage” striations, as highlighted by a black rectangle in Fig. 8d with a magnified subsection from it, which was not counted in the measurement. It is thus reasonable to consider the striation spacing corresponds well to the globally measured FCGR. By comparing the fracture features in different loading frequencies, no significant differences could be observed.

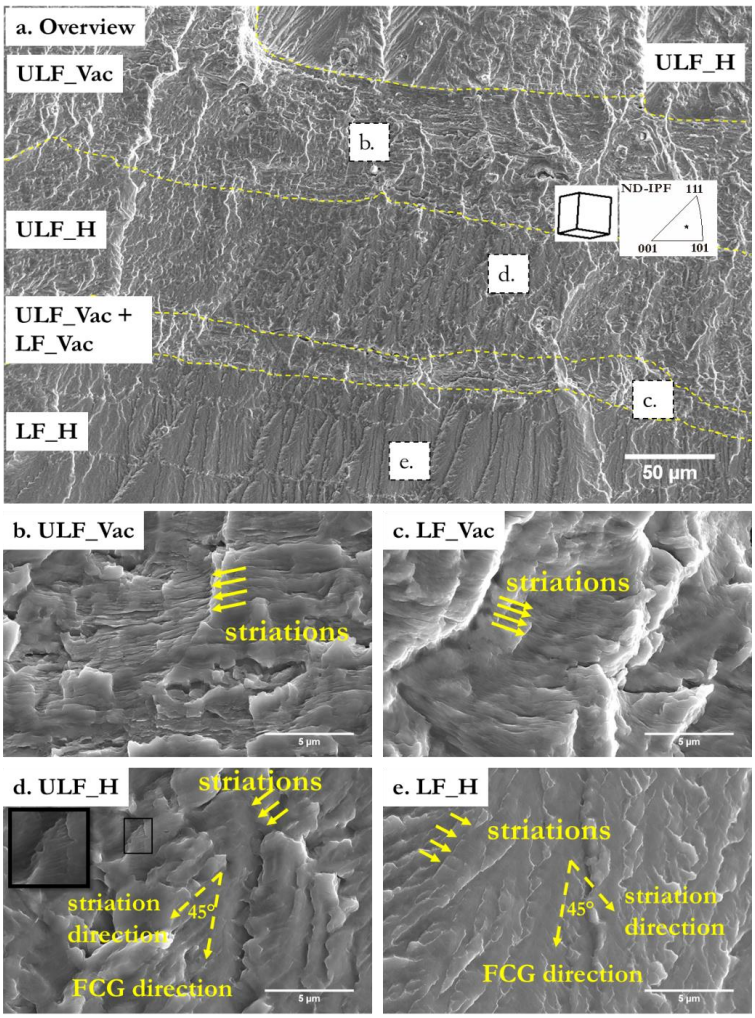

Fig. 8 Fracture surface with features from different loading and environmental conditions (a. overview; b. ULF, Vac; c. LF, Vac; d. ULF, H; e. LF, H). The global FCG direction is from top to bottom. All the ROIs are in the same grain and the representative unit cell with the ND-IPF on this grain is shown in a.

4. Discussion

4.1 Plasticity-related fracture procedure

Based on the microstructure observation near the fatigue crack, it could be inferred that the FCG procedure was a plasticity-related procedure both in Vac and with H-charging. Before FCG, the notched specimen was subjected to cyclic loading to initiate the fatigue pre-crack. A certain plastic deformation zone was produced during this procedure. This plasticity could be observed in the upper left corner of Fig. 5. Due to text length concerns, the crack initiation procedure would not be discussed in this work and only the stable crack growth stage was considered.

Depending on the material's properties and loading conditions, the externally applied energy could be released either by crack growth (new surface opening) or by plastic deformation (e.g. dislocation motion, mechanical twinning or phase transformation), or in most cases by mixed mode of both of them. The experimental observations of a relatively larger plastic zone and a smaller crack advance in Vac case indicated that the energy was largely released by plastic deformation mechanisms. Since no phase transformation or mechanical twinning was observed in the studied material, it was inferred that the outwards dislocation motion into the material matrix from the crack-tip gave a significant contribution to the plastic energy release. As a result, fracture surface in Vac case showed a large plastic zone (Fig. 5 and Fig. 6) and a small crack advance (smaller striation distances as in Fig. 8b and c). According to Laird and Smith [37], the fatigue striations formed on the fracture surface are a result of blunting and sharpening of the crack tip under cyclic loading via a plastic deformation mechanism. This can confirm that the FCG in the current study is a plasticity-related procedure.

Based on the discrete-dislocation plasticity simulation results by Chakravarthy and Curtin [38], noticeable dislocations slipping could be observed around the crack-tip during crack growth, and the local strain field could extend to several microns away. Conventional large-scale investigations such as optical microscopy could capture the fracture or mechanical behavior at macro-scale but were difficult to reveal the quantitative measurement of the small-scale local strain. The micro-scale characterizations in this work, however, could successfully capture the plasticity at this level. Combining with EBSD technique, some quantitative crystallographic and microstructural data could also be obtained. In this test, the plasticity extension could

range to about 30 μm in Vac, with a crystal rotation (misorientation) up to 30° based on the measurements shown in Fig. 5 and Fig. 6, depending on the loading conditions. This investigation gave strong proof to the simulation results in [38] that the FCG procedure was associated with plasticity evolution in the vicinity of the crack-tip.

When dislocations are introduced into the crack system, there is an effect named dislocation shielding, simply describing the phenomenon that dislocations are trying to lower the stress of the crack-tip. As is generally accepted, the vicinity of a crack-tip is often highly stressed. The shielding dislocations are thus emitted from the crack-tip and move into the material matrix and in this way make the crack blunt and thus lower the stress state at the crack-tip. However, dislocations also interact with themselves if they are emitted. A large amount of dislocations ahead can also restrict the new dislocations from emitting, therefore, the dislocations will accumulate in the nearby area close to the crack path but not extend into the matrix infinitely. When the shielding dislocations are sufficient to prevent new dislocations from emitting, the stress state will again be elevated by the external loading and thus the crack grows after the critical stress condition is reached. This mechanism could explain why we see discontinuous plastic zones along the crack path.

4.2 The HE effect from H-plasma charging

In a previous study [31], the HE effect on the same ferritic alloy was observed by H-plasma charging during slow strain rate tensile tests. With monotonic loading, the global elongation (final elongation value in percentage up to complete fracture) was reduced by about 5% in comparison with the reference test in Vac. The reasons were given as the combined effect from localized deformation and localized H-concentration. Following this conclusion, a notch was introduced and a sharp fatigue crack was initiated from the notch by cyclic loading, which could give a stress-concentrated location and thus controlling the crack path. From the FCG results, the H-charging by the plasma phase did take part in the FCG behavior, giving an increase of about one in magnitude of the FCGR. This result could be used as a confirmation to our previous proposal and a convincing proof of the HE effect from H-plasma charging.

As a direct comparison, the resulting fatigue fractography from H-charging in Fig. 8 was comparable with that under monotonic tensile loading in Ref. [31], with the only difference from fatigue striations. The characteristic “quasi-cleavage” facets were

observed in the H-charged case in both works, c.f. Fig. 8 and Fig. 9. Previous literature showed similar H-induced "quasi-cleavage" features in various Fe-based BCC alloys under different H-rich environments [24, 39-46]. It is thus considered that one characteristics by H-charging in fractography is the "quasi-cleavage" fracture features.

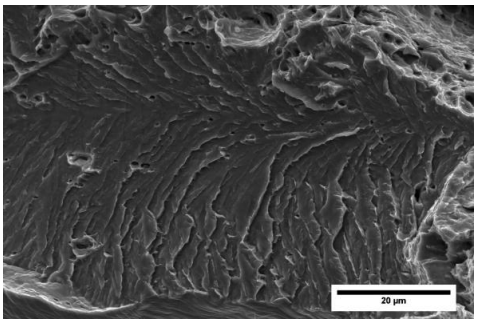

Fig. 9 Fracture feature with monotonic tensile loading with H-plasma charging on the investigated material, from Ref. [31].

The "quasi-cleavage" feature after H-enhanced FCG in a pure iron specimen was studied in a recent work [47]. They observed the "quasi-cleavage" regions were parallel to the {100} planes and concluded the H-enhanced FCG was due to the contribution of local cleavage fracture. However, this proposal contradicts our results. Based on our investigations, the fatigue crack did not change direction significantly during the whole test, either in Vac or in H. From the EBSD scans, the FCG direction was closer to {110} traces rather than {100}, as marked in Fig. 5a. From the crystallographic analysis, the ND of the fracture surface was approximately parallel to the crystallographic <1 3 5> direction, which did not correspond to the cleavage fracture surface of this material. Several reasons could attribute to this difference. The investigated material in [47] was a polycrystalline pure iron, the cleavage fracture could be activated due to local stress state and local crystal orientation accompanied by accommodations between grains. Furthermore, only selected grains were indexed in [47] with the cleavage orientation relationship, which did not contribute much to statistics. Another important factor was the stress state. The investigation area in [47] came from the mid-thickness of the CT specimen, which was experiencing more plane-strain condition. While most of other works including the present one focused on the surface area which was experiencing more plane-stress condition. This could give some differences since the plane-strain condition gave higher lattice dilatation. Under plane-strain condition, the material

experienced a higher hydrostatic stress, and this stress state was a major reason for the elastic volume expansion, which could lead to a locally higher H-concentration. Therefore, a stronger HE phenomenon (cleavage fracture feature) was expected.

The previously proposed models for the H-enhanced FCG were mainly based on the HELP mechanism assumptions, which emphasize that H is aiding the deformation processes by enhancing the mobility of dislocations, and consequently making the plastic deformation zone smaller in size (e.g. [2, 7]). However, based on our investigations, there is no clear proof of enhanced dislocation mobility, but instead, a restricted mobility of dislocations seems to be more evident. It is observed that both the size of the deformation zone and the total amount of plasticity were smaller in the H cases comparing with the Vac cases, as was also pointed out in [47]. The misorientation distribution in Fig. $6a_2$ and b_2 showed this relation clearly. The maximum misorientation angle values were in general much smaller in the H cases than that of the corresponding Vac cases. If we consider the plasticity was only "localized", a stronger plasticity, i.e. higher misorientation angle than the maximum value in the Vac case, should be observed when it gets closer to the crack. However, this was not the case based on the EBSD results. In another way, the misorientation profile, i.e. plastically deformed area, was strongly suppressed by H in comparison with the Vac cases. The same story could be told from the SPM results in Fig. 7 as well. The scanned areas were directly from the region connecting the primary fatigue crack, and no strong peaks could be seen in the H cases. This means the plasticity was impaired during the FCG in H. The reduced plastic zone by H was also confirmed by in-situ micro-cantilever bending test in the case of monotonic loading and step-wise loading in other BCC materials [48-50].

Based on the investigation from both fractography and plastic zone characterization, a model on the H-enhanced FCG was proposed. Fig. 10 is a schematic of the proposed mechanism. When a pre-crack is under cyclic loading, the loading would give contribution to both crack growth and plasticity independent of H influence. The cracking is considered as atomic plane separation (fast brittle cracking) while the plastic response results in deformation zones with higher misorientation (dislocation shielding and slow ductile cracking). It has been calculated by atomistic simulations that the strong trapping sites of H are distributed around the dislocation cores [51]. As an

interstitial solid solute atom, H in general has a pinning effect on dislocation slipping, which will increase the critical resolved shear stress of some specific slip systems [52, 53]. Consequently, by impairing the mobility of the dislocation in hydrogen enriched volume in vicinity of the crack, the dislocation shielding effect on the stress intensity of the crack will be reduced in comparison with the H-free case such that the plasticity extension is smaller in H than in Vac (see the middle illustration in Fig. 10). The investigation results of the plastic zone size in the early section give convincing proof to this proposed mechanism. Another feature is the distribution of the plastic zone. The H-free case gives a more concentrated deformation zone while the H case gives more separated plastic zones (c.f. Fig. 5 and Fig. 6). This could be explained by the right-side illustration in Fig. 10 that the dislocation shielding effect is competing with the crack growth. Since the dislocation shielding is restricted by H, the extended distance of the plastic zone in the H case is shorter than that in the H-free case. A locally higher stress intensity at the crack tip is expected when the dislocation shielding on crack is restricted. Therefore, the critical stress state for crack growth is more easily reached in H than in Vac. In the assumptions, it is considered that the crack growth is free of plastic behavior, and thus, a larger undeformed distance between the plastic zones in H than in Vac could be seen. Hence, as a short conclusion, the mechanism of H-enhanced FCG is proposed as the H-restricted dislocation shielding and thus enhanced cracking.

Furthermore, as was also observed in Inconel 718 alloy [54], a secondary slip system would get more easily activated when H is present during the FCG procedure. According to our investigations, a secondary pile-up direction was observed in the H-charged case while no similar traces were found in the Vac case (c.f. Fig. 7). In the Vac case, the primary slip system was activated by the local stress intensity K, and the dislocations could partly shield the local K by the dislocation motion along the activated slip system. However, when H was present, the dislocation mobility was impeded based on our assumptions. Therefore, the local K was less shielded and this stress intensity could further activated new slip systems. The influence from a secondary slip system would also confine the motion of the primary slip system, which gives a more restricted dislocation shielding effect and thus less-extended plastic zone in the H case. This might be another mechanism of the restricted plasticity.

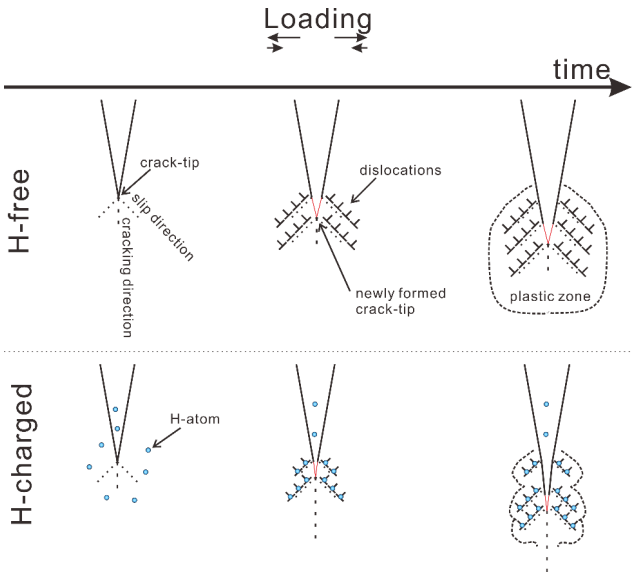

Fig. 10 Proposed H-enhanced cracking mechanism. Explanation in text.

4.3 Frequency effect

Typically, increasing the frequency of cyclic loading affects the kinetic of hydrogen uptake at the crack tip and reduces the FCGR of metals in a wide range. Consequently, a lower frequency leads to a higher FCGR. However, when it comes to a very low frequency range, this relation can deviate. Matsunaga et al.[28] did FCG tests on steels under high pressure H_2 gas with a wide range of loading frequency and found that when the frequency is higher than 0.1 Hz, the FCG acceleration in 0.7 MPa H_2 gas is decreasing with increasing frequency; while when the frequency is in the range of 10^{-3} Hz to 0.1 Hz, this relation is reversed. This result agrees with the result in the present study. In this work, two loading frequencies were adopted as ULF (~0.015 Hz) and LF (~0.15 Hz) that fall in the range of the peculiar frequency dependency range. As can be seen from Fig. 3, when tested in Vac, the frequency did not give strong influence of the FCGR, but during H-charging, the FCGR was clearly accelerated and this increment was depending on the frequency. The LF gave an acceleration about one magnitude in the FCGR, but the ULF gave a less acceleration.

The mechanisms of this peculiar frequency effect on H-enhanced FCGR in steels have been discussed in several different works [28, 55, 56]. This dependency was concluded to be attributed to the distribution of H concentration, i.e. local H-gradient, in the

vicinity of the crack-tip, which affects the HELP process in the crack-tip zone. The basic idea was built on the assumption that a local steep gradient of H-concentration will result in the slip localization at the crack-tip. At ULF, the H has relatively more time to diffuse deeper into the material's matrix, which gives a smoother H-concentration profile. Assuming that the same H-concentration in the environment and the same crack-tip is under a higher loading frequency, the H diffuses less into the material, which means that in the vicinity of the crack-tip, the H-concentration is decreasing strongly as the distance to the crack-tip increases and consequently giving a local steep gradient of H-concentration. From the basic assumption, the local steep H-concentration gradient will make the dislocation slip behaviors more localized at the crack-tip (basic HELP mechanism) and thus leading to less crack blunting and faster crack advancement. Based on the assumptions, this model could explain the peculiar frequency dependency to an extent, but the detailed embrittlement mechanism seems to be a black box and remains unclear. To understand the possible mechanisms, three scenarios can be presented regarding a) the H concentration gradient, b) the H uptake and c) the H influence on the dislocation motion.

a) H concentration gradient

Based on the analytical model presented by Sofronis and McMeeking [57], the H profile ahead of the crack-tip is not monotonic, but instead, the peak concentration would appear some distance away from the tip, which was calculated to be 1.53 times of the crack opening displacement. Kotake et al. [58] updated this model by including the case under cyclic loading at load ration $R = 0.5$, which is corresponding to the present study. In the updated model, the loading time effect was also considered: longer time (lower frequency) gives higher peak concentration at full loading, but at the end of the unloading (to 0.5 of the maximum load) the concentration is lower. That is to say, lower frequency gives a larger amplitude of the H concentration value. The scenario could be schematically presented as Fig. 11. The Y-axis is the relative concentration ratio C_L/C_0 (local H concentration C_L over the constant initial concentration C_0). The X-axis is the relative distance to the crack-tip X/b (X is the absolute distance and b is the crack opening displacement as shown in the corner of Fig. 11). However, the calculation results from [57] and [58] do not give a significant different between the concentration resulting from ULF and LF loading. Considering the loading time effect on the H

concentration resulting from 100 s loading and 10 s loading (which are in the similar magnitude as the presented study), there is a difference of roughly 10% in the peak H concentration. This value, however, seems to be insufficient to cause one magnitude different FCGR and such significant plasticity difference in the fracture process zone. Furthermore, due to the sharpness of the studied crack-tip, the crack opening displacement should be in the range of less than 1 μm. According to the above-mentioned model, the peak H concentration happens about 1~2 μm away from the crack-tip. This value does not necessarily agree with the measured plastic zone size. As a short summary, the effect from stress-controlled local H concentration could not satisfactorily explain the whole story.

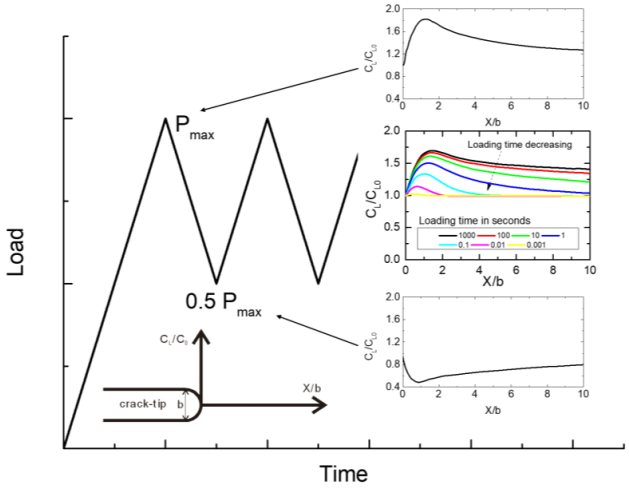

Fig. 11 Local H concentration profile at the crack-tip area during cyclic loading with the loading time effect on the profile. Concentration profiles adopted from [58].

b) H uptake

The major factor controlled by the frequency is the loading time difference. And the most possible consequence from this difference seems to be the H diffusion and uptake into the fracture process. If the surface H uptake is a controlling factor in this process, a higher H concentration is expected at ULF and thus a more significant embrittlement effect. However, this did not happen in our case nor in the study in [28]. Furthermore, by adopting the diffusion calculations, the time needed for H diffusion into the fracture process zone of several tens of microns is in the magnitude of 0.001 s, which can be fully covered by any single cycle in the current study. On the other hand, due to the

relatively low solubility limit of H in BCC ferrite (atomic solubility of about $5*10^{-8}$, according to [59]), the fracture process zone was reasonably assumed to be saturated with H during the test. Hence, it is concluded that the H uptake situation should be similar for both the ULF and the LF cases, and is not the controlling factor in the embrittlement dependency on loading frequency.

c) H influenced dislocation motion.

When the above-mentioned points are somehow ruled out, we try to think about the fundamental theory of dislocation motion with the influence from strain rate since fundamentally we had a different displacement rate (more physically a different strain rate) during the test. From the classical theory, dislocation motion is associated with a thermally activated process that is dependent on the strain rate [60]. The higher the strain rate is, the lower thermal activation energy could be provided, and namely a higher external force is needed to move the dislocations. Consequently, higher strain rate hardens the material and lower strain rate softens the material. This relation could be expressed by the following empirical equation:

$$\dot{\varepsilon} = \dot{\varepsilon}_0 \exp\left(-\frac{\Delta G}{kT}\right) \qquad \text{Eq. 4}$$

where $\dot{\varepsilon}_0$ is a constant initial strain rate depending on the material system, k is the Boltzmann constant and T is the temperature. The macroscopic plastic strain rate $\dot{\varepsilon}$ could then be directly linked to the thermal activation energy ΔG for dislocation motion. From this relation, a higher strain rate leads to a smaller thermal activation energy and vice versa, when all other parameters keep constant. From a perceptual aspect, a lower strain rate means more time for dislocation jumping over the barrier and easier dislocation slipping and thus leading to a softened material, while a higher strain rate means more difficult dislocation motion and thus a harder material. Considering the testing conditions in the present study, the ULF condition (lower strain rate) gave a higher thermal activation energy, which gave the dislocations more chance to overcome the energy barrier for movement, compared to the LF condition. Quantitatively, there is a difference of about $kT \cdot \ln 10$ in the thermal activation energy. When no H is presented, this amount of difference seems insufficient to cause such a difference (the plastic zone sizes in ULF Vac and LF Vac cases are similar, c.f. Fig. 5.). Back to the proposed model in the above section, H has the effect of restricting dislocation motion,

which makes the energy barrier larger. The ULF condition seems to lead to a higher thermal activation energy such that dislocations overcame the H enhanced barrier, while in the LF condition, a relatively lower thermal activation made dislocation motion less possible and thus a restricted plastic zone was observed. Based on the data with a wider frequency range in Ref. [28], a continuously weaker HE effect was observed when the frequency went lower from 0.1 Hz to 10^{-3} Hz. By ruling out the H diffusion as well as the H distribution in the system, the thermal activation process of dislocation motion in combination with the hydrogen impaired mobility of the dislocation seems to be the most successful mechanism to explain the peculiar frequency dependency of the H-enhanced FCGR at low frequency range. Analytically, this relation is shown in Fig. 12. At lower frequency range, the dislocation kinetics becomes a controlling factor that influences the HE effect, while when the frequency becomes higher, the H diffusion problem comes into play and the HE effect is mainly dependent on the diffusion. At the intersection range (about 0.1 Hz from [28]), the H-enhanced FCGR gets its peak enhancement. To prove this proposal, researchers in the numerical methodology fields are encouraged to shed some light on it.

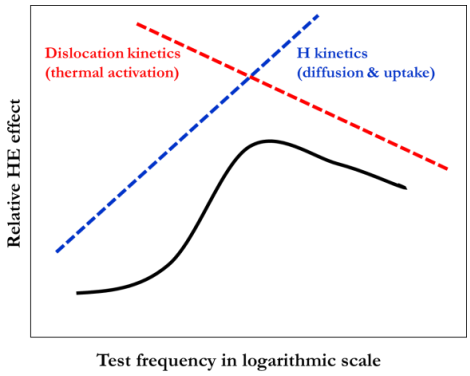

Fig. 12 Schematic description of the frequency dependency and the influencing factors. Solid line is the HE effect from the FCGR ratio in [28]. Red dash-line represents the thermal activation process influence and blue dash-line represents the H diffusion influence.

It should be noted that the form of H (diffusible H or trapped H) was not differentiated in the current study. From the presented scenarios, the effect of the enhancement in FCGR is more possibly coming from the trapped H because the diffusion and uptake

mechanisms can be ruled out. However, due to the current technical limitations, the exact form of H in the vicinity of the crack-tip was not validated and only the possible assumptions are presented in the current study.

5. Conclusions

A SENT specimen with large grained ferritic structure was tested under low frequency cyclic loading in an ESEM with in-situ H-plasma charging and in Vac. The FCG behavior was observed by SEM. Some conclusions could be drawn as follows:

- The plasticity evolution in the vicinity of the crack-tip plays a dominating role in the FCG of the studied Fe-3wt%Si steel. The dislocation shielding effect on the crack could influence the FCGR.
- In H-plasma, the FCGR was enhanced by about one magnitude when compared with the FCGR in Vac with the same loading parameters.
- A mechanism on the H-enhanced FCG process was proposed based on the constrained dislocation shielding effect. The plastic zone near the crack-tip was restricted by the H-charging.
- In the tested frequency range (0.015 ~ 0.15 Hz), a higher frequency gave a higher FCGR value in H and vice versa. While in Vac, the frequency did not play a significant role. The frequency dependency of the HE effect was explained by the competition between thermally activated dislocation motion and the H diffusion.

Acknowledgement

This study was financially supported by the Research Council of Norway through the HyF-Lex project (Petromaks2 Programme, project number 244068/E30).

Reference

[1] W.H. Johnson, On Some Remarkable Changes Produced in Iron and Steel by the Action of Hydrogen and Acids, Proc. R. Soc. London 23(156-163) (1875) 168-179.

[2] C.D. Beachem, A new model for hydrogen-assisted cracking (hydrogen “embrittlement”), Metall. Mater. Trans. B 3(2) (1972) 441-455.

[3] H.K. Birnbaum, P. Sofronis, Hydrogen-enhanced localized plasticity—a mechanism for hydrogen-related fracture, Mater. Sci. Eng., A 176(1-2) (1994) 191-202.
[4] I.M. Robertson, The effect of hydrogen on dislocation dynamics, Eng. Fract. Mech. 64(5) (1999) 649-673.
[5] I.M. Robertson, H.K. Birnbaum, An Hvem Study of Hydrogen Effects on the Deformation and Fracture of Nickel, Acta Metall. 34(3) (1986) 353-366.
[6] I.M. Robertson, H.K. Birnbaum, P. Sofronis, Hydrogen Effects on Plasticity, in: J.P. Hirth, L. Kubin (Eds.), Dislocations in Solids, Elsevier, Amsterdam, 2010, pp. 249-293.
[7] S. Wang, A. Nagao, P. Sofronis, I.M. Robertson, Hydrogen-modified dislocation structures in a cyclically deformed ferritic-pearlitic low carbon steel, Acta Mater. 144 (2018) 164-176.
[8] R.P. Gangloff, Critical issues in hydrogen assisted cracking of structural alloys, in: S.A. Shipilov, R.H. Jones, J.-M. Olive, R.B. Rebak (Eds.), Environment-Induced Cracking of Materials, Elsevier, Amsterdam, 2008, pp. 141-165.
[9] W.W. Gerberich, P.G. Marsh, J.W. Hoehn, Hydrogen Induced Cracking Mechanisms - Are There Critical Experiments?, in: A.W. Thompson, N.R. Moody (Eds.), Hydrogen Effects in Materials, Minerals, Metals & Materials Society (TMS), Warrendale, Pennsylvania, USA, 1996, pp. 539-554.
[10] R.A. Oriani, Whitney Award Lecture—1987:Hydrogen—The Versatile Embrittler, Corrosion 43(7) (1987) 390-397.
[11] R.A. Oriani, P.H. Josephic, Equilibrium and kinetic studies of the hydrogen-assisted cracking of steel, Acta Metall. 25(9) (1977) 979-988.
[12] S.P. Lynch, Environmentally Assisted Cracking - Overview of Evidence for an Adsorption-Induced Localized-Slip Process, Acta Metall. 36(10) (1988) 2639-2661.
[13] S. Lynch, Hydrogen embrittlement phenomena and mechanisms, Corros. Rev. 30(3-4) (2012) 105-123.
[14] S.P. Lynch, Metallographic contributions to understanding mechanisms of environmentally assisted cracking, Metallography 23(2) (1989) 147-171.
[15] S.P. Lynch, Comments on “A unified model of environment-assisted cracking”, Scr. Mater. 61(3) (2009) 331-334.
[16] Y. Fukai, Formation of superabundant vacancies in M–H alloys and some of its consequences: a review, J. Alloys Compd. 356-357 (2003) 263-269.

[17] M. Nagumo, Hydrogen related failure of steels – a new aspect, Mater. Sci. Technol. 20(8) (2013) 940-950.

[18] D.S. Shih, I.M. Robertson, H.K. Birnbaum, Hydrogen embrittlement of α titanium: In situ tem studies, Acta Metall. 36(1) (1988) 111-124.

[19] M.L. Holzworth, M.R. Louthan, Hydrogen-Induced Phase Transformations in Type 304L Stainless Steels, Corrosion 24(4) (1968) 110-124.

[20] N. Narita, C.J. Altstetter, H.K. Birnbaum, Hydrogen-related phase transformations in austenitic stainless steels, Metall. Trans. A 13(8) (1982) 1355-1365.

[21] H.K. Birnbaum, Mechanical properties of metal hydrides, J. Less Common Met. 104(1) (1984) 31-41.

[22] P. Peralta, C. Laird, Fatigue of Metals, in: D.E. Laughlin, K. Hono (Eds.), Physical Metallurgy (Fifth Edition), Elsevier, Amsterdam, 2014, pp. 1765-1880.

[23] H. Matsunaga, M. Yoshikawa, R. Kondo, J. Yamabe, S. Matsuoka, Slow strain rate tensile and fatigue properties of Cr-Mo and carbon steels in a 115 MPa hydrogen gas atmosphere, Int J Hydrog Energy 40(16) (2015) 5739-5748.

[24] Y. Ogawa, D. Birenis, H. Matsunaga, A. Thogersen, O. Prytz, O. Takakuwa, J. Yamabe, Multi-scale observation of hydrogen-induced, localized plastic deformation in fatigue-crack propagation in a pure iron, Scr. Mater. 140 (2017) 13-17.

[25] Y. Ogawa, J. Yamabe, H. Matsunaga, S. Matsuoka, Material performance of age-hardened beryllium–copper alloy, CDA-C17200, in a high-pressure, gaseous hydrogen environment, Int J Hydrog Energy 42(26) (2017) 16887-16900.

[26] M. Nakamura, S. Okazaki, H. Matsunaga, S. Matsuoka, SSRT and fatigue life properties of austenitic stainless steel weld metal 317L in high-pressure hydrogen gas, Transactions of the JSME (in Japanese) 84(857) (2018) 1-20.

[27] J. Yamabe, M. Yoshikawa, H. Matsunaga, S. Matsuoka, Hydrogen trapping and fatigue crack growth property of low-carbon steel in hydrogen-gas environment, Int. J. Fatigue 102 (2017) 202-213.

[28] H. Matsunaga, O. Takakuwa, J. Yamabe, S. Matsuoka, Hydrogen-enhanced fatigue crack growth in steels and its frequency dependence, Philosophical Transactions A 375(2098) (2017).

[29] S. Matsuoka, J. Yamabe, H. Matsunaga, Criteria for determining hydrogen compatibility and the mechanisms for hydrogen-assisted, surface crack growth in austenitic stainless steels, Eng. Fract. Mech. 153 (2016) 103-127.

[30] T.L. Anderson, Fracture Mechanics: Fundamentals and Applications, third ed., CRC Press, Boca Raton, 2005.

[31] D. Wan, Y. Deng, A. Barnoush, Hydrogen embrittlement effect observed by in-situ hydrogen plasma charging on a ferritic alloy, Scr. Mater. 151 (2018) 24-27.

[32] C.G. Morgan, R. Vane, Removal of Carbon Contamination using Hydrogen with Low-Power Downstream Plasma Cleaning. https://evactron.com/wp-content/uploads/2016/10/cleaningwithh2advlith2011.pdf, 2011).

[33] G.M. Bond, I.M. Robertson, H.K. Birnbaum, On the determination of the hydrogen fugacity in an environmental cell tem facility, Scripta Metall. 20(5) (1986) 653-658.

[34] S.-S. Rui, Y.-B. Shang, W. Qiu, L.-S. Niu, H.-J. Shi, S. Matsumoto, Y. Chuman, Fracture mode identification of low alloy steels and cast irons by electron back-scattered diffraction misorientation analysis, Journal of Materials Science & Technology 33(12) (2017) 1582-1595.

[35] S.-S. Rui, Y.-B. Shang, Y. Su, W. Qiu, L.-S. Niu, H.-J. Shi, S. Matsumoto, Y. Chuman, EBSD analysis of cyclic load effect on final misorientation distribution of post-mortem low alloy steel: A new method for fatigue crack tip driving force prediction, Int. J. Fatigue 113 (2018) 264-276.

[36] H. Vehoff, P. Neumann, In situ sem experiments concerning the mechanism of ductile crack growth, Acta Metall. 27(5) (1979) 915-920.

[37] C. Laird, G.C. Smith, Crack propagation in high stress fatigue, Philos. Mag. 7(77) (1962) 847-857.

[38] S.S. Chakravarthy, W.A. Curtin, Origin of plasticity length-scale effects in fracture, Phys. Rev. Lett. 105(11) (2010) 115502.

[39] M. Nagumo, K. Miyamoto, Microscopic Process of Failure and Mechanism of Hydrogen Embrittlement of Iron, J. Jpn. Inst. Met. 45(12) (1981) 1309-1317.

[40] M. Nagumo, T. Takahashi, Hydrogen embrittlement of some Fe-base amorphous alloys, Mater. Sci. Eng. 23(2-3) (1976) 257-259.

[41] Y. Ogawa, D. Birenis, H. Matsunaga, O. Takakuwa, J. Yamabe, Ø. Prytz, A. Thøgersen, Hydrogen-assisted fatigue crack propagation in a pure BCC iron. Part I: Intergranular crack propagation at relatively low stress intensities, MATEC Web of Conferences 165 (2018) 03011.

[42] Y. Ogawa, H. Matsunaga, J. Yamabe, M. Yoshikawa, S. Matsuoka, Unified evaluation of hydrogen-induced crack growth in fatigue tests and fracture toughness tests of a carbon steel, Int. J. Fatigue 103 (2017) 223-233.

[43] Y. Ogawa, H. Matsunaga, M. Yoshikawa, J. Yamabe, S. Matsuoka, Fatigue Life Properties and Anomalous Macroscopic Fatigue Fracture Surfaces of Low Carbon Steel JIS-SM490B in High-Pressure Hydrogen Gas Environment, ASME 2016 Pressure Vessels and Piping Conference, 2016, p. V06BT06A027.

[44] F. Terasaki, T. Kawakami, A. Yoshikawa, N. Takano, Mechanism of crack propagation due to hydrogen embrittlement in iron single crystals stressed along [001] axis, Revue de Métallurgie 95(12) (2017) 1519-1529.

[45] H. Vehoff, W. Rothe, Overview .30. Gaseous-Hydrogen Embrittlement in Fesi-Single and Ni-Single Crystals, Acta Metall. 31(11) (1983) 1781-1793.

[46] D. Wan, A. Alvaro, V. Olden, A. Barnoush, Hydrogen-assisted fatigue crack growth in ferritic steels – a fractographic study, MATEC Web of Conferences, 2018, p. 03004.

[47] D. Birenis, Y. Ogawa, H. Matsunaga, O. Takakuwa, J. Yamabe, Ø. Prytz, A. Thøgersen, Interpretation of hydrogen-assisted fatigue crack propagation in BCC iron based on dislocation structure evolution around the crack wake, Acta Mater. 156 (2018) 245-253.

[48] Y. Deng, A. Barnoush, Hydrogen embrittlement revealed via novel in situ fracture experiments using notched micro-cantilever specimens, Acta Mater. 142 (2018) 236-247.

[49] B.R.S. Rogne, N. Kheradmand, Y. Deng, A. Barnoush, In situ micromechanical testing in environmental scanning electron microscope: A new insight into hydrogen-assisted cracking, Acta Mater. 144 (2018) 257-268.

[50] T. Hajilou, Y. Deng, B.R. Rogne, N. Kheradmand, A. Barnoush, In situ electrochemical microcantilever bending test: A new insight into hydrogen enhanced cracking, Scr. Mater. 132 (2017) 17-21.

[51] S. Taketomi, R. Matsumoto, N. Miyazaki, Atomistic study of hydrogen distribution and diffusion around a {112}<111> edge dislocation in alpha iron, Acta Mater. 56(15) (2008) 3761-3769.

[52] Y. Murakami, T. Kanezaki, Y. Mine, Hydrogen Effect against Hydrogen Embrittlement, Metall. Mater. Trans. A 41(10) (2010) 2548-2562.

[53] R. Kirchheim, Solid solution softening and hardening by mobile solute atoms with special focus on hydrogen, Scr. Mater. 67(9) (2012) 767-770.
[54] S. Puydebois, A. Oudriss, P. Bernard, L. Briottet, X. Feaugas, Hydrogen effect on the fatigue behavior of LBM Inconel 718, MATEC Web of Conferences 165 (2018) 02010.
[55] T. Matsuo, S. Matsuoka, Y. Murakami, Fatigue crack growth properties of quenched and tempered Cr-Mo steel in 0.7 MPa hydrogen gas, The 18th European Conference on Fracture: Fracture of Materials and Structures from Micro to Macro Scale, Dresden, Germany, 2010.
[56] M. Yoshikawa, T. Matsuo, N. Tsutsumi, H. Matsunaga, S. Matsuoka, Effects of hydrogen gas pressure and test frequency on fatigue crack growth properties of low carbon steel in 0.1-90 MPa hydrogen gas, Transactions of the JSME 80(817) (2014) SMM0254.
[57] P. Sofronis, R.M. McMeeking, Numerical analysis of hydrogen transport near a blunting crack tip, J. Mech. Phys. Solids 37(3) (1989) 317-350.
[58] H. Kotake, R. Matsumoto, S. Taketomi, N. Miyazaki, Transient hydrogen diffusion analyses coupled with crack-tip plasticity under cyclic loading, International Journal of Pressure Vessels and Piping 85(8) (2008) 540-549.
[59] K. Kiuchi, R.B. McLellan, The solubility and diffusivity of hydrogen in well-annealed and deformed iron, Acta Metall. 31(7) (1983) 961-984.
[60] D. Hull, D.J. Bacon, Introduction to Dislocations 5th Edition, Elsevier, Amsterdam, 2011.

Paper 4

Plasticity in cryogenic brittle fracture of ferritic steels: dislocation versus twinning

Di Wan*, Afrooz Barnoush

Mater. Sci. Eng., A 744 (2019) 335-339, DOI: 10.1016/j.msea.2018.12.038.

Plasticity in cryogenic brittle fracture of ferritic steels: dislocation versus twinning

Di Wan, Afrooz Barnoush

Department of Mechanical and Industrial Engineering, Norwegian University of Science and Technology, Richard Birkelands vei 2B, 7491 Trondheim, Norway.

Abstract

The sub-surface deformation structure after cryogenic (77 K) brittle fracture in a ferritic steel was characterized by scanning electron microscopy (SEM). Twin-like structures were found in many grains below the fracture surface. Electron backscatter diffraction (EBSD) was used to identify the crystallography of the structures, and the twin relation in body-centered cubic (BCC) systems was indexed. The twins in the sub-surface area were characterized further by electron channeling contrast imaging (ECCI). This study clarifies the low temperature brittle fracture behavior in the ferritic Fe-3wt%Si steel consists of both cleavage and plastic deformation in the form of dislocation activities and twinning.

Keywords: cleavage fracture, twinning, scanning electron microscopy, EBSD, ECCI, BCC.

1. Introduction

It is universally acknowledged that metals can change their mechanical performances when the temperature reaches a certain low level. A famous disaster is the sinking of the RMS Titanic, in which the brittle fracture of steel at extreme cold temperature after a collision with an iceberg was a major reason [1]. As the most dangerous form of fracture, the brittle cleavage fracture is a transgranular fracture by the separation of well-defined crystallographic planes, which in ferritic steels are the {100} planes [2]. Based on the classical theory, this kind of brittle fracture is typically associated with no plastic deformation, and the loading energy is normally released by the separation of certain atomic bonds defined by crystallography. This concept was integrated into the famous Griffith model in explaining fracture toughness. From literature, major characterizations are focusing on the fractography, and the microstructural changes in the vicinity of the crack are simply ignored. This is mainly due to the challenging

requirement for sample preparation. Recent development by means of focused ion beam (FIB) and lift-out method plus transmission electron microscopy (TEM) observation [3-5] is promising, but still the observation is limited to a very small area, and on the other hand this technique is very time-consuming. In this study, we shift the key point from the fracture surface to the sub-surface area. Specifically by means of scanning electron microscopy (SEM) based techniques including electron backscatter diffraction (EBSD) and electron channeling contrast imaging (ECCI), we are extending our observation to a much larger area along and below the crack, while still capable of observing single dislocation as in the case of TEM. This new method has a potential to make a paradigm shift in the study of the fracture process and as an example, we show its application for understanding the mechanism of low temperature brittle fracture.

Dislocation slipping and mechanical twinning are two common plastic deformation mechanisms. Despite the difficulties, twinning deformation in body-centered cubic (BCC) metals is reported and summarized in some review articles [6-8]. The occurrence of twinning was linked to brittle fracture in some BCC metals [9]. Cheng et al. [10] observed ferrite twins in a Fe-Mn-Al alloy by quenching the material from high temperature, and categorized them as mechanical twins induced by the thermal strain energy relief. This mechanism could contribute to a large portion of the energy release since the intrinsic stacking fault energy (SFE) in BCC materials is relatively high [11, 12].

The present study shows that the deformation structure under a cryogenic (77 K) fracture surface is associated with some plasticity in the form of dislocation activities and the formation of twin-like structures. BCC steels are one of the most widely used structural materials served in various industries subjected to low temperature, such as the oil and gas industries or marine industries in the arctic regions. To understand the fundamental deformation and fracture mechanisms under low temperature is significantly supportive to know the behaviors of the engineering structures in the extreme conditions.

2. Experimental

In this study, compact tension (CT) specimens according to the ASTM E647-13 standard were cut by electrical discharge machining (EDM) from a large-grained (grain size approx. 300 μm) Fe-3wt%Si ferritic steel. The chemical composition is the same

as in [13]. Pre-cracks were initiated by fatigue loading. Pliers were used to hold the CT specimen in the holes with fixed relative position, and the specimen was put into liquid nitrogen (77 K) with the pliers jaws. Manual loading was applied through the pliers handles outside of the liquid nitrogen in an opening manner and the specimen fractured in the liquid nitrogen, as schematically described in Fig. 1. With this method, the loading was exerted when the specimen was inside the liquid nitrogen, which means the fracture happened in cryogenic environment. The reproducibility of the presented result was confirmed after loading more than 10 specimens using the same method, and the fracture morphology was confirmed as completely cleavage type in all cases. The fractography was done by a Quanta 650 SEM (Thermo Fisher Scientific Inc., USA). After fractography, the low temperature fractured part of the specimen was cut and the fracture surface was electrodeposited with Fe. The cross-section of the sample was then prepared by grinding to #4000 emery paper plus final electropolishing in H2SO4-methanol electrolyte. Thanks to the coating, the deformation zone near the fracture surface could be well preserved. The cross-section of the fractured sample was further investigated by EBSD and ECCI in the same SEM. With the help of ECCI, plasticity such as dislocations and twins can be investigated in bulk samples in SEM. Detailed technical information of this imaging technique can be found in [14].

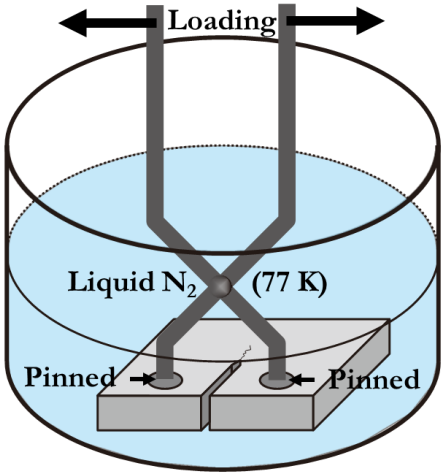

Fig. 1 Schematic description of the loading condition: CT specimens with pre-crack fractured inside liquid nitrogen by manual loading.

3. Results and discussion

Fig. 2 shows the fracture surface after low temperature loading. The whole surface has a pure transgranular brittle cleavage-like pattern. Clear river patterns can be observed over the surface. Sharp facets having an angle of roughly 90° can be seen at the end of some grains. This is common since the cleavage plane in BCC structure is {100} planes. This figure confirms the brittle cleavage behavior of the test piece under such loading conditions.

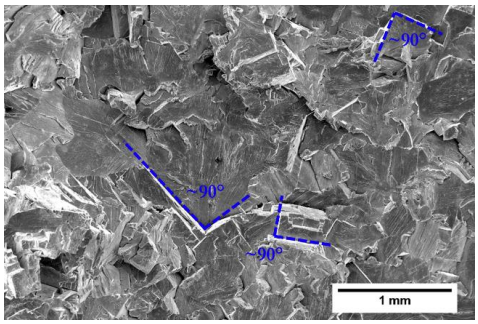

Fig. 2 Fractography showing pure cleavage type fracture of the investigated sample. The blue dash lines indicate that an approximate angle of 90° can be found between the facets.

Fig. 3 is the sub-surface microstructure characterized by ECCI. An overview is shown in Fig. 3a. A plastic zone can extend into the matrix by about 100 μm. Some twin-like structures with a width up to one micrometer can be found, and these structures can influence the direction of some secondary cleavage cracks, deflecting the cracks by small steps, as shown by the yellow arrows. A magnified view of the twin-like structure is shown in Fig. 3b. Dislocation slipping lines can go through this band structure with the outgoing direction unchanged. Individual dislocation lines can be observed at the end of the twin-like structure. Secondary cracks are seen inside the grain matrix as indicated by the yellow arrows in Fig. 3a. Some of the secondary cracks are stopped by the twin-like structures, as indicated by the white arrow. Fig. 3c shows a magnified view of the end of one secondary crack. Individual dislocations are found near the crack. Fig. 3d shows an interaction area between a twin-like structure and a grain boundary (GB). Plasticity is observed emitting from the intersection zone. Heavy plastic deformation (large dislocation density) can be found near the intersection area, and it becomes less and less significant when going into the grain, as indicated by the dash-lines with arrows heading dislocation emitting directions. To clarify the nature of this twin-like structure, EBSD was used to check the crystallographic information.

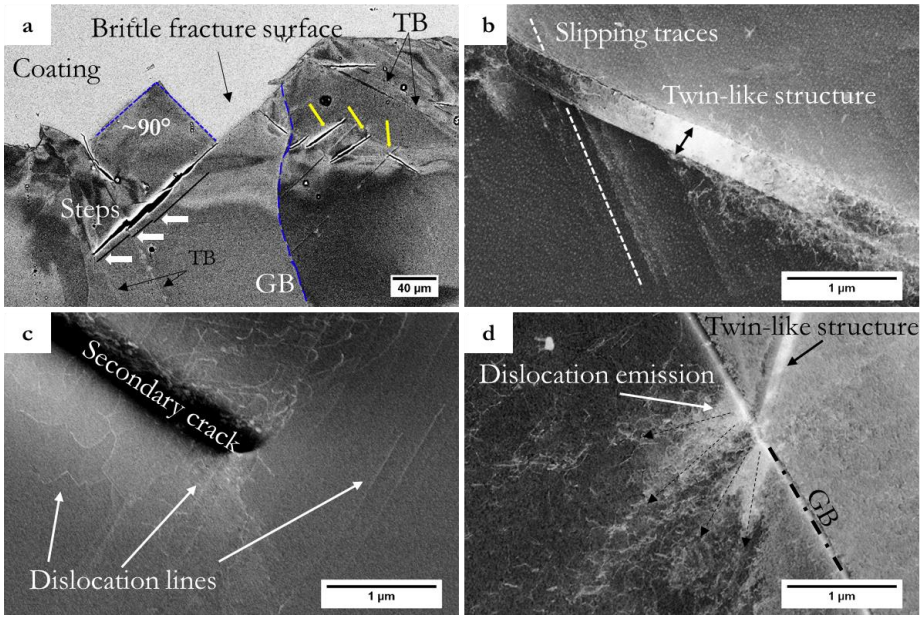

Fig. 3 Deformation structure below the fracture surface. (a. overview showing the sub-surface microstructure; b. twin-like structure with dislocations; c. dislocations near a secondary crack; d. intersection between a twin-like structure and a GB). The white arrows in a. indicate the steps introduced by the twin-like structures. The yellow arrows in a. indicate secondary cracks formed inside the matrix. Electronic version in color.

Fig. 4 shows the normal direction (ND) – inverse pole figure (IPF) map of an area below the cleavage fracture surface by EBSD scan. High angle grain boundaries (HAGBs) and twin boundaries (TBs) are indexed. The TBs in this map are defined as 60° with respect to <111> axis and the twin plane is defined as {112} [6]. The {112} pole figure (PF) is plotted for the red (grain matrix) and blue (twin-like structure) parts of the big grain in the lower part of the IPF map, and the poles were plotted as red and blue, respectively. It can be seen that three poles are overlapping each other as the highlighted circles in the PF. This means the red and blue parts share same {112} planes, which is the twinning plane of BCC crystals. The misorientation profile over a distance of about 5 µm across the blue part is plotted, as shown in the lower right corner of Fig. 4. A misorientation of about 60° can be seen between the red and blue part, which suggests a typical twinning relation. {100} traces are marked near the fracture surface, all of which show parallel relation to the fracture plane, suggesting cleavage separation of the {100} planes. Some regions of interest (ROIs) are highlighted in this figure and further characterized in details.

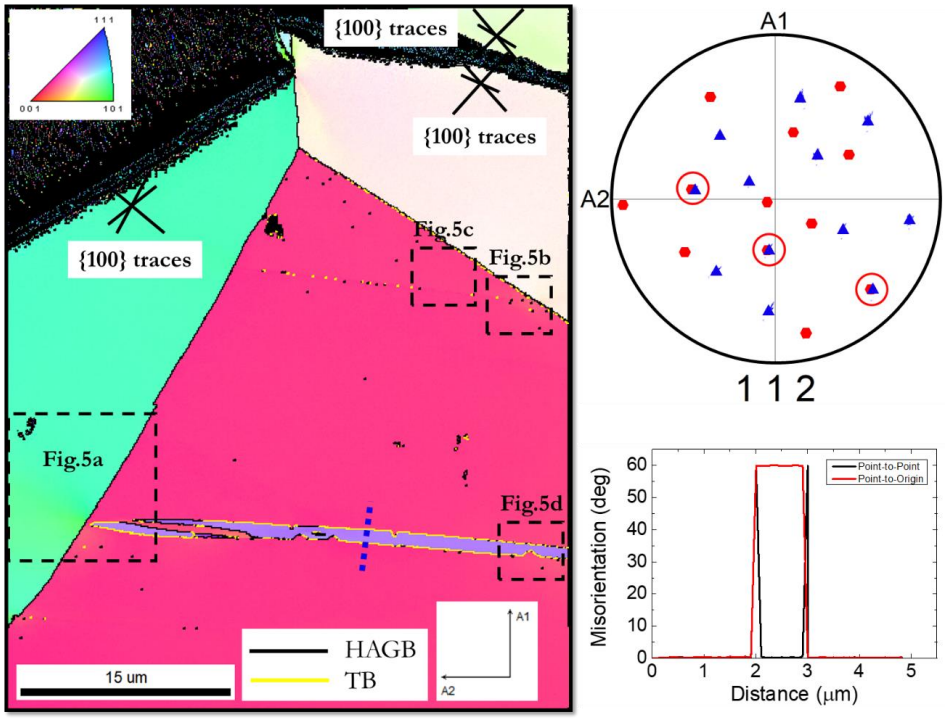

Fig. 4 ND-IPF map and the corresponding {112} PF of the red grain and the blue part inside the red grain of the area below the fracture surface. {100} plane traces are marked near the fracture surface. TB can be indexed between the blue and the red parts. Three overlapping poles are highlighted in the pole figure. Misorientation profile is plotted over the highlighted blue dot-line in the IPF map.

Fig. 5 shows a close-up investigation of the twin-like structures highlighted in Fig. 4. A large area of plastic deformation in the neighboring grain can be observed in Fig. 5a. The plasticity was emitting from the intersection between the twin-like structure and the HAGB. In Fig. 5b, a plastic zone was found also inside the grain containing the twin-like structure. Clear individual dislocations can be observed near the plastic zone. These individual dislocations can generally be found in the grain, as in Fig. 5c. From the EBSD information, most of these dislocation lines are parallel to the <111> directions of this grain, suggesting a large fraction of screw dislocation components. In Fig. 5d, an imperfection in the twin-like structure is presented. A triangular shaped zone is observed connecting the boundary, and arrays of dislocations are emitted from the intersecting points on the straight boundary. The arrays are also parallel to the <111> directions. From this figure, the largest width of this twin-like structure is measured to be about 1 μm.

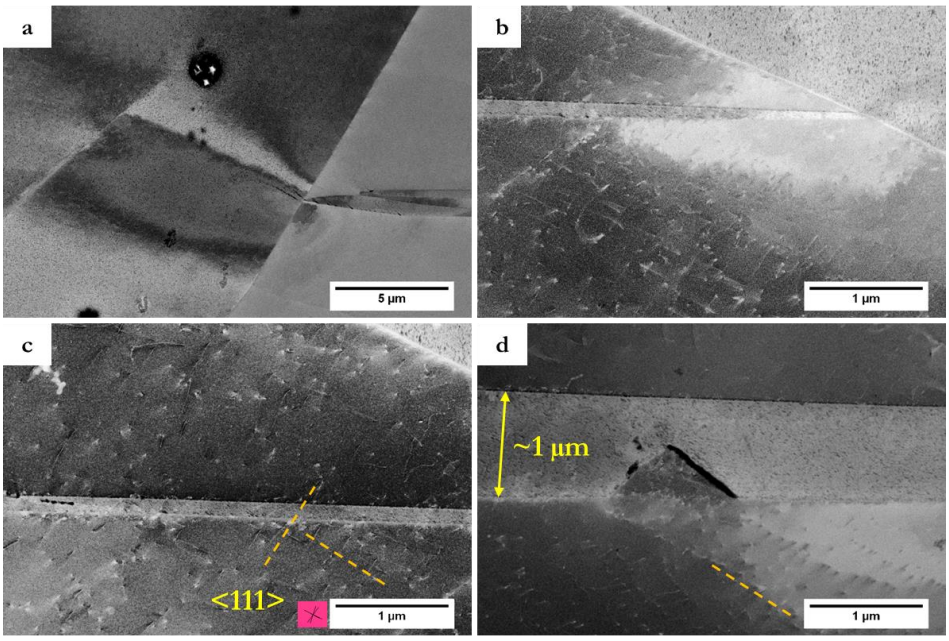

Fig. 5 Detailed investigation of the twin-like structure. (a. induced plasticity in the neighboring grain; b. plasticity near the intersection zone between the twin-like structure and a grain boundary; c. dislocation structure near the twin-like structure; d. imperfection in the twin-like structure. The lines in the red rectangular in c. and the yellow dash lines indicate the <111> directions indexed by EBSD. All corresponding ROIs are marked in Fig. 4.)

As is pointed out by Chen [2], a plasticity should be expected locally to trigger the cleavage fracture of ferritic steels at low temperature. The energy release, as well as the stress redistribution, is strongly associated with the distribution of this plastic zone. The local plastic flow is a necessary precursor to cleavage and yielding, which might be induced by dislocation slipping or twinning [15]. In the present investigation, local plasticity was observed generally spread near the fracture surface. Both dislocation slip and twinning are found contributing to the local plasticity (c.f. Fig. 3). According to the results in both Fig. 3 and Fig. 5, the twins could also influence the plasticity in the surrounding area.

The low temperature deformation behavior of pure iron has been studied using small-scale mechanical testing (micro-pillar bending) and molecular dynamics (MD) simulations [16, 17]. It is suggested that the dislocation slipping behavior at low temperature is mainly controlled by the screw components due to the intrinsic core structure. As shown in Fig. 5c, the dislocation lines are generally parallel to the <111> directions of the grain, and since the perfect dislocations in BCC lattice have the burgers

vector of ½ <111>, it could be concluded that the dislocations here are containing a large fraction of screw components.

As is generally investigated and modelled, the screw dislocation motion in BCC materials is mainly realized by the double kink mechanism [18-21]. Since this mechanism is a thermally activated process, the screw dislocation motion depends strongly on the temperature. When the temperature decreases, the thermal activation energy of screw dislocation motion is also decreasing. According to the dislocation dynamics simulation results [21], at low temperature the dislocations prefer to form long straight lines. When looking at the investigated dislocation lines inside the grain such as Fig. 3c and Fig. 5b-d, long straight dislocation lines parallel to the <111> crystallographic directions are found, which give proof to the simulation results in [21]. We could thus conclude that although pure cleavage brittle fracture happened to the investigated specimen under cryogenic temperature, some plastic activities were still happening in the grains near the fracture surface in the form of screw dislocation motion. However, if we start talking about the twinning behavior in the investigated material, it is considered as a less popular topic that was paid less attention.

Conventionally, twinning in ferrite is relatively difficult since the intrinsic stacking fault energy (SFE) is extremely high that can reach up to ~1 J/m2 [11, 22]. The MD simulations indicate that twinning can happen in pure Fe micro-pillar when the temperature is lowered to 15 K [16, 17]. However, the twinning phenomenon has already been observed at 77 K in the Fe-3wt% bulk specimen in the present study. Several reasons could be attributed to this discrepancy. Das [23] reported Si can decrease the stacking fault energy of an alloy, which is an important parameter of the twinning possibility of a material. During unexpected brittle fracture, the stress concentration at the crack-tip will be much higher than the static loading condition. And deformation twins in BCC materials can be induced by this heavy deformation [6]. Based on the facts stated above, the twinning phenomenon can happen more easily in the studied material than the prediction to pure iron [16, 17]. Although previous works found proof of twins in ferritic materials [24-26], they focus only on the fracture surface and no detailed crystallographic information was given. Instead, we used advanced high resolution SEM techniques to characterize the twin structure and successfully correlated the structure with crystallography. The <111>-60° twin boundary with a

common {112} plane was confirmed and thus giving explicit proof to the twinning behavior in the studied BCC material.

Reid [9] summarized the relation between twinning and brittle fracture. The relation is different from case to case, but most cases fall in these four categories: 1. twinning and brittle fracture are independent processes; 2. twins are nucleated by cracking; 3. cracks are nucleated by twins, but the cracks may or may not continue propagation; 4. twins provide preferred path for crack propagation. According to Fig. 3a, most of the secondary cracks are located away from the twins, and some are stopped by the twins. No strong proof can correlate the primary crack (corresponding to the fracture surface) and the twin structures. It is thus inferred that the twins would not induce the crack nucleation in the studied case. From the same figure, the cracks are not along the same direction as the twins, although they are located in the same grain. Thus the twins in the studied case could not provide a preferred path for the crack propagation. From literature, some proof of twinning in ferrite could be found on fractographs after cyclic loading at 123 K [25] or monotonic tensile loading at 77 K [24]. Except that the twins were found together with cleavage fracture, there is no unique association between twinning and fracture in BCC metals and alloys [9].

A possible mechanism of the twin nucleation was described in detail in Ref. [22]. One ½ <111> screw dislocation is considered to dissociate into three 1/6 <111> fractional dislocations with a configuration symmetric to the <111> screw axis. This configuration is stable under zero stress state. However, the fractional dislocations will translate on the most stressed {112} plane under external loading, and form a three-layer stacking fault. This is considered as the nucleus of the twin, and further dislocation motion on the {112} plane would be considered as twin growth. The screw dislocation motion requires a thermal activation due to the dissociated core structure, thus the dislocation mobility is strongly reduced at low temperature. Therefore, the twinning mechanism mentioned above could contribute partly to the plastic energy release from the external loading. This mechanism is in good agreement with some proposed mechanisms and the corresponding experimental results [27-29].

4. Summary

To sum up, we did combined high resolution ECCI and EBSD characterizations on a ferritic specimen that was fractured at cryogenic temperature (77 K). Some of the conclusions could be drawn:

- The cryogenic cleavage fracture of the studied ferritic Fe-3wt%Si steel was associated with plastic deformation near the fracture surface in the form of dislocation emission and twinning.
- For the first time, a <111> 60° type twin boundary with common {112} plane relation in the studied material was characterized by the combined ECCI + EBSD technique. The characterizations provide both detailed crystallographic information and microstructure feature with resolution up to single dislocation line level. This technique is promising in the analysis of the fracture process zone in a much larger area than conventional TEM investigations.
- The twinning mechanism in BCC structure was discussed, which was considered to be related with the dissociation of <111> screw dislocations and the dislocation motion on stressed {112} planes.

A promising outlook of this work is to construct a proper experimental setup that is able to control the load and testing environment (e.g. temperature control) as well as record the mechanical data for further analysis. This is ongoing in the authors' research group and will be the prospect of the future work.

Author contributions

D. Wan conducted all experimental work, data analysis, interpretation and prepared the manuscript. A. Barnoush is the supervisor of this work. Both authors discussed the manuscript and approved for submission.

Competing interests statement

The authors do not have competing interests.

Acknowledgement

This work was supported by the Research Council of Norway through the project HyF-Lex (project number: 244068/E30). Discussion on dislocation and twinning behavior characterization from Prof. Yanjun Li at Department of Materials Science and

Engineering, Norwegian University of Science and Technology is gratefully acknowledged.

Data availability statement

The raw/processed data required to reproduce these findings cannot be shared at this time due to technical or time limitations.

References

[1] K. Felkins, H.P. Leigh, A. Jankovic, The royal mail ship Titanic: Did a metallurgical failure cause a night to remember?, JOM 50(1) (1998) 12-18.
[2] J.H. Chen, R. Cao, Micromechanism of Cleavage Fracture of Metals, Elsevier, Amsterdam, 2015.
[3] S. Lee, J. Jeong, Y. Kim, S.M. Han, D. Kiener, S.H. Oh, FIB-induced dislocations in Al submicron pillars: Annihilation by thermal annealing and effects on deformation behavior, Acta Mater. 110 (2016) 283-294.
[4] M.J. Pfeifenberger, M. Mangang, S. Wurster, J. Reiser, A. Hohenwarter, W. Pfleging, D. Kiener, R. Pippan, The use of femtosecond laser ablation as a novel tool for rapid micro-mechanical sample preparation, Materials & Design 121 (2017) 109-118.
[5] Y. Deng, A. Barnoush, Hydrogen embrittlement revealed via novel in situ fracture experiments using notched micro-cantilever specimens, Acta Mater. 142 (2018) 236-247.
[6] J.W. Christian, S. Mahajan, Deformation twinning, Prog. Mater Sci. 39(1-2) (1995) 1-157.
[7] S. Mahajan, D.F. Williams, Deformation Twinning in Metals and Alloys, International Metallurgical Reviews 18(2) (2013) 43-61.
[8] M.A. Meyers, O. Vöhringer, V.A. Lubarda, The onset of twinning in metals: a constitutive description, Acta Mater. 49(19) (2001) 4025-4039.
[9] C.N. Reid, The association of twinning and fracture in bcc metals, Metall. Trans. A 12(3) (1981) 371-377.

[10] W.-C. Cheng, Y.-S. Lin, K.-F. Chen, The formation of ferrite quenching twins in a body-centered cubic Fe–Mn–Al alloy during high-temperature quenching, Scr. Mater. 81 (2014) 36-39.

[11] J.-A. Yan, C.-Y. Wang, S.-Y. Wang, Generalized-stacking-fault energy and dislocation properties in bcc Fe: A first-principles study, Phys. Rev. B 70(17) (2004).

[12] V. Vítek, Intrinsic stacking faults in body-centred cubic crystals, Philos. Mag. 18(154) (1968) 773-786.

[13] D. Wan, Y. Deng, A. Barnoush, Hydrogen embrittlement effect observed by in-situ hydrogen plasma charging on a ferritic alloy, Scr. Mater. 151 (2018) 24-27.

[14] S. Zaefferer, N.N. Elhami, Theory and application of electron channelling contrast imaging under controlled diffraction conditions, Acta Mater. 75 (2014) 20-50.

[15] D.A. Curry, Cleavage micromechanisms of crack extension in steels, Metal Science 14(8-9) (2013) 319-326.

[16] A.B. Hagen, B.D. Snartland, C. Thaulow, Temperature and orientation effects on the deformation mechanisms of α-Fe micropillars, Acta Mater. 129 (2017) 398-407.

[17] A.B. Hagen, C. Thaulow, Low temperature in-situ micro-compression testing of iron pillars, Mater. Sci. Eng., A 678 (2016) 355-364.

[18] C. Domain, G. Monnet, Simulation of screw dislocation motion in iron by molecular dynamics simulations, Phys. Rev. Lett. 95(21) (2005) 215506.

[19] L.H. Yang, J.A. Moriarty, Kink-pair mechanisms for a/2 〈111〉 screw dislocation motion in bcc tantalum, Mater. Sci. Eng., A 319-321 (2001) 124-129.

[20] M. Wen, A.H.W. Ngan, Atomistic simulation of kink-pairs of screw dislocations in body-centred cubic iron, Acta Mater. 48(17) (2000) 4255-4265.

[21] S. Naamane, G. Monnet, B. Devincre, Low temperature deformation in iron studied with dislocation dynamics simulations, Int. J. Plast. 26(1) (2010) 84-92.

[22] A. Ojha, H. Sehitoglu, L. Patriarca, H.J. Maier, Twin nucleation in Fe-based bcc alloys—modeling and experiments, Modell. Simul. Mater. Sci. Eng. 22(7) (2014) 075010.

[23] A. Das, Revisiting Stacking Fault Energy of Steels, Metall. Mater. Trans. A 47(2) (2015) 748-768.

[24] T. Sakaki, T. Nakamura, Cleavage Fracture of Iron Single Crystals, Tetsu-To-Hagane 59(7) (1973) 955-966.

[25] W. Yu, K. Esaklul, W.W. Gerberich, Fatigue threshold studies in Fe, Fe-Si, and HSLA steel: Part II. thermally activated behavior of the effective stress intensity at threshold, Metall. Trans. A 15(5) (1984) 889-900.

[26] F. Nakasato, I.M. Bernstein, Crystallographic and fractographic studies of hydrogen- induced cracking in purified iron and iron- silicon alloys, Metall. Trans. A 9(9) (1978) 1317-1326.

[27] S. Mahajan, Interrelationship between slip and twinning in B.C.C. crystals, Acta Metall. 23(6) (1975) 671-684.

[28] A.W. Sleeswyk, Emissary dislocations: Theory and experiments on the propagation of deformation twins in α-iron, Acta Metall. 10(8) (1962) 705-725.

[29] A.W. Sleeswyk, Twinning and the origin of cleavage nuclei in α-iron, Acta Metall. 10(9) (1962) 803-812.

Paper 5

Hydrogen-assisted fatigue crack growth in ferritic steels – a fractographic study

Di Wan*, Antonio Alvaro, Vigdis Olden, Afrooz Barnoush

MATEC Web of Conferences, 2018, p. 03004, DOI:
10.1051/matecconf/201816503004.

Hydrogen-assisted fatigue crack growth in ferritic steels – a fractographic study

Di Wan[1,*], Antonio Alvaro[2], Vigdis Olden[2], Afrooz Barnoush[1]

1. Department of Mechanical and Industrial Engineering, Norwegian University of Science and Technology, Richard Birkelands vei 2B, 7491 Trondheim, Norway

2. SINTEF Materials and Chemistry, 7456 Trondheim, Norway

Abstract Fatigue crack growth (FCG) behavior of a Fe-3wt.%Si ferritic alloy under different environmental conditions using in-situ electrochemical (cathodic) hydrogen (H) charging has been investigated. Three frequencies have been applied. Results clearly show that the FCG rate increased by a factor spanning from 20 to 1000 times, depending on the loading frequencies, when compared to the reference test in air. Lower frequency leads to higher FCG rate. A comprehensive fractographic analysis was carried out: the area fraction of different fracture surface features was measured and taken into statistical analysis. Based on these investigations, the possible mechanisms of H-enhanced FCG are discussed. Similar tests in high-pressure H gas from other studies were also compared and discussed. These results give a preliminary understanding of H effect in fatigue crack propagation procedure in ferritic alloys.

1. Introduction

It is generally acknowledged that engineering structures are normally experiencing different loads such as static load, cyclic load, impact load or a combination of several loads from the above-mentioned category. And a very common condition is cyclic loading combining a static loading. Researches regarding the fracture behavior from repeated loading have been published over a century and continue increasing. According to the data from Battele Laboratory under contract to United States Government agencies in 1983, the costs of fractures and efforts to prevent fracture amounted to 119 billion US dollars per year, which occupied a considerable part of the gross national product at that time [1]. It can be expected that this number becomes different today due to a faster development in industry. The classical fatigue crack growth behavior can be simplified by a logarithmic linear relation, which is called the Paris' law (or Paris-Erdogan law), as shown in Eq. (1):

$$da/dN = C \cdot \Delta K^m \qquad (1)$$

where a is the crack length, N is the number of cycles and da/dN is the crack growth rate, describing the infinitesimal crack length per increasing number of load cycles. C and m on the right-hand side are constants depending on material and test conditions. ΔK is the range of the stress intensity factor during fatigue loading, and is defined as Eq. (2):

$$\Delta K = K_{max} - K_{min} \qquad (2)$$

where K_{max} and K_{min} are the maximum and minimum value of the stress intensity factor, respectively.

This relation is favored by many engineers since by taking a simple logarithmic operation, the crack growth rate and the stress intensity factor range can be treated as a linear relation, and it's easier for engineers to predict how fast the crack can grow without repairing it.

A factor that degrades the mechanical behavior of materials is the environmental effect, especially the environment containing hydrogen (H), in which the materials can become more brittle than in other cases. This phenomenon is named hydrogen embrittlement (HE) and has been studied since the first publication by Johnson [2] in 1875. The HE effect of metallic materials has been intensively discussed over the past century. It draws engineers' attention since it can cause catastrophic failure of metallic structures that serve in a H-containing environment. Several different mechanisms have been developed, and the most common ones are hydrogen-enhanced localized plasticity (HELP) [3-8], hydrogen-enhanced decohesion (HEDE) [9-12], adsorption-induced dislocation emission (AIDE) [13], hydrogen-enhanced vacancy production [14, 15], hydrogen-induced phase transformation [16-18] etc. These mechanisms describe the HE effect in terms of different aspects ranging from chemical bonding up to microstructure level. A systematic review has been established by Murakami et al. [19] regarding the H effect on the fatigue crack propagation in steels.

For most oil and gas industries in the arctic region, the metallic structures will serve in a H-containing environment (e.g. ocean) with a continuous vibrational loading. Hence the fatigue properties with environmental effect of those structures are of significant importance. The purpose of this study is to study the mechanism in the degradation of

structural materials that serve in the condition with cyclic loading and H environment and try to correlate the physical mechanism with engineering aspects. For this purpose, Fatigue Crack Growth Rate (FCGR) tests were done on a ferritic alloy with large grain size in different environments. The FCGR data were analyzed and correlated with the classical Paris' law. The results showed a strong effect of promoting crack propagation in H environment by a factor spanning from 20 to 1000 times. Scanning Electron Microscopy (SEM) characterization was done on the fractured specimens. The reasons for the degradation were discussed.

2. Experimental

2.1 Materials

The materials used in this study is a Fe-3wt.%Si alloy with pure ferritic structure. The grain size of the as-received material is about 300 μm. The chemical composition of this material is shown in Table 1.

Compact Tension (CT) specimens according to the ASTM E647 standard were cut from the raw material by Electric Discharge Machining (EDM). The geometry is shown in Figure 1.

Table *1*. Chemical composition of the investigated material.

Element	C	Si	Mn	P
wt.%	0.018	3.000	0.055	0.008
Element	Cu	Al	Ti	Nb
wt.%	0.013	0.015	0.001	0.002
Element	S	Cr	Ni	Mo
wt.%	0.003	0.010	0.006	0.003
Element	V	B	Zr	Fe
wt.%	0.001	0.0002	0.0010	Bal.

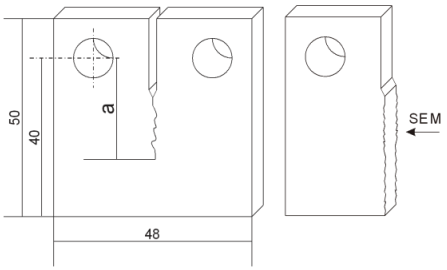

Figure *1*. Schematic of the CT specimen (thickness = 8, unit: mm). SEM characterization was done on the fractured half-specimen.

2.2 Fatigue crack growth rate test

The CT specimens were first pre-cracked by fatigue test by the same procedure as described in Ref.[20]. The final pre-cracks normally have a length ranging between 1 to 3 mm. For the FCGR test, an initial stress intensity factor range (ΔK) corresponding to a 2.5% increase from the last ΔK value of the pre-crack test was applied. The fatigue crack growth rates and the crack length were recorded via an alternate current potential

drop (AC-PD) device. The tests were done at room temperature in lab air and in an electrochemical cell. The frequencies were chosen to be 0.1 Hz, 1 Hz and 10 Hz and the load ratio R was kept 0.5 during the test to reduce the crack closure effect.

For H-charging, the electrolyte was chosen to be a neutral 0.1M Na_2SO_4 solution. The specimen was in-situ cathodically charged with a constant potential of -1400 mV_{SCE}. Multimeters were used during the charging procedure, to make sure the whole circuit runs as designed.

After tests, the specimens were put into liquid nitrogen and broken into two parts. The half-specimens were used for further characterization.

2.3 Characterization

For characterization, a Quanta 650 environmental scanning electron microscope (ESEM, Thermo Fisher Scientific Inc., USA) was used. The ESEM was operated at an accelerating voltage of 20 kV. To investigate the dislocation structure induced during the FCG test, electron channeling contrast imaging (ECCI) was performed on the cross-section of the fractured specimens. A solid-state four-quadrant backscatter electron (BSE) detector was used, and the contrast was controlled to an optimum state for dislocation imaging.

3. Results

3.1 FCGR results

The FCGR data is shown in Figure 2. It can be seen from the data that when H was applied, the crack propagation rate increased significantly. The enhancement depends strongly on the test frequency. When the frequency decreases, the crack propagation becomes faster. With the highest frequency (10 Hz) in the present study, the FCGR increased by about 20 times with respect to the test in lab air, while the lowest frequency (0.1 Hz) made the FCGR increase by about 1000 times. These data show a relatively good linear relation and were fitted by the Paris' law. The fitted parameters are shown in Table 2.

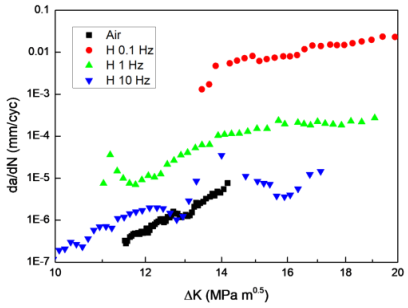

Figure *2*. d*a*/d*N* vs Δ*K* data for the studied specimens.

Table *2*. Fitted parameters based on the Paris' law.

Test condition	*C'*	*m'*
Air, R=0.5, f=10 Hz	3E-17	7.890
H, R=0.5, f=10 Hz	3E-15	7.898
H, R=0.5, f=1 Hz	5E-13	6.986
H, R=0.5, f=0.1 Hz	7E-9	5.048

3.2 Fractography

Fractography was taken on all half-specimens after the FCGR test. The fracture features were statistically analyzed. As shown in Figure 3a, the fracture surface of the specimens can be divided into three different regions, namely the EDM region, pre-crack region and the FCG region. It should be noted that the crack front was not necessarily a straight line due to non-uniform distribution of the stress field ahead of the crack tip. To avoid ambiguity between the pre-crack region and the FCG region, 1 mm was skipped from the measured starting place, and 0.6 mm was skipped from the edges through the thickness direction. As a result, only the highlighted part in Figure 3a was considered in the statistics. For fracture features, normally three distinct features can be identified, namely transgranular (TG) type, intergranular (IG) type and the so-called "quasi-cleavage" ("QC") type, as shown in Figure 3b-d. The area percentage of each fracture mode was analyzed on all H-charged specimens from the fractography, and the result is shown in Figure 4. The specimen tested in air showed only TG fracture and a minor percentage of IG fracture over the tested Δ*K* range. It should be noted that the name of "QC" fracture is somehow ambiguous, but it has been such named in many literature regarding crack growth with H environment (e.g. [8, 15, 21, 22]) and we just keep the convention. It can be seen from the results that H mainly changes the relative amount between TG and "QC" fracture modes. When H is charged to the specimen, "QC" fracture starts to happen to the material. When the frequency decreases, the "QC"

percentage increases and the TG percentage decreases, with minor change in the IG percentage.

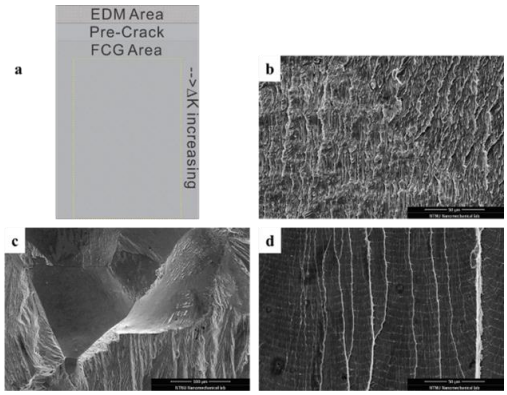

Figure 3. a. schematic description of the statistical analysis; b. typical TG fracture; c. typical IG fracture; d. typical "QC" fracture.

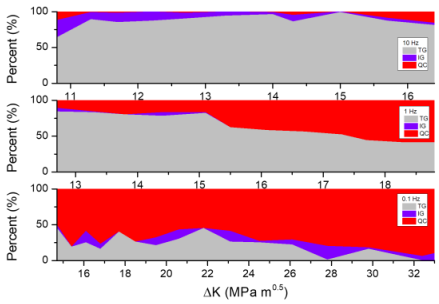

Figure 4. Fracture mode distribution with respect to ΔK level.

Images with high magnification were taken regarding each fracture feature on specimens tested in all conditions. The results are shown in the following figures.

In the TG fracture zone (as shown in Figure 5), the structures are similar in H-free and H-charged cases. Small and fine striations that are almost vertical to the global crack growth direction could be observed over the fracture surface. Tear edges are commonly observed, and the striations are normally vertical to the direction of the tear edges.

Figure 6 shows the magnified IG fracture surface. The figures show clearly fracture following grain boundaries (GBs), leaving a smooth surface from the boundaries without visible striations. There is not much different between the H-free and all the H-charged conditions. It is worth noting that the IG fracture type occupies only a small fraction according to the statistics in Figure 4.

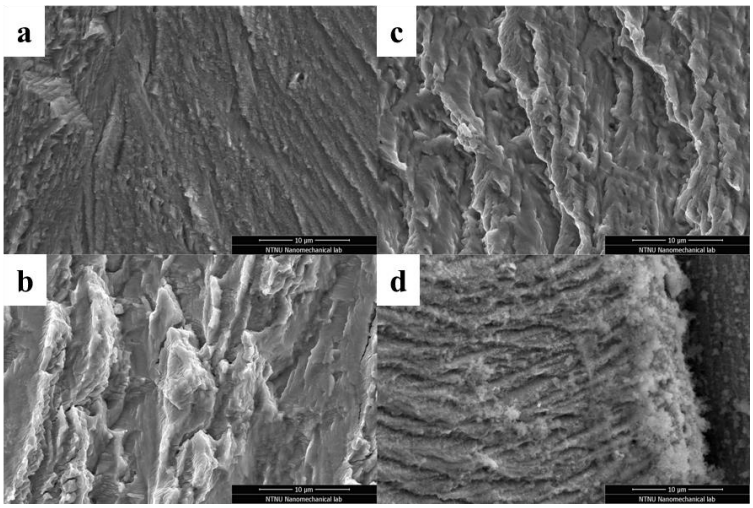

Figure *5*. Magnified images showing structure in TG fracture region (a. in Air; b. in H, f = 10 Hz; c. in H, f = 1 Hz; d. in H, f = 0.1 Hz; global FCG direction from top to bottom for each case)

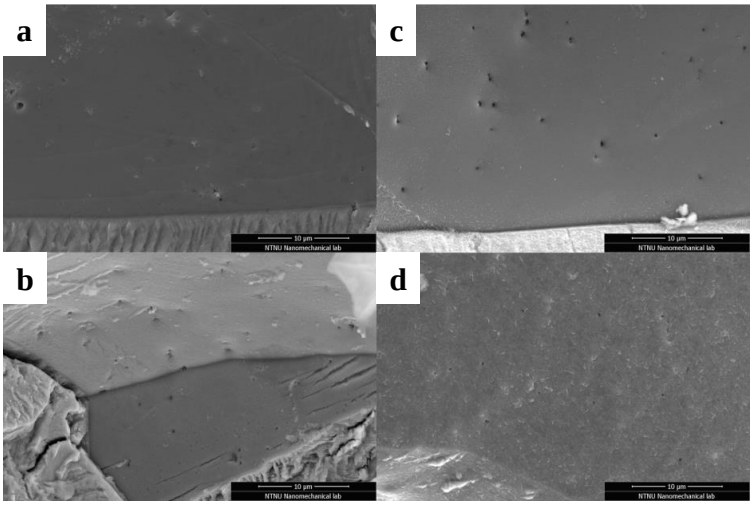

Figure *6*. Magnified images showing structure in IG fracture region (a. in Air; b. in H, f = 10 Hz; c. in H, f = 1 Hz; d. in H, f = 0.1 Hz; global FCG direction from top to bottom for each case)

Figure 7 shows the "QC" fracture in all conditions. Sparsely distributed brittle-like striations that are almost perpendicular to the global FCG direction could be observed on the surfaces. In the H-charged cases the fracture left sharp edges on the surface, and the striations were faceted in all H-cases. River-lines are visible on the fracture surfaces, and the lines are more or less parallel to the global FCG direction. It is important to be pointed out that the "QC" feature could not be observed in the air case. Figure 7a shows

the most similar feature in air as “QC” in H-cases, but the striations are not faceted and the tear ridges are not as sharp as the H-cases. The “QC” feature is characteristic from the H influence.

3.3 ECCI characterization

Preliminary ECCI characterization was performed on the cross-section of the fractured specimen to investigate the dislocation structures below the fracture surface. The result is shown in Figure 8. The global FCG direction is from left to right, but local variations could be observed. Plastic zones can be identified by the bright contrast due to a high dislocation density. The bright contrast above the yellow dash-line in Figure 8a comes from Fe-coating. Away from the plastic zone, sparsely distributed dislocations were observed in the H-free case, while in the H-charged case, dislocations were better organized into vein-like structures. This is the preliminary result and further systematic and detailed work is ongoing.

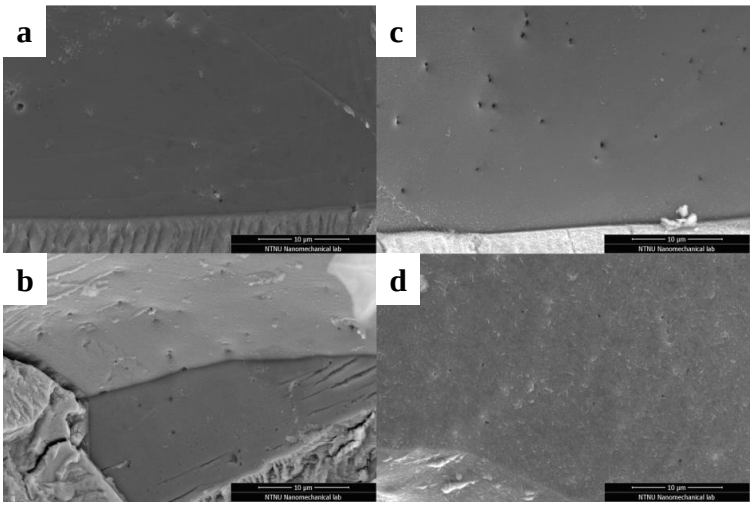

Figure *7*. Magnified images showing structure in “QC” fracture region (a. in Air; b. in H, f = 10 Hz; c. in H, f = 1 Hz; d. in H, f = 0.1 Hz; global FCG direction from top to bottom for each case)

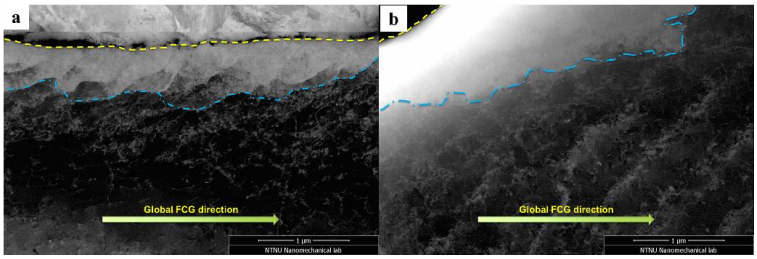

Figure *8*. Dislocation structures observed by ECCI in a. H-free case and b. H-charged case from the region fractured at similar ΔK level. The yellow dash-line is the fracture surface and the light blue broken-line is the indicated plastic zone under the fracture surface.

4. Discussion

4.1 Paris' relation

It is clearly shown that the measured crack growth data can be properly correlated with the Paris' law. This relation can describe the crack growth procedure in a mathematically simple and linear relation, also when aggressive environment applies. These data show that the Paris' law is validated for these test conditions. However, the local variation in different grains or different fracture features can give error in the estimation. A systematic verification at the microscale level is ongoing. This will be analyzed and discussed in a future work by the present authors.

4.2 H effect on FCG procedure

It is clearly shown in the crack growth data that when H was charged, the crack growth rate was increased up to 1000 times in comparison with the reference test in air. The test frequency also played a significant role in the crack growth rate enhancement. It could be inferred that the H degradation is a time-dependent process. When the frequency decreases, H has more time to invade the lattice and deteriorate the mechanical behavior, globally makes the crack grows faster. Chen et al. [23] also suggested that the H-assisted cracking is time-dependent in Fe-3%Si single crystals.

From the statistics in Figure 4, the frequency also influences the fracture mode distribution. A higher frequency leads to more TG fracture and a lower frequency gives more "QC" fracture, with the IG fraction almost keeps unchanged. The possible reasons might be that the "QC" fracture was transformed from the TG fracture by the effect from H.

Matsuoka et al. [24, 25] has explained the formation of this fracture feature in terms of reduced plasticity expansion in the crack-tip region. Based on their model, these striations are the results from slip localization, which is compatible with the HELP mechanism [3, 4]. They suggested that when the cyclic load was exerted to the specimen, the stress would be localized in the vicinity of the crack-tip, and the H atoms would be attracted by the highly localized tensile stress field. The localized H concentration made the crack propagation much easier even at a lower stress level during unloading procedure. Consequently, the distances between striations are larger in the H-charged specimens than the one tested in air. Similar features have also been observed in polycrystalline pure iron [22] and Fe-Si single crystals [26, 27] with H influence.

Another key point from Figure 4 is that when ΔK level increases, there is always a tendency of increasing "QC" fraction and decreasing TG fraction. This is the most significant for 1 Hz, but a clear tendency is also seen for 0.1 Hz and 10 Hz. Since "QC" feature is characteristic for the H influence, we can assume the fraction of "QC" fracture is a factor that can give an estimation of the HE level. Since the HE happens generally in high strength materials, it is suggested that the combination of high stress level and high H concentration makes the embrittlement possible. During FCGR tests, there is always a stress concentrated zone ahead of the crack-tip, which can also attract H atoms and enhance the local H concentration.

4.3 Dislocation structure

The ECCI results shown in Figure 8 are some preliminary results from dislocation investigations. The regions of interest came from a similar ΔK level during the FCGR tests. The H-case shows highly organized vein-like dislocation structure while the H-free case does not show similar feature. This could be the effect from H that dislocations were localized along some specific crystallographic directions, while impeded in other directions. As a result, concentration to some organized structures. However, there are some points still remain unclear such as the grain orientations, the accommodation from nearby grains, the local stress field, etc. Further investigations are ongoing and will be discussed more in detail in a future work by the present authors.

Nevertheless, some proof could be found from literature. For example, Wang et al. [8] did a similar work on pure iron with the help of scanning transmission electron microscope (STEM). It has been explained in this work that the attachment of H to

dislocations or other obstacles will change the stress field associated with crystallographic defects, and consequently enhancing the dislocation motion preferred in some specific directions while suppressing in other directions. As a result, the observed dislocation structure should be more organized in the H-charged case than that from the H-free case.

5. Conclusions

In this study, the fatigue crack growth behavior of a ferritic Fe-3wt.%Si alloy was tested both in lab air and with in-situ cathodic H-charging. Post-mortem fractography analysis was done through SEM. The main results can be summarized in the following points:

- The FCGR is increased by in-situ cathodic H-charging by a number ranging from 20 to 1000 times in comparison with a reference test in air;
- The higher crack growth rate is attributed to the increasing proportion of the "QC" type fracture, and it depends on the loading frequency and ΔK level;
- IG fracture occupies only a small part in comparison with TG type and "QC" type. GBs are not preferred crack propagation path;
- The preliminary investigations on dislocation structures show difference in H-free and H-charged cases, and more detailed systematic work is ongoing.

This work is financially supported by the Research Council of Norway through the HyF-Lex project (Petromaks 2 Programme, Project Number: 244068/E30).

References

[1] P. Peralta, C. Laird, Fatigue of Metals, in: D.E. Laughlin, K. Hono (Eds.), Physical Metallurgy (Fifth Edition), vol 2, Elsevier, Amsterdam, (2014), pp. 1765-1880.
[2] W.H. Johnson, P R SOC LONDON 23 (1875) 168-179.
[3] C.D. Beachem, METALL MATER TRANS B 3 (1972) 441-455.
[4] H.K. Birnbaum, P. Sofronis, MAT SCI ENG A 176 (1994) 191-202.
[5] I.M. Robertson, ENG FRACT MECH 64 (1999) 649-673.
[6] I.M. Robertson, H.K. Birnbaum, ACTA METALL 34 (1986) 353-366.

[7] I.M. Robertson, H.K. Birnbaum, P. Sofronis, Hydrogen Effects on Plasticity, vol 15, (2009), pp. 249-293.

[8] S. Wang, A. Nagao, P. Sofronis, I.M. Robertson, ACTA MATER 144 (2018) 164-176.

[9] W.W. Gerberich, P.G. Marsh, J.W. Hoehn, Hydrogen Induced Cracking Mechanisms - Are There Critical Experiments?, in: A.W. Thompson, N.R. Moody (Eds.), Hydrogen Effects in Materials, Minerals, Metals & Materials Society (TMS), Warrendale, Pennsylvania, USA, (1996), pp. 539-554.

[10] R.A. Oriani, CORROSION 43 (1987) 390-397.

[11] R.A. Oriani, P.H. Josephic, ACTA METALL 25 (1977) 979-988.

[12] R.P. Gangloff, Environment-Induced Cracking of Materials 1, (2008) 141-165.

[13] S.P. Lynch, ACTA METALL 36 (1988) 2639-2661.

[14] Y. Fukai, J ALLOY COMPD 356-357 (2003) 263-269.

[15] M. Nagumo, MAT SCI ENG 20 (2013) 940-950.

[16] H.K. Birnbaum, J LESS COMMON METALL 104 (1984) 31-41.

[17] N. Narita, C.J. Altstetter, H.K. Birnbaum, METALL TRANS A 13 (1982) 1355-1365.

[18] D.S. Shih, I.M. Robertson, H.K. Birnbaum, ACTA METALL 36 (1988) 111-124.

[19] Y. Murakami, R.O. Ritchie, Effects of hydrogen on fatigue-crack propagation in steels, Gaseous Hydrogen Embrittlement of Materials in Energy Technologies, vol 2, Woodhead Publishing, (2012), pp. 379-417.

[20] A. Alvaro, O.M. Akselsen, X. Ren, P.-A. Kane, Fatigue Properties of a 420 MPa Structural Steel at Low Temperature, The 25th International Ocean and Polar Engineering Conference, vol 4, Kona, Big Island, Hawaii, USA, 2015, pp. 331-337.

[21] Y. Ogawa, H. Matsunaga, J. Yamabe, M. Yoshikawa, S. Matsuoka, I J FATIGUE 103 (2017) 223-233.

[22] Y. Ogawa, D. Birenis, H. Matsunaga, A. Thøgersen, Ø. Prytz, O. Takakuwa, J. Yamabe, SCR MATER 140 (2017) 13-17.

[23] X. Chen, W.W. Gerberich, METALL TRANS A 22 (2012) 59-70.

[24] S. Matsuoka, H. Tanaka, N. Homma, Y. Murakami, I J FRACT 168 (2010) 101-112.

[25] S. Matsuoka, N. Tsutsumi, Y. Murakami, T JAP SOC MECH ENG A 74 (2008) 1528-1537.

[26] H. Vehoff, P. Neumann, ACTA METALL 28 (1980) 265-272.

[27] H. Vehoff, W. Rothe, ACTA METALL 31 (1983) 1781-1793.